uOttawa

L'Université canadienne
Canada's university

FACULTÉ DES ÉTUDES SUPÉRIEURES ET POSTOCTORALES

uOttawa

L'Université canadienne
Canada's university

FACULTY OF GRADUATE AND POSDOCTORAL STUDIES

Eve Heafey
AUTEUR DE LA THÈSE / AUTHOR OF THESIS

M.Sc. (Chemistry)
GRADE / DEGREE

Department of Chemistry
FACULTÉ, ÉCOLE, DÉPARTEMENT / FACULTY, SCHOOL, DEPARTMENT

Applications of Spectroscopy to the Creation and Study of Nanostructures
TITRE DE LA THÈSE / TITLE OF THESIS

J.C. Scaiano
DIRECTEUR (DIRECTRICE) DE LA THÈSE / THESIS SUPERVISOR

CO-DIRECTEUR (CO-DIRECTRICE) DE LA THÈSE / THESIS CO-SUPERVISOR

Natalie Goto

Sean Barry

Gary W. Slater
Le Doyen de la Faculté des études supérieures et postdoctorales / Dean of the Faculty of Graduate and Postdoctoral Studies

APPLICATIONS OF SPECTROSCOPY TO THE CREATION AND STUDY OF NANOSTRUCTURES

Eve Heafey

A thesis submitted to the
Faculty of Graduate and Postdoctoral Studies
in partial fulfillment of the requirements for the degree of
Master of Science
Specialization in Chemistry

uOttawa

in the Ottawa-Carleton Chemistry Institute
Department of Chemistry, University of Ottawa

Your file Votre référence
ISBN: 978-0-494-65498-9
Our file Notre référence
ISBN: 978-0-494-65498-9

To my parents, for their undying love and support.

ABSTRACT

With the technological advances of today, comes the increasing need for device miniaturization. This thesis focuses on the construction of nanostructures, approached from both bottom-up (synthesis) and top-down (lithography) methods.

First, a bottom-up method to construct cadmium selenide semiconductor nanoparticles under mild conditions in reverse micelles is described and investigated. A detailed spectroscopic study of nanoparticle growth is provided, whereby the growth was monitored over a period of up to a year. The nanoparticles were removed from the surfactant using ethanol precipitation and were subjected to surface derivatization in order to stabilize them.

Secondly, photoreversible cycloaddition of an anthracene derivative is studied for use in double-exposure lithography. The system was found to be adequately reversible, though possible side photoreactions were investigated. Spectroscopic studies were also conducted and photophysical pathways of the compound were examined. The compound was found to have a cleaving quantum yield of 0.67 ± 0.04 and was established as an actinometer to assess the efficacy of future candidate compounds.

TABLE OF CONTENTS

LIST OF FIGURES

CHAPTER 1. THE ADVENT OF NANO

CHAPTER 2. SEMICONDUCTOR PARTICLE NANOCONSTRUCTION

CHAPTER 3. A PROMISING WINDOW FOR NANOLITHOGRAPHY

LIST OF TABLES

CHAPTER 3. A PROMISING WINDOW FOR NANOLITHOGRAPHY

LIST OF EQUATIONS

CHAPTER 1. THE ADVENT OF NANO

CHAPTER 2. SEMICONDUCTOR PARTICLE NANOCONSTRUCTION

CHAPTER 3. A PROMISING WINDOW FOR NANOLITHOGRAPHY

ABBREVIATIONS & TERMINOLOGY

Å	*Angstrom unit (10^{-10} m)*
AQ	*Anthraquinone*
APO	*Anthracene endoperoxide*
AOT	*Aerosol-OT (docusate sodium salt, bis(2-ethylhexyl) sulfosuccinate)*
b.p.	*Boiling point*
cal	*Calorie (1 cal = 4.184 J)*
CEL	*Contrast enhancement layer*
cycloDAME	*"Dianthracene methyl ether" cycloadduct*
DAME	*"Dianthracene methyl ether"*
DAMEPO	*"Dianthracene methyl ether" endoperoxide*
DPCP	*Diphenylcyclopropenone*
Δ OD	*Change in absorbance*
eins	*Einstein unit of light energy (one mole of photons)*
EUV	*Extreme ultraviolet light (13.4 nm)*
ε	*Extinction coefficient*
Hz	*Hertz (s^{-1}), basic S.I. unit for frequency*
J	*Joule*
k	*Rate constant*
LFP	*Laser flash photolysis*
m	*Meter, basic S.I. unit for length*
M	*Molar*
mL	*Milliliter (10^{-3} L)*

mJ	*Millijoule (10^{-3} J)*
mM	*Millimolar (10^{-3} M)*
m.w.	*Molecular weight*
μL	*Microliter (10^{-6} L)*
μm	*Micrometer (10^{-6} m)*
μs	*Microsecond (10^{-6} s)*
nm	*Nanometer (10^{-9} m)*
NMR	*Nuclear magnetic resonance spectroscopy*
NP	*Nanoparticle*
ns	*Nanosecond (10^{-9} s)*
PAB	*Post-application bake*
PAG	*Photoacid generator*
PMMA	*Polymethylmethacrylate*
QD	*Quantum dot*
Φ	*Quantum yield*
Φ_{fl}	*Quantum yield of fluorescence*
rCEL	*Reversible contrast enhancement layer*
s	*Second, basic S.I. unit for time*
S_0	*Singlet ground state*
S_1	*First singlet excited state*
T	*Triplet state*
T_g	*Glass transition temperature*
τ	*Lifetime*
UVA	*ultraviolet radiation ranging from 315-400 nm*
UVB	*ultraviolet radiation ranging from 280-315 nm*
UVC	*ultraviolet radiation ranging from 200-280 nm*
w	*Water-to-surfactant ratio ($w = [H_2O]/[surfactant]$)*
W	*Watts (Joules per second)*

It is important to comment on the definitions and usages of the terms nanoscience and nanotechnology. These seem to be used frivolously and without thought, though it is clear that a distinction exists between science and technology; the latter being comprised of theory and experiment while the former is mainly the realm of development, applications and commercial implications. In the case of "nano" however, it is often difficult to distinguish the two.[1] *Indeed, what is studied by nanoscience is morphed into application and what is used in nanotechnology is in turn thoroughly studied. For the purposes herein, the terms will be used without distinction.*

1. Hornyak, G. L.; Dutta, J.; Tibbals, H. F.; Rao, A. K., *Introduction to Nanoscience*. CRC Press – Taylor & Francis Group: Boca Raton, 2008.

ACKNOWLEDGEMENTS

My supervisor, Professor Tito Scaiano, has inspired me from the very beginning of my university life. Tito - you are an extraordinary chemist, supervisor, mentor and individual and I still have much to learn from you. I am forever grateful to you for all you have given me academically and personally. You have wisely guided me and always allowed me to pursue my many projects and ambitions. Words cannot express the impact that you have made on my career, my vision and my life.

Dr. Marta Liras was to me an endless source of information and she has provided me with useful guidance and advice. I would like to thank her more specifically for her generous help with synthesis and NMR. Working alongside Paul Billone, enjoying the sciences of chemistry and wine, has led to many interesting discussions and valuable insight for which I am thankful.

I am indebted to Dr. Robert Bristol from Intel Corporation as well as Dr. James M. Blackwell and Katherine Esswein from Intel's Molecules for Advanced Patterning (MAP) Program for their support and helpful contributions.

I am also grateful for Michel Grenier's assistance. He has made the laser lab a haven of interesting music and interesting science: giving me CBC Radio 2, countless entertainment recommendations and indispensable help with the laser systems.

I would like to express my heartfelt thanks to the entire research group, current and past members that I have worked with. Anyone who has been in the Scaiano Group knows that this is truly a unique environment to work in, which hardly feels like work and more often feels like discovering new and interesting things with friends. Members of this group are kind and always willing to help. I would like to

mention my pseudo-deskmate Kevin Stamplecoskie, for putting a smile on my face and coming to the rescue whenever I needed it; Dr. Marie Laferrière who took me under her wing, shared the joys and tribulations of quantum dots with me, always encouraging and guiding me; Dr. Maria Gonzalez-Bejár, for generously sharing her space with me and making time to lend a helping hand, even when she was overwhelmed with work; the very generous Dr. Kathy-Sarah Focsaneanu whose door is always open to talk NIN or chemistry or anything else; and Dr. Alexis Aspée, who happily dropped what he was doing to answer my many questions and help me in any way he could. For his help in the wet lab, I am also grateful to Matt Decan who is generous and kind... though he unsuccessfully tries to hide it. On that note, I'd also like to thank kumquats for making our lunchtimes hilarious. I will dearly miss being around Tito and the group, at meetings and social outings alike. I will always conserve fond memories of wonderful times spent together as well as Tito and Elda's warmth and generosity at BBQs, Christmas dinners, ski and cottage weekends.

I am grateful for all the support I have received from fellow labmates and in particular for Matt's undying patience. To my Matt - who generously gave me his TLC spotters, perfectly cut plates, NMR tubes, fumehood space and blackberries - thank you for columns and lunches and dancing in the morning and everything else. You were an unexpected and bright encounter on my convoluted journey: you are my sunshine. I also thank Elyse and Maurice from the bottom of my heart, for understanding when I neglected them, for coffees and kind gestures which never failed to brighten my day, and for generally being the best, most supportive friends a girl can have.

I would like to give special thanks to my family, for always taking an interest in what I do and always being there for me. To my parents - Dad, who listened to my hard-to-follow stories and always rescued me when I needed; Mom, who has and always will want the best for me. I know that you are always thinking of my well-being. This endeavor would have been impossible without your support. You are in my thoughts always and I am very lucky to have you. Thank you...

CHAPTER 1

THE ADVENT OF NANO –

SMALL SCIENCE MAKING BIG WAVES

The prefix nano, stemming from the greek word for dwarf, was first used in the scientific literature by Lohmann in 1908 to classify very small organisms (now known to measure approximately 200 nm).[1, 2] *Over 65 years later, Taniguchi first defined the term nanotechnology as "the processing of, separation, consolidation, and deformation of materials by one atom or one molecule",*[3] *though that definition has since been extended to include features as large as 100 nm. Indeed the nanoworld as it is conceived today, is a borderland between the realm of atoms and molecules (~ Å), dominated by electrostatic interactions, Brownian motion as well as quantum mechanics, and the macroworld where properties depend on the collective action of trillions of atoms in a bulk material (~ μm).*[4]

The conception of nanotechnology today has emerged from groundbreaking scientists and innovative thinkers, such as Dr. Richard P. Feynman. Fifty years ago, Feynman launched an invitation to the American Physical Society, to enter a new field of physics.[5] *He described a new realm of science on the small scale that would open yet unimagined possibilities for useful technologies on the atomic and molecular levels. His enlightened and innovative lecture is widely acknowledged as one of the foundations of current nanotechnology.*[6] *The development of the field was also enabled by the many advances in microscopic techniques that allow atomic resolution, including those that emerged from the research of Binning and Rohrer who were awarded the 1986 Nobel prize in physics for their design of the scanning tunneling microscope.*[7] *Drexler's well-known book "Engines of Creation" was also published that same year, in which the author gave his vision of nanotechnology's future and its possibilities.*

At the start of the new millennium, the field of nanotechnology had already evolved to produce real examples of nanodevices.[6] Today, nanotubes and nanowires are being used to build electronic display panels,[8] and nanoparticles have found possible use in solar cells as well as drug carriers.[9-11] In fact, there is a well-established history of protein absorption to gold nanoparticles, from antibodies to enzymes which have been typically studied as probes and sensors in medicine.[12] Interestingly, recent work has shown that gold nanoparticles can be modified to inhibit HIV-1 fusion to human T cells.[13]

Nanoresearch has indeed become one of the most highly energized disciplines in science and technology today.[4] This is exemplified by the swelling number of scientific publications in the field, as shown in Figure 1 below.

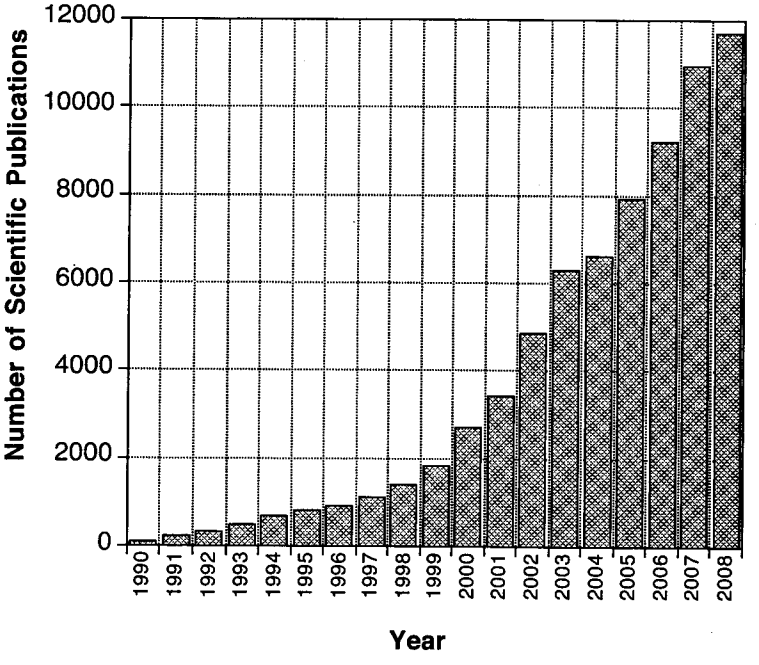

Figure 1. Number of peer-reviewed scientific publications per year since 1990 pertaining to "nano", determined by SciFinder.

The increasing number of publicly traded nanotech companies and soaring business interests also attest to this fact. Companies, such as Nanophase Technologies who notably produces zinc oxide nanoparticles for use in sunscreens, strive to deliver nano-engineered materials to enable innovative products that revolutionize the world and improve people's lives.[14] The ZnO nanoparticles are designed to protect

the skin from sun exposure by scattering harmful UV radiation, while remaining invisible to the eye because they are too small to scatter visible light.

Silver nanoparticles on the other hand, have long been known to possess antibacterial properties.[15, 16] *On this basis, Samsung has recently launched a new line of antibacterial home appliances under the Silver Nano Health System trademark, which uses silver nanoparticles in washing machines, refrigerators, air conditioners, air purifiers and vacuum cleaners with silver nanoparticle coatings on their inner surfaces.*[17]

Indeed, as we gradually reduce the size of functional devices and materials, we open the way to new technologies in a multitude of fields including medicine, computing, environment, energy, materials and nanorobotics.[18]

Evidently, the reach of nanoscience is considerable as revealed by the recently instituted Kavli Prize in Nanoscience, which is awarded for "outstanding achievement in the science and application of the unique physical, chemical, and biological properties of atomic, molecular, macromolecular, and cellular structures and systems that are manifest in the nanometer scale".[19] *The prestigious Kavli Prize was established through a partnership between The Norwegian Academy of Science and Letters, The Kavli Foundation and The Norwegian Ministry of Education and Research to recognize outstanding scientific research and honor highly creative scientists. Three prizes are awarded every second year in the biggest (astrophysics), the smallest (nanoscience), and the most complex (neuroscience) scientific fields, according to Kavli himself.*[20]

Although much progress has already been made since the visionary days of Feynman, it is clear that nanofabrication will continue to be "the foundation and enabler of the entire field of nanotechnology and nanoscience".[21] *The topic of nanofabrication is at the very core of this thesis and will be explored from the two fabrication approaches: top-down and bottom-up.*

i. Top-down fabrication

All top-down approaches remove, reduce, subtract, or subdivide a bulk material to make structures on the nanoscale.[22] These usually fall within the realm of engineering and physics, as opposed to chemistry, using methods such as film laser-beam processing, lithography and mechanical techniques.[23]

Such a reliance on big machines to make small devices can be cumbersome and often limits nanoscience to the institutions with the largest pocketbooks.[24] Another disadvantage of the top-down approach is the introduction of imperfections in the surface structure, that can be introduced in etching steps in lithography for example.[25, 26] Many powerful top-down techniques today nevertheless involve some form of lithography, which can easily be considered as "the workhorse of fabricating patterned surfaces".[27]

Lithography was invented by Alois Senefelder at the end of the eighteenth century. The name is derived from the Greek word "lithos" for stone as limestone was the canvas used for lithography in its beginnings.[28] The lithographic techniques used today are essentially extensions of photography and begin with a pattern which is usually reduced in the lithographic process.[29] Briefly, the pattern is transferred to the substrate using a three-component system consisting of a mask through which light is passed onto a photosensitive material (resist). The resist is a material that undergoes a change in chemical resistance to a developer solution when exposed to light. If the resist is placed in a developer solution after selective exposure to a light source, it will etch away one of the two regions (exposed or unexposed).

The integrated circuit and computing industry was built on the technology offered by lithography, which continues to be the most reliable way to fabricate nanostructures with widespread applications.[22] In fact, there is no doubt that the current "nano fever" is driven, at least in part, by the computing industry ceaselessly trying to keep up with Moore's Law,[25] which predicted in 1965 that the device density on integrated circuits would double every 18 months.[30] Increasing device density inevitably means reducing feature size and was successfully achieved in the past by decreasing the lithographic wavelength used. This was a valid strategy until about 15 years ago, when the feature size required became smaller than the possible lithographic wavelengths, as shown in Figure 2.

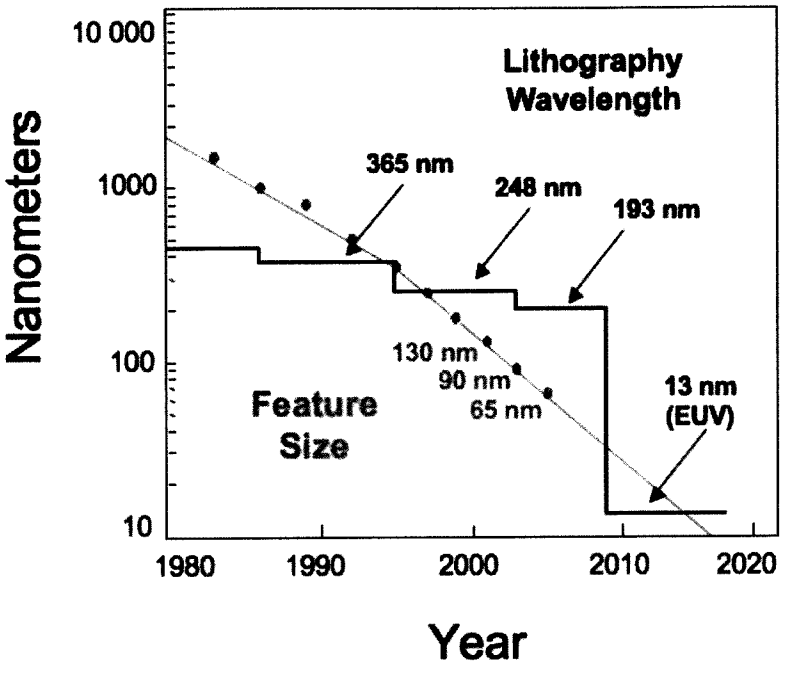

Figure 2. Schematic representation of the progression of lithographic feature sizes and lithographic wavelengths in nanometers, showing the crossover point around 1995. Diagram modified from Dr. Robert Bristol's (Intel Corporation, Portland, Oregon) presentation at the University of Ottawa on September 25, 2008.

It is well-known that the laws of physics restrict lithographic resolution to approximately λ/4 to λ/2, where λ is the wavelength of the light used to image.[31] *Indeed resolution, determined by the half pitch critical dimension (CD), is limited by the Rayleigh equation as shown below, where k is the process aggressiveness constant depending on specific resist material, process technology and image-formation techniques used,*[25] *and NA is the numerical aperture of the imaging lens:*[32]

Equation 1. $CD = k\lambda / NA$

The half pitch can therefore be reduced by decreasing the imaging light wavelength or the aggressiveness factor, or by increasing the numerical aperture. The current half pitch limit is ~ 38 nm, given the technologies available today.[32]

The imaging process is said to be diffraction-limited when the first diffraction minimum of the image of one source point coincides with the maximum of another.

In other words, lithographic features smaller than 38 nm would not be properly resolved using conventional techniques. This is known as the diffraction limit, where features begin to blur and meld together.[29] Beyond this optical barrier, lithography becomes much more difficult and requires a number of complex tactics to achieve adequate resolution. Although the integrated circuit industry has been successful at circumventing these limitations, the current technology is approaching the physical barrier to minimum achievable size.[32] Novel materials and techniques are now needed to create structures and devices on a smaller scale and allow imaging beyond the classical Rayleigh equation limits.

ii. Bottom-up construction

Opposite top-down methods exists the so-called bottom-up approach; an approach intimately associated with Feynman's idea of "manipulating and controlling things on a small scale".[5, 24] This approach enters the sphere of chemistry and completely bypasses limitations such as those imposed by the diffraction limit, employing methods such as chemical synthesis, self-assembly and chemical vapor deposition to construct nanostructures.[33] Some advantages of this approach include atomic feature sizes as well as ease and speed of adaptation to new technologies.[24, 34] Furthermore, where top-down techniques introduce internal stress and surface defects, bottom-up ones produce nanostructures that are in a state closer to a thermodynamic equilibrium because they are driven by the reduction of Gibbs free energy.[25]

It is also interesting to note that while lithographic techniques are limited by the inherent two-dimensionality of each lithographic step, bottom-up methods allow nanofabrication with three-dimensional control.[35] Nevertheless, while bottom-up techniques can produce very small and advanced nanostructures, the complexities and still widely unchartered territory limit large-scale commercial manufacturing.

In spite of that, bottom-up methods undoubtedly have the capability of complementing top-down fabrication techniques, but such an amalgam will require broad and profound knowledge of structure, dynamics and growth mechanisms of the nanostructures being synthesized.[36] The following chapters are an attempt at broadening our understanding of these important facets of nanofabrication.

REFERENCES

1. Joachim, C., To be nano or not to be nano? *Nature Materials* **2005**, 4, 107 - 109.

2. Lohmann, H., Untersuchungen zur Feststekkung des Vollstandigen Gehaltes des Meeres an Plankton. *Helgolander wiss Meeresunters* **1908**, 10, 131 - 370.

3. Tanigushi, N., On the Basic Concept of 'Nanotechnology'. *Proceedings of the International Conference on Production Engineering, Part II. Japan Society of Precision Engineering.* **1974**.

4. Stix, G., Little Big Science. *Scientific American* **2001**, 285, (3), 32 - 37.

5. Feynman, R. P., There's Plenty of Room at the Bottom. *Engineering and Science* **1960**, 23, 22 - 36.

6. Kricka, L. J.; Fortina, P., Nanotechnology and Applications: An All-Language Literature Survey Including Books and Patents. *Clinical Chemistry* **2002**, 48, 662 - 665.

7. online at http://nobelprize.org/nobel_prizes/physics/laureates/1986/.

8. Collins, P. G.; Arnold, M. S.; Avouris, P., Engineering Carbon Nanotubes and Nanotube Circuits Using Electrical Breakdown. *Science* **2001**, 292, (5517), 706 - 709.

9. Huynh, W. U.; Dittmer, J. J.; Alivisatos, A. P., Hybrid Nanorod-Polymer Solar Cells. *Science* **2002**, 295, (5564), 2425 - 2427.

10. Lambert, G.; Fattal, E.; Couvreur, P., Nanoparticulate Systems for the Delivery of Antisense Oligonucleotides. *Advanced Drug Delivery Reviews* **2001**, 47, 99 - 112.

11. Gibson, J. D.; Khanal, B. P.; Zubarev, E. R., Paclitaxel-Functionalized Gold Nanoparticles. *Journal of the American Chemical Society* **2007**, 129, 11653 - 11661.

12. Pasquato, L.; Pengo, P.; Scrimin, P., Biological and Biomimetic Applications of Nanoparticles. In *Nanoparticles - Building Blocks for Nanotechnology*, Rotello, V., Ed. Kluwer Academic/Plenum Publishers: New York, 2004.

13. Bowman, M.-C.; Ballard, T. E.; Ackerson, C. J.; Feldheim, D. L.; Margolis, D. M.; Melander, C., Inhibition of HIV Fusion with Multivalent Gold Nanoparticles. *Journal of the American Chemical Society* **2008**, 130, 6896 - 6897.

14. *online at http://www.nanophase.com/.*

15. Morones, J. R.; Elechiguerra, J. L.; Camacho, A.; Holt, K.; Kouri, J. B.; Ramirez, J. T.; Yacaman, M. J., The Bacterial Effect of Silver Nanoparticles. *Nanotechnology* **2005**, 16, 2346 - 2353.

16. Lansdown, A. B., Silver I: Its Antibacterial Properties and Mechanisms of Action. *Journal of Wound Care* **2002**, 11, 125 - 130.

17. online at http://www.samsung.com/au/silvernano/site.html.

18. Balzani, V.; Credi, A.; Venturi, M., Light-powered Molecular-scale Machines. *Pure Applied Chemistry* **2003**, 75, (5), 541 - 547.

19. *online at http://www.kavliprize.no/.*

20. *online at http://www.kavlifoundation.org/.*

21. Wang, Y.; Mirkin, C. A.; Park, S.-J., Nanofabrication Beyond Electronics. *ACS Nano* **2009**, 3, (5), 1049 - 1056.

22. Hornyak, G. L.; Dutta, J.; Tibbals, H. F.; Rao, A. K., *Introduction to Nanoscience*. CRC Press - Taylor & Francis Group: Boca Raton, 2008.

23. Skaff, H.; Emrick, T., Semiconductor Nanoparticles: Synthesis, Properties, and Integration Into Polymers for the Generation of Novel Composite Materials. In *Nanoparticles - Building Blocks for Nanotechnology*, Rotello, V., Ed. Kluwer Academic/Plenum Publishers: New York, 2004.

24. Wade, T. L.; Wegrowe, J.-E., Template Synthesis of Nanomaterials. *The European Physical Journal - Applied Physics* **2005**, 29, 3 - 22.

25. Cao, G., *Nanostructures & Nanomaterials: Synthesis, Properties and Applications*. Imperial College Press: London, UK, 2004.

26. Das, B.; Subramaniam, S.; Melloch, M. R., Effects of Electron-Beam Induced Damage in Back-Gated GaAs/AlGaAs Devices. *Semiconductor Science & Technology* **1993**, 8, 1347 - 1351.

27. Wang, D.; Mohwald, H., Template-directed Colloidal Self-assembly: The route to 'Top-down' Nanochemical Engineering. *Journal of Materials Chemistry* **2004**, 14, 459 - 468.

28. Senefelder, A., *The Invention of Lithography*. The Fuchs & Lang Manufacturing Company: New York, 1911.

29. Whitesides, G.; Love, J., The Art of Building Small. *Scientific American* **2001**, 285, (3), 39 - 47.

30. Moore, G. E., Cramming more components onto integrated circuits. *Electronics* **1965**, 38, (8), 114 - 117.

31. Balzani, V., Nanoscience and Nanotechnology: The Bottom-up Construction of Molecular Devices and Machines. *Pure and Applied Chemistry* **2008**, 80, (8), 1631 - 1650.

32. Lee, S.; Jen, K.; Willson, C.; Byers, J.; Zimmerman, P.; Turro, N., Materials modeling and development for use in double-exposure lithography applications. *Journal of Micro/Nanolithography* **2009**, 8, (1), 011011/1-11.

33. Yu, B.; Meyyappan, M., Nanotechnology: Role in Emerging Nanoelectronics. *Solid State Electronics* **2006**, 50, 536 - 544.

34. Huie, J. C., Guided Molecular Self-assembly: A Review of Recent Efforts. *Smart Materials and Structures* **2003**, 12, 264 - 271.

35. Shenhar, R.; Rotello, V. M., Nanoparticles: Scaffolds and Building Blocks. *Accounts of Chemical Research* **2003**, 36, 549 - 561.

36. Zhang, S., Building From the Bottom Up. *Materials Today* **2003**, 6, (5), 20 - 27.

CHAPTER 2

SEMICONDUCTOR PARTICLE NANOCONSTRUCTION – AN AQUEOUS ROOM TEMPERATURE SYNTHESIS

SEMICONDUCTOR PARTICLE NANOCONSTRUCTION – AN AQUEOUS ROOM TEMPERATURE SYNTHESIS

Colloidal semiconductor nanocrystals or nanoparticles (NPs), often referred to as quantum dots (QD), and their interesting properties were discovered in 1983 by Louis E. Brus.[1] In 2008, he received the inaugural Kavli Prize in nanoscience for this outstanding contribution to science.

QDs are indeed at the forefront of nanotechnology, enabling the advancement of various devices such as transistors, solar cells, LEDs and diode lasers.[2] The unique characteristics of quantum dots, such as broad absorbance and narrow emission, are due to their small size which provides confinement of the electron-hole pairs in all three dimensions,[3] which will be explained further. Interestingly, the electronic states of quantum dots ressemble something between those of an atom or molecule and those of a bulk material.[3] Quantum dots therefore exhibit strong size-dependence of their electrical and optical properties.[4, 5]

As explained by Alivisatos, the electronic bands of a solid are centered around the atomic energy levels.[6] As a cluster size increases, the center of the band develops first and the edges last. The Fermi level is by definition the energy level having the probability that it is exactly half filled with electrons. It can therefore be thought of as an analog of the highest occupied molecular orbital (HOMO) in a molecule. Indeed, energy levels below the Fermi level tend to be entirely filled with electrons, whereas energy levels above the Fermi level tend to be empty.

In metals, the Fermi level lies in the band (see Figure 3). Since the energy spacing to the next level is small, the properties of a metal at temperatures above a few Kelvin ressemble those of a continuum, even for small particle sizes. In an semiconductor however, the Fermi level lies at the top of the conduction band. As the semiconductor particle size increases, the density of states will develop in the band gap and alter the relevant energy spacing between the top of the conduction band and the bottom of the valence band, thus leading to the characteristic size dependent properties of semiconductor nanoparticles.

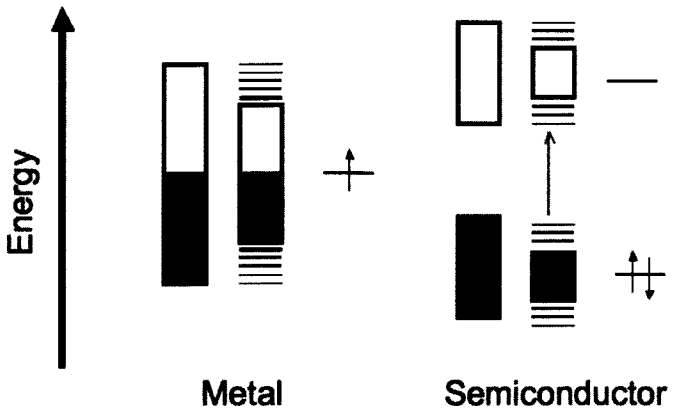

Figure 3. Schematic illustration of the density of states in metal and semiconductor clusters, for (from left to right) bulk, nanoparticle and molecular realms, showing the band gap reduction occurring in semiconductor particles due to the density of states development in the band gap as the size increases.[6]

Briefly, higher energy photons are required to generate electron-hole pairs when these are confined to a smaller volume.[7] *These electron-hole pairs (termed excitons when the pairs are in intimate contact and have not dissociated) are formed when an electron is excited from the valence to the conduction band.*[8] *Indeed, when the semiconductor is in the ground state, the valence band is completely filled and separated from the conduction band by a narrow band gap. If sufficient energy is applied, electrons are promoted into the conduction band thereby leaving a hole in the valence band and creating an electron-hole pair. Quantum confinement is said to occur when the nanoparticle radius is smaller than the average distance between electron and hole, termed the bulk exciton Bohr radius (~11 nm for CdSe).*[8] *In other words, when the particle is reduced to a size comparable to or smaller than the Bohr radius, the space in which the charge carriers (excitons) move is also reduced which confines their motion. Like the motion of an electron in a box, as the size of the box decreases, its kinetic (as well as its excitation) energy increases. Thus, when the semiconductor particle size becomes smaller than the Bohr radius, the band gap energy increases.*[9]

As quantum dot light emission is produced upon the recombination of the charge carriers generated upon light absorption, larger particles which have smaller energy band gaps will exhibit emission at a lower energy.[10] *For example, the emission in CdSe can be tuned from blue (390 nm) to deep red (690 nm) by increasing the particle size from 1.5 to 12 nm.*[11]

CdSe nanoparticles are typically prepared at high temperatures, from cadmium oxide and selenium, using the procedure developed by Peng and Peng.[12] However, there is a growing interest in a synthetic path involving gentler conditions, such as reactions at room temperature. The main advantages of such methods are simplicity and convenience. Another appealing advantage of room temperature synthesis, is the option of altering the luminescence properties of the nanoparticles, for example by doping them with lanthanides, which cannot be readily accomplished at high temperatures.

It was found that CdSe nanoparticles can be synthesized at room temperature in aqueous phase, using cadmium and selenium salts.[13] As physical and optical properties are extremely dependant on semiconductor nanoparticle size, a crucial aspect of quantum dot synthesis is size control. Hence, reverse micelles were used in this project to confine the hydrophilic reactants to the aqueous nanoreactors formed by the surfactant and water.[14, 15] The structural conformation of Aerosol-OT (docusate sodium salt, AOT) which has two hydrocarbon tails is conducive to the formation of reverse micelles and is therefore a preferred surfactant in this synthesis. AOT forms well defined water droplets and it has been found that the water pool size of AOT reverse micelles is directly dependant on w, the water-to-surfactant molar ratio.[16]

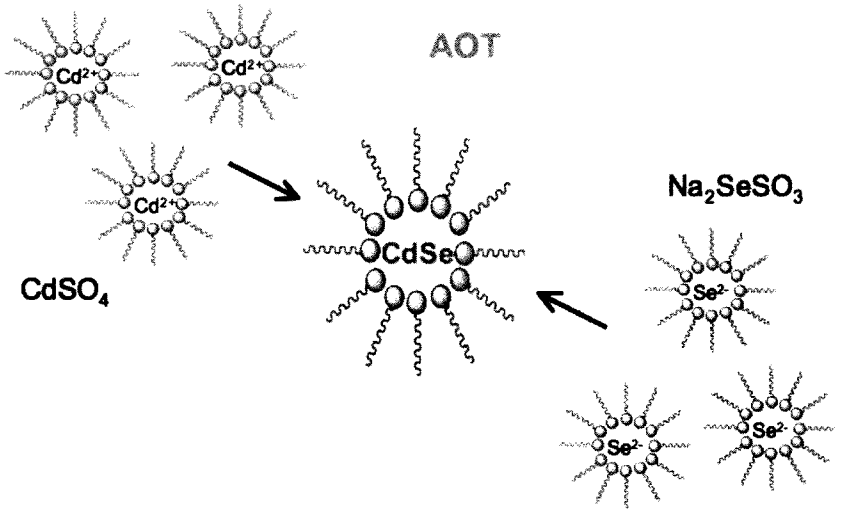

Scheme 1. Graphical depiction of the reverse micelle synthesis of quantum dots. Blue structures represent the surfactant, AOT.

METHODS

Spectra were measured using precision quartz cuvettes with optical paths of 1 cm.

UV-visible spectra were recorded on a Varian Cary-50 single beam spectrometer with zero/baseline corrections, using air and solvent as the zero and baseline absorbance curves, respectively unless otherwise noted.

Steady-state fluorescence (photoluminescence) spectroscopy was carried out with an instrument from Photon Technology International (PTI) utilizing a continuous xenon lamp for excitation at 350 nm and Felix32 Analysis software version 1.2. Spectral resolution was set at 2 nm. Photoluminescence lifetime measurements were carried out on a PTI EasyLife LS system, with excitation from a 350 nm diode. Light from the diode was filtered from the detected emission using a 375 nm longpass filter.

Ultraviolet light was provided by a UVP compact UV lamp (PL series, 4 W) with shortwave (254 nm) and longwave (365 nm) options, for quantum dot photoluminescence photography. Continuous lamp irradiation was carried out in a Luzchem photoreactor, model LZC-4, with Sylvania® Cool White bulbs (4.8 W/m^2 per bulb) providing visible light spanning the whole visible range (400 - 700 nm).

MATERIALS

For all applications, the water used was filtered with a Millipore MilliQ system, using a Quantum™ EX cartridge. The water resistivity at 25°C was 18.2 MΩ. Solvents were purged with nitrogen gas and all experiments were conducted under an inert nitrogen atmosphere to avoid selenium oxidation which occurs readily at ambient conditions.

The cadmium sulfate ($CdSO_4$, 99.999%, Aldrich), selenium powder (99.5+%, 100 mesh, Aldrich), sodium sulfite anhydrous (Na_2SO_3, Aldrich), trioctylphosphine oxide (TOPO, Aldrich), triethylamine (99%, Aldrich), 3-mercapto-1-propane sulfonic acid sodium salt (MPSA, technical grade 90%, Aldrich), heptane (99%, Aldrich) and ligroin were used as received. Sodium selenosulfite (Na_2SeSO_3, 0.1 M) was synthesized by refluxing 0.0789 g Se-powder in 10 mL 0.2 M $Na_2SO_{3\,(aq)}$, vigorously stirring under argon gas for 24 hours at 80°C. Note that the excess sodium sulfite is important in order to prevent selenosulfate decomposition and selenium precipitation.[17]

The surfactant, docusate sodium salt (AOT, SigmaUltra minimum 99%, Aldrich) was purified by dissolving it in petroleum ether and filtering through a Whatman #1 paper filter. The solvent was removed by rotary evaporation.

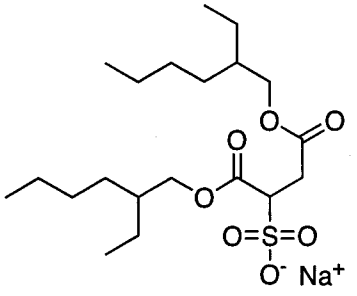

Structure 1. Aerosol-OT surfactant (docusate sodium salt).

Purified AOT (0.444 g) was dissolved in 20 mL heptane and this solution was purged with nitrogen for three hours in a test tube with stirring. This AOT solution (0.05 M) was divided in two 10 mL aliquots. In the first aliquot, 100 µL of 1.0 M aqueous $CdSO_4$ solution was added and briefly stirred to ensure homogeneous dispersion. An

excess of the cadmium precursor, which is less reactive than the selenium precursor, was found beneficial for the system to reach the desired balance between nucleation and growth,[12, 18] hence 100 µL of 0.1 M aqueous Na_2SeSO_3 was added in the same manner to the second aliquot. These reverse micelle solutions (w = 10) were left to equilibrate for one hour, after which the solutions were magnetically stirred once again and allowed to turn clear. At this point, the two solutions were mixed together and stirred briefly. From then on the quantum dots were allowed to develop without stirring.

According to literature, a probable pathway for formation of CdSe nanoparticles is hydrolysis of $SeSO_3^{2-}$ to HSe^-:[19]

$$SeSO_3^{2-} + OH^- \rightarrow HSe^- + SO_4^{2-}, \text{ followed by } CdSO_3^{2-} + HSe^- \rightarrow HSO_3^- + CdSe$$ [§]

For all spectroscopy, an aliquot of growing quantum dots was transferred to a cuvette after 1 minute of stirring and monitored over a period of several hours to several months. New aliquots were regularly taken to ensure that the cuvette solution and the initial stock solution were developing in the same manner.

Control experiments confirmed that the reactants used are not independently fluorescent. Furthermore, it was established that the micellar environment was significant in the synthesis. Indeed, when the reaction was made to occur strictly in water, with nothing to restrain the quantum dot growth, the resulting solution was a turbid, heterogeneous, non-fluorescent solution that exhibited no properties expected of quantum dots. In the reverse micelle solution however, the quantum dots grew in size and the initially clear solution evolved from pale to deep yellow.

It is important to note that a peak growing in the photoluminescence spectra at approximately 375 nm, was found to be caused by a compound being extracted by heptane from the rubber septa used. Therefore, glass or Teflon stoppers were used in all syntheses. In addition, Teflon tape was used to cover the rubber septa during purging.

[§] Although there are likely various equilibria between HSe^- and Se^{2-}, HSO_3^- and SO_3^{2-} and probable final formation of SO_4^{2-} these are not elaborated here.

RESULTS

Spectroscopic Properties of Studied Compounds

The position of the first excitonic absorption peak of a QD solution reflects the size of the QD contained therein and can be described by an empirical relationship, shown in Equation 2, where D is the diameter of a given nanocrystal sample in nanometers, and λ is the wavelength of the first excitonic absorption peak of the corresponding sample in nanometers:

***Equation 2. Empirical relationship for CdSe QDs.*[20]**

$$D = (1.6122 \times 10^{-9})\lambda^4 - (2.6575 \times 10^{-6})\lambda^3 + (1.6242 \times 10^{-3})\lambda^2 - (0.4277)\lambda + (41.57)$$

It is important to note that for any quantum dot solution, there is an inherent size distribution around the mean. This contributes to the absorbance peak width, where the most abundant nanoparticles have the size corresponding to the peak maximum.

It is also known that for very small particles, this band disappears completely.[21] *Hence, the band of the synthesized nanoparticles does not appear until several hours of growth when the particles have reached this critical size. As initial QD growth cannot be monitored via absorbance because of the small particle size, photoluminescence provides us with a useful tool, especially in the early stages of growth. In fact, the QD photoluminescence is observable almost immediately after putting cadmium in contact with selenium. Similarly to the absorbance plasmon band, the photoluminescence emission of quantum dots is directly related to their size. Indeed, shorter wavelength emissions will be observed from smaller nanoparticles. The photoluminescence peak shift can therefore be monitored over time and is a reflection of quantum dot growth. It is quite clear from both absorbance and emission profiles, as those shown in Figure 4, that the nanoparticles are in fact growing.*

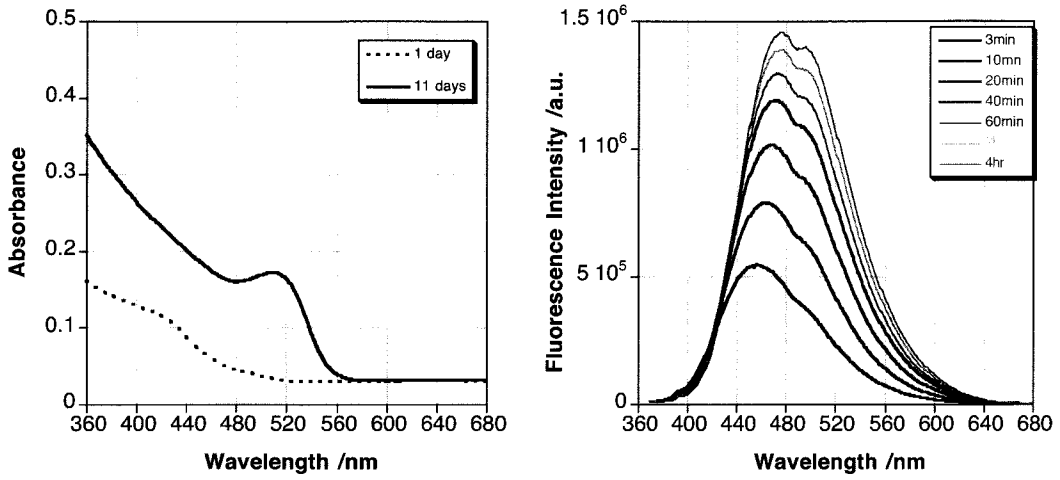

Figure 4. Absorbance [LEFT] and emission [RIGHT] spectra of CdSe nanoparticles in 0.05 M AOT/heptane (w = 4.9). Excitation wavelength is 350 nm for emission measurements.

The emission profiles above seem to show two distinct maxima. Although the double peak has yet to be fully explained by our research, it has been reported in the literature though not discussed.[22] We can suppose that they reflect two distinct distributions of reverse micelle size, due to the mixing of two reverse micelle solutions during synthesis.

The smallest fluorescent nanoparticles synthesized had an absorbance band at around 385 nm, reflecting a diameter of approximately 1.4 nm according to the literature.[20]

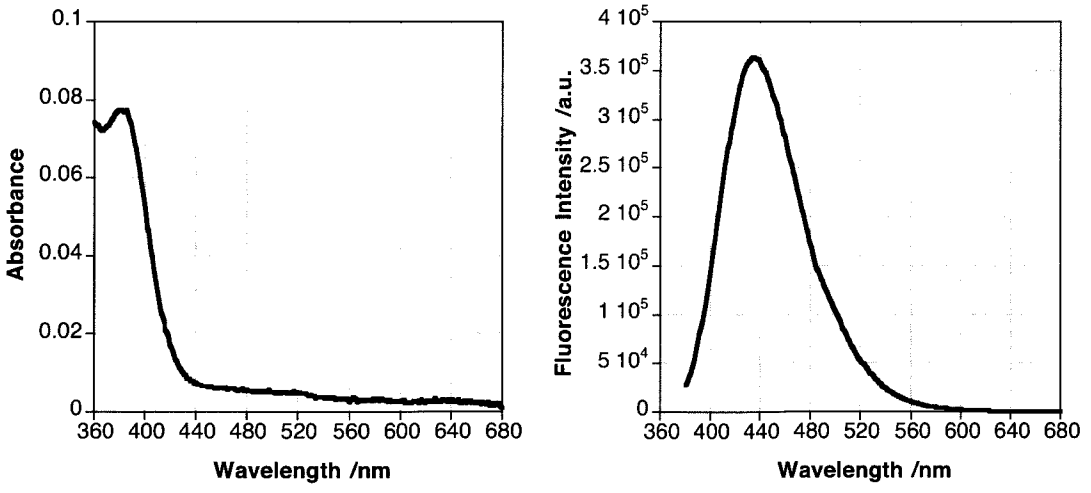

Figure 5. Absorbance [LEFT] and emission [RIGHT] spectra of smallest fluorescent CdSe nanoparticles after 24 hours of growth, in 0.05 M AOT/heptane (w = 10) reverse micelles. Excitation wavelength is 350 nm for emission measurement.

The spectroscopic properties of growing quantum dots were also monitored for longer growth times. Nanoparticles synthesized were found to persist in the reverse micelle solution for several days and these are shown in Figure 6 below.

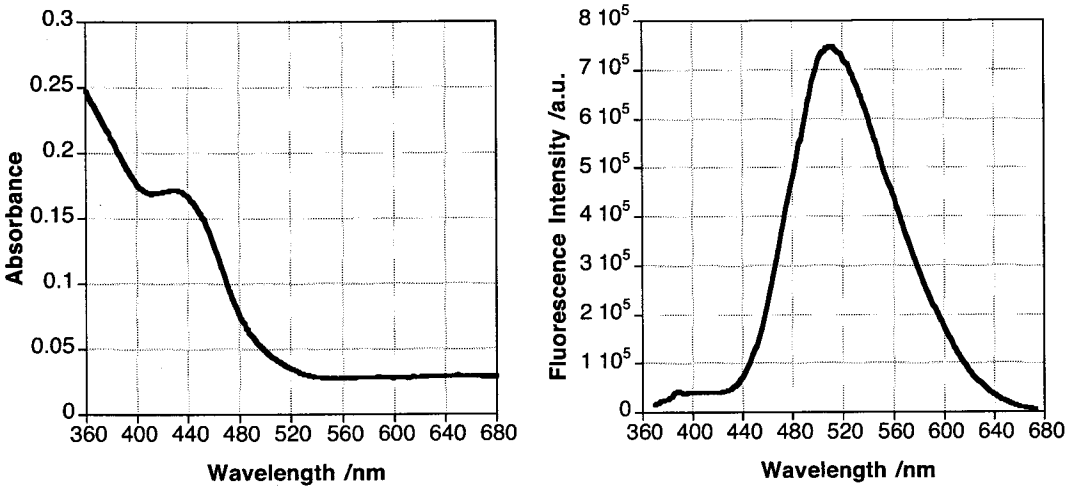

Figure 6. Absorbance [LEFT] and photoluminescence emission [RIGHT] spectra of CdSe nanoparticles in 0.05 M AOT/heptane (w = 10). Spectra taken after 10 days of growth time. Excitation wavelength is 350 nm for emission measurements.

These experiments showed luminescence increasing and red-shifting with growth time. This was found initially for all experiments, regardless of the amount of precursor, the AOT concentration or the water-to-surfactant ratio. After much longer growth times however, nanoparticles ceased to emit. The duration of luminescence was inconsistent, though the cause of nanoparticle darkening is likely coalescence of the nanoparticles. Indeed, it has been explained that most of the photogenerated charge carriers undergo recombination at the surface vacancies and therefore the smaller particles, that have a large surface-to-volume ratio, are more highly luminescent.[13] It follows that larger particles would be less luminescent.

Thus, the evolution of quantum dot emission was monitored over an extended period of growth time, to observe the increase and later decrease of emission intensity. This evolution is illustration below in two graphs, identical to one another, though shown with different perspectives.

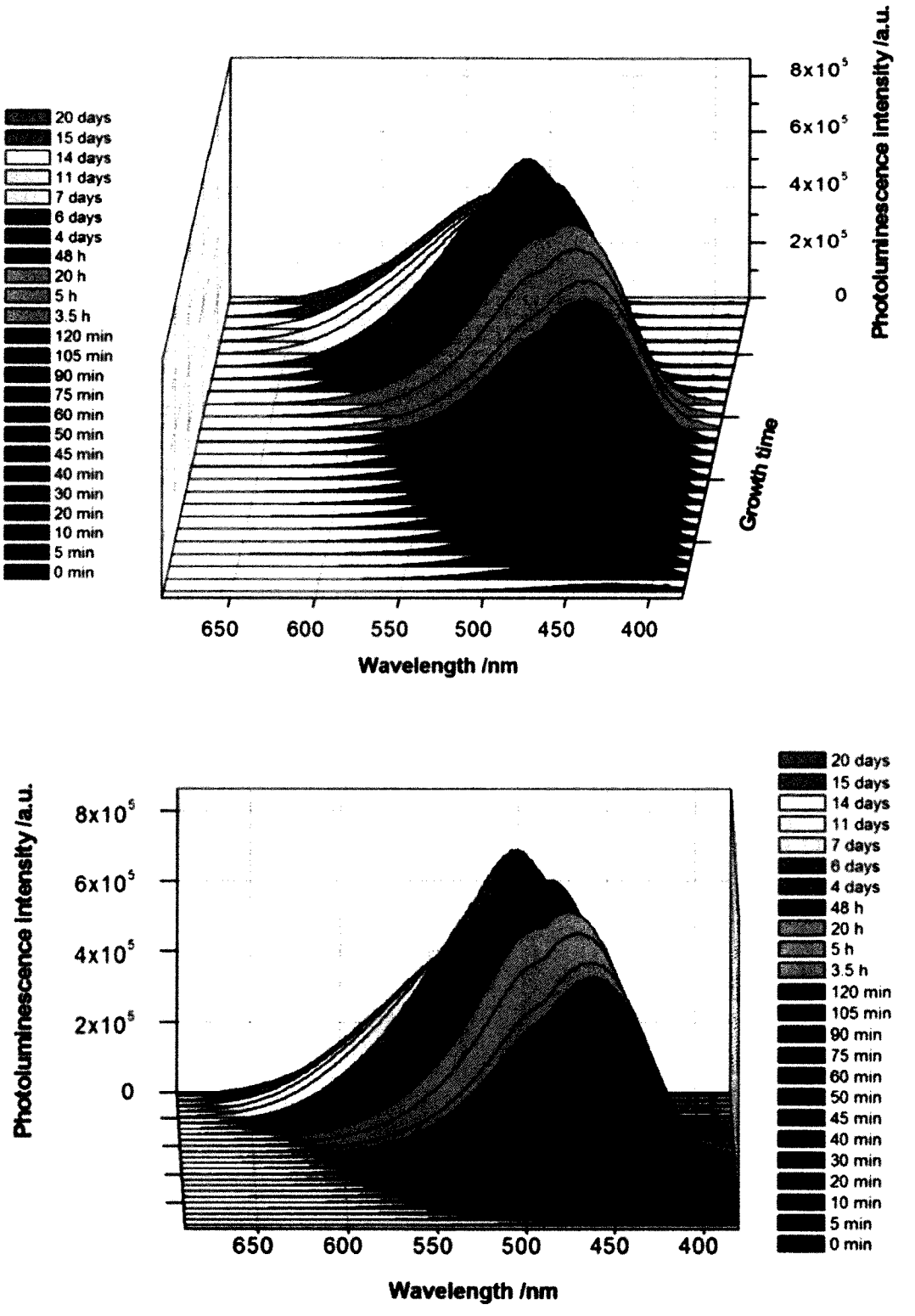

Figure 7a. Photoluminescence emission traces of CdSe nanoparticles growing in 0.1 M AOT/heptane (w = 4.9). Time after precursor mixing is shown. Both plots represent the same data, while giving two different perspectives.

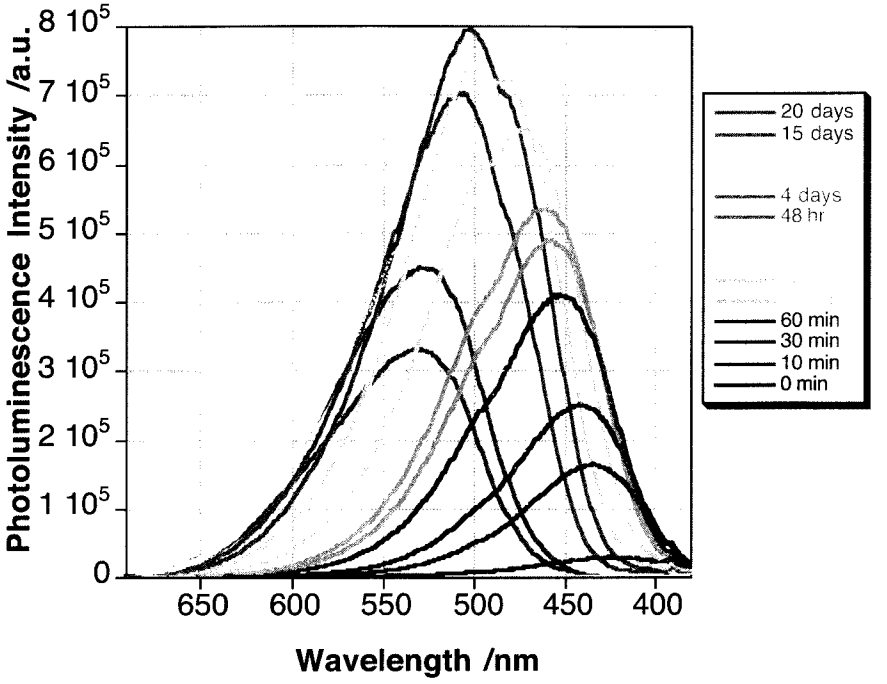

Figure 7b. Two-dimensional version of photoluminescence emission traces of CdSe nanoparticles shown in Figure 7a.

As before, we observe the red shifting emission peak due to the nanoparticle size increasing. The emission intensity, which increases initially and then decreases, is revealing. We attribute the initial increase to the formation of small QDs until depletion of ionic reactants, where the maximum emission is reached. After this point, the smaller dots coalesce to form fewer, larger QDs. The particles continue to merge until their emission is no longer detectable, though absorbance measurements indicate that particles are still present in solution as large clusters. As previously mentioned, it is expected that the smaller particles are more highly luminescent.[13]

The photoluminescence intensity of these synthesized quantum dots is excellent, of the same order of magnitude as commercial dots. Nevertheless, we attempted to further increase the emission yield. Light irradiation of the quantum dots is believed to affect their luminescence.[23-25] *QD solutions were therefore irradiated in reverse micelles with visible light in a photoreactor (28.8 W/m^2 for up to 3 hours) and exposed to direct sunlight for up to 5 days, with no significant change in emission intensity. Triethylamine has also been shown to enhance photoluminescence,*[13] *but concentrations up to 3 mM did not have any effect on the luminescence of these quantum dots.*

i. Effect of the water-to-surfactant (w) ratio

Reverse micelles are a powerful tool to prepare nanoparticles and control their size, acting as nanoreactors for the synthesis of Pd, Pt, CdS and CdSe to name a few.[26-29] *If the reverse micelle acts as a cage confining the quantum dots' growth, the size of this cage should influence the size of the final quantum dot formed. Therefore, by varying the w ratio and consequently changing the water pool size, the nanoparticle size could be controlled.*

This size control was observed and is illustrated in Figure 8, which shows the absorbance and emission spectra of nanoparticles formed in reverse micelles with w-ratios of 1.0 (smaller) and 4.9 (larger). To compare results, the precursor concentration inside nanoreactors was kept constant and the nanoreactor size (w-ratio) was varied. This implies though, that the amount of precursor present in the solution with a higher water-to-surfactant ratio is larger.

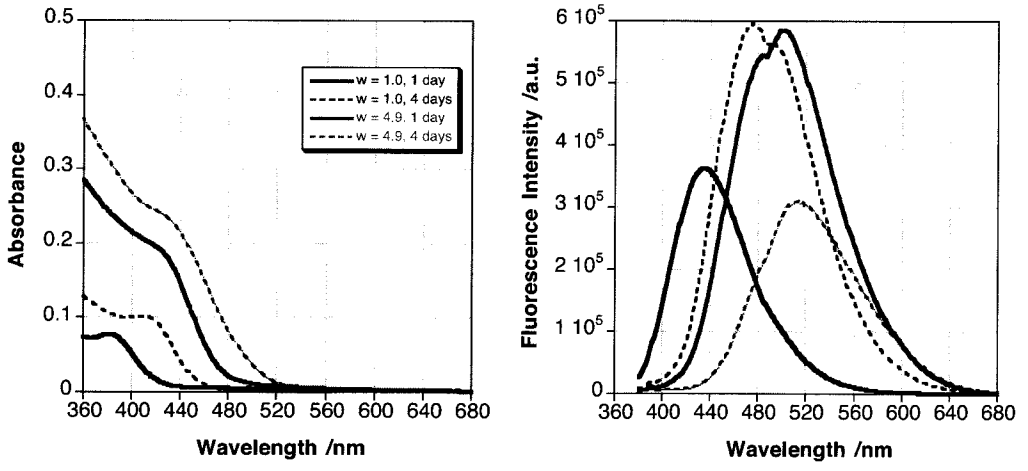

Figure 8. Absorbance [LEFT] and photoluminescence emission [RIGHT] spectra of CdSe nanoparticles in 0.5 M AOT/heptane with varied water-to-surfactant ratios. Measurements were taken after 1 and 4 days of growth time.

As expected, the absorbance and emission peaks red shift as the nanoparticles grow. The intensity increase with higher w-ratios observed in both plots is indicative of a more concentrated solution of nanoparticles. This can easily be explained by the simple fact that the higher w-ratio solution ($QD_{4.9}$) contained a greater amount of precursor, likely leading to a greater number of nanoparticles.

Furthermore it was found that although nanoparticles were formed more quickly in larger water pools, their emission decreased quickly as well. Indeed, after 4 days, the emission of $QD_{4.9}$ decreased to half the emission intensity of $QD_{1.0}$. This could be due to greater coalescence within a large nanoreactor, that might contain a higher number of nanoparticles. On the other hand, the surfactant can protect the nanoparticles contained in small nanoreactors from agglomeration with nanoparticles in adjacent nanoreactors.

Interestingly, the emission intensity of the nanoparticle solution reaches a maximum when the emission peak is around 490 nm. This would agree with our previous statements if this point represents the depletion of ionic precursors.

ii. Effect of surfactant concentration

Our results indicate that higher AOT concentrations produce more highly luminescent solutions. This observation is true even when probed at various growth times, as shown in Figure 9 below.

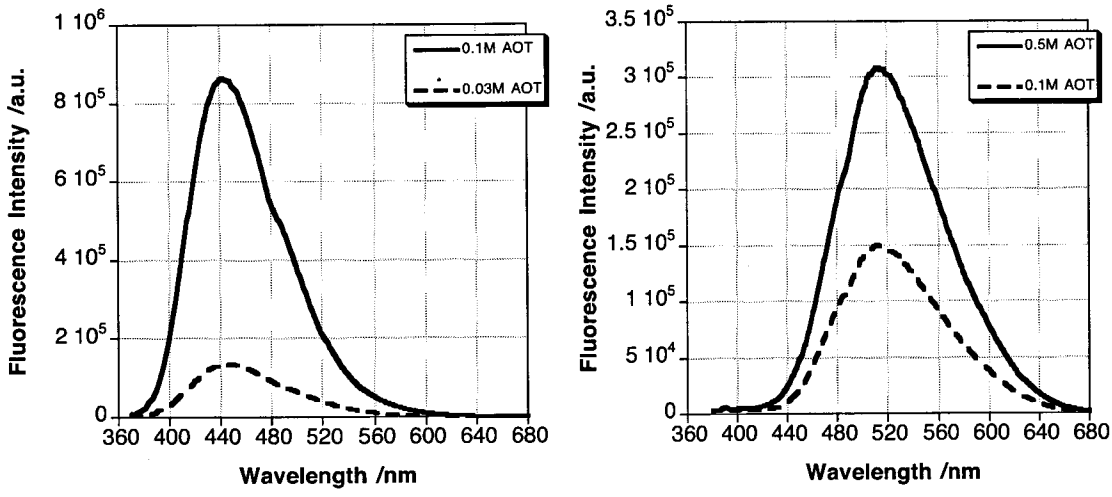

Figure 9. Photoluminescence emission of quantum dot solutions in heptane/AOT/H_2O systems, with w = 4.9 and varying AOT concentrations. Spectra taken 3 hours [LEFT] and 4 days [RIGHT] after mixing of reactant solutions.

In these experiments, the water-to-surfactant ratio was maintained at a constant value of 4.9, while the AOT concentration was varied. It is important to mention that the reactant solution concentration was not altered, though the total volume of reactant increased with increasing w-ratio, which signifies that the overall

concentration of reactant in the observed volume also increased. A clear trend of increasing emission intensity with increasing AOT concentration was observed. This finding, for equal w ratios, is not surprising. Indeed, higher surfactant concentrations will lead to more nanoreactors, which we presume would produce a higher number of nanoparticles. The quantity of precursors is proportionally increased with the w-ratio which would allow for such an increase in the number of nanoparticles produced. It is therefore not the particles that have higher individual emission, but rather the number of nanoparticles emitting that is increased.

It is probable that even higher AOT concentrations would produce still more nanoparticles, but these systems were avoided in order to make future surfactant removal easier.

Photoluminescence Lifetime Measurements

The photoluminescence lifetime was measured as the nanoparticles were growing in the reverse micelle system. The growth time, and likely the nanoparticle size, were found to affect the measured lifetime distributions.

Indeed, the photoluminescence decay time increases with quantum dot growth time. This behaviour is shown in Figure 10 below.

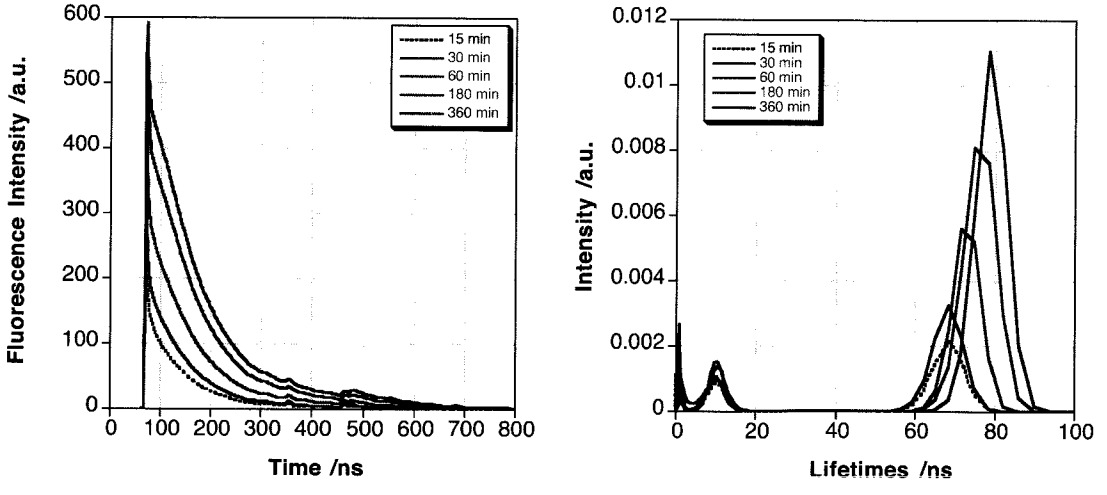

Figure 10. Photoluminescence decay traces [LEFT] and lifetime distributions [RIGHT] of CdSe nanoparticles growing in 0.1 M AOT/heptane (w = 4.9). Time after precursor mixing is shown. 375 nm longpass filter used to avoid diode excitation light (350 nm) reaching the detector.

The decay lifetimes were fit with the Exponential Series Method (ESM) decay function by the Felix software and this analysis led to the lifetime distributions shown in the right plot of Figure 10. ESM is designed to fit lifetime distributions without initial assumptions about their shapes. This method uses a series of exponentials (up to 200 terms) as a probe function with fixed lifetimes and variable pre-exponentials.[30]

The distributions obtained indicate that there are three lifetime components. The first and second components (1 and 10 ns) are quite short and remain unchanged for the growth period monitored.[‡] *On the other hand, the longer component becomes longer as growth time is increased. For the longer component, the average decay lifetime was found to increase from 70 to 80 ns within the first 5 hours of nanoparticle growth. This behaviour was found for other samples studied, though only the trend was consistent rather than the exact values. Indeed, while the lifetimes obtained and their absolute weights varied from day-to-day, the longest lifetime component increased with growth time and the shorter component remained constant, as is shown in Figure 11.*

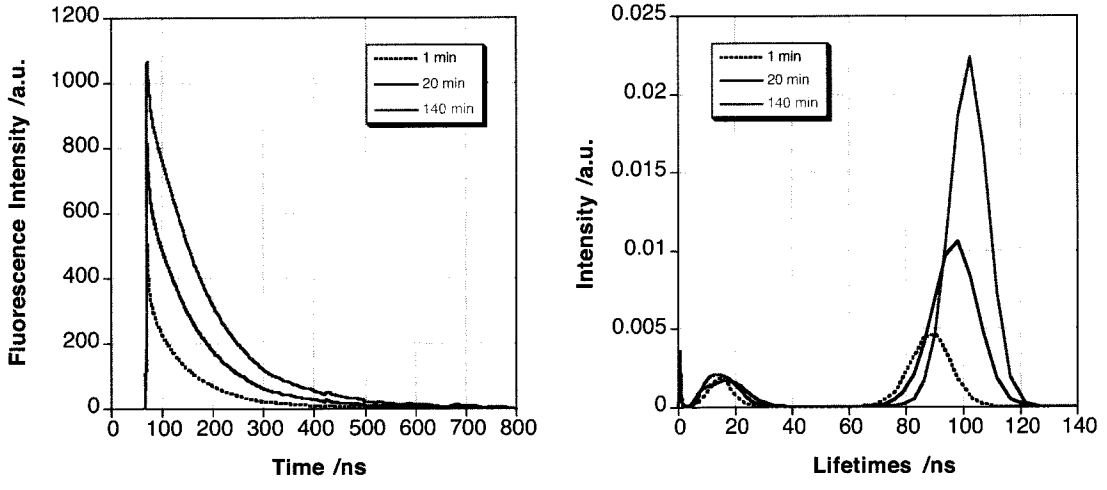

Figure 11. Photoluminescence decay traces [LEFT] and lifetime distributions [RIGHT] of CdSe nanoparticles growing in 0.1 M AOT/heptane (w = 4.9). Time after precursor mixing is shown. 375 nm longpass filter used to avoid diode excitation light (350 nm) reaching the detector.

[‡] The very short and modest lifetime component of 1 ns is likely an artefact, caused by diode generated light.

Surface defects, mostly associated with surface vacancies (such as surface nonstoichiometry and dangling bonds), are known to decrease the emission lifetime and luminescence properties due to the recombination of charge carriers at these defect sites.[31, 32] *Hence, the increase in lifetime observed might be a reflection of surface defect reduction due to nanoparticle ripening.*

Surface Derivatization

It is known that surface derivatization is helpful in stabilizing QDs,[33] *raising their quantum yields and generally improving their luminescence properties.*[34] *Surface passivation essentially removes local trap (defect) sites from the surface thus enhancing radiative recombination of photogenerated charge carriers.*[35]

CdSe nanoparticles have traditionally been coated with a with a large bandgap semiconductor shell such as ZnS.[13] *Indeed, the use of materials with a higher band gap prevents defect sites from competing with the radiative recombination of the exciton, thus enhancing the yield of the excitonic emission.*[36] *Capping of other nanoparticles has been achieved notably by thiols and amines for CdS NPs*[37, 38] *as well as phosphines and dendrimers for Pd NPs.*[27]

We found that the photoluminescence of nanoparticles synthesized in reverse micelles persisted even after several weeks, and it is believed that the surfactant is acting as a stabilizer in this system. This behaviour has been reported by Harruff et al. who found surface passivation by AOT of CdS QDs,[35] *as well as Xu et al. in the case of CdSe.*[34] *Nevertheless it is useful to protect the QD surface with other capping agents, in order to eventually remove the surfactant from the system. The use of mercapto acids has been an important landmark in synthesizing CdSe quantum dots.*[22, 39, 40] *In this project, 3-mercapto-1-propane sulphonic acid (MPSA) was successfully employed as a capping agent.*

A reverse micellar vehicle was used to introduce the MPSA to the growing nanoparticle system. Indeed, similarly to the cadmium and selenium precursors, 100 μL of an aqueous solution of the capping agent (0.2 M) was added to 10 mL of the AOT/heptane mixture (0.05 M) which led to a MPSA-containing reverse micelle system (w = 10). Various volumes of reverse micellar MPSA were added to a 10-day

aged solution of QDs in reverse micelles. The capping agent caused an immediate photoluminescence enhancement, which continued for a period of at least one year. The addition of MPSA also successfully restricted nanoparticle growth and protected them significantly against flocculation.

Any close association of particles, such as aggregates and agglomerates, can be defined as a floc and flocculation as the process of forming them.[41] Although aggregation is usually thought of as a close, irreversible association and agglomeration as a loose, reversible association of particles, the term flocculation can be generically used to describe the "instability of colloids".[42] Precipitation commonly follows flocculation, which was found to be irreversible for some nanoparticles synthesized with this method. Flocculation should be avoided as it decreases the stability of the nanoparticle solution and alters the size of nanoparticles which is so fundamental to their properties, as previously explained. While surface passivation does provide luminescence enhancement via defect state trapping, nanoparticle coatings can also prevent flocculation and eventual precipitation.[38]

We show the most successful passivation trial below, achieved with a 100 μL addition of 0.2M MPSA-containing reverse micelles (0.05M AOT/heptane, w = 10) to a 3 mL sample.

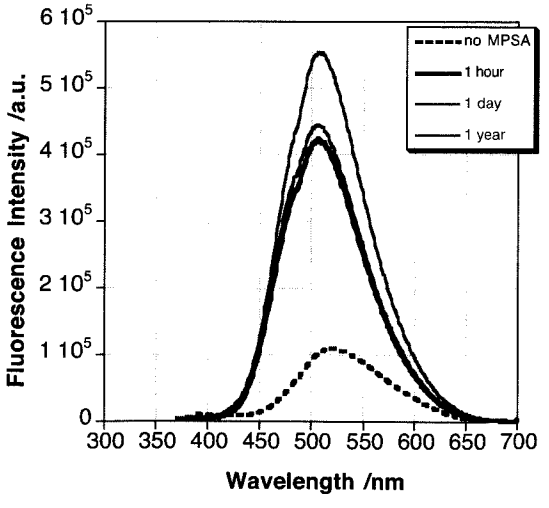

Figure 12. CdSe QDs synthesized in reverse micelle solution modified with 3-mercapto-1-propane sulphonic acid. After 10-day aging period, 100 μL of 0.2M MPSA-containing reverse micelles (0.05M AOT/heptane, w = 10) was injected to a 3 mL quantum dot solution. Time after MPSA addition is shown.

Other volume additions also lengthened the quantum dot luminescence to a period of years, but appeared to allow more flocculation as reflected by red-shifting of emission peak and broadening of the signal. For instance, QDs modified with 500 μL of MPSA-containing reverse micelles have a significantly red-shifted emission, as the photograph below illustrates.

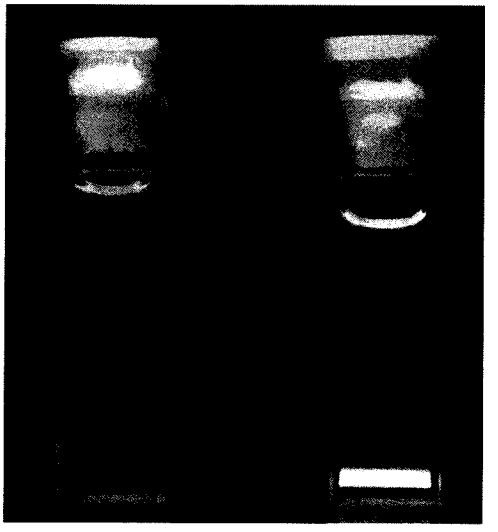

Figure 13. MPSA-modified CdSe quantum dot photoluminescence (shortwave compact UV lamp excitation). QDs in reverse micelle solution (0.05 M AOT/heptane, w = 10) with 100 μL [LEFT] and 500 μL [RIGHT] of 0.2M MPSA-containing reverse micelles, injected to 3 mL solution of growing CdSe nanoparticles. Photograph taken two years after synthesis.

Nevertheless, the nanoparticles were found to be highly robust and luminescent after extended periods of time as shown in Figure 13, a photograph taken two years after synthesis. No special precautions were taken to conserve the quantum dots as these were left in a capped cuvette at ambient conditions. Even after complete evaporation of the solvent, the nanoparticle-containing AOT was redissolved in heptane, thereby recovering the nanoparticle luminescence.

Surfactant Removal

To fully take advantage of the synthesized QDs, it would be useful to remove the surfactant that is used in synthesis. It has been reported that ethanol is a successful candidate for AOT precipitation and removal.[27, 38, 43, 44]

Ethanol was therefore added dropwise while stirring to a 7-day aged solution of quantum dots in reverse micelles, until the solution turned turbid. Stirring was ceased and the phases were allowed to separate for approximately 30 minutes. The heptane phase contained QDs and these were highly fluorescent. The absorbance and emission spectra of this phase are shown below. The emission of the quantum dot solution before AOT removal is shown for comparison, but has been normalized to match emission intensity at 505 nm. The actual emission intensity of the nanoparticles in heptane was approximately twice that of the solution with AOT present which could be caused by AOT acting as an inner filter.

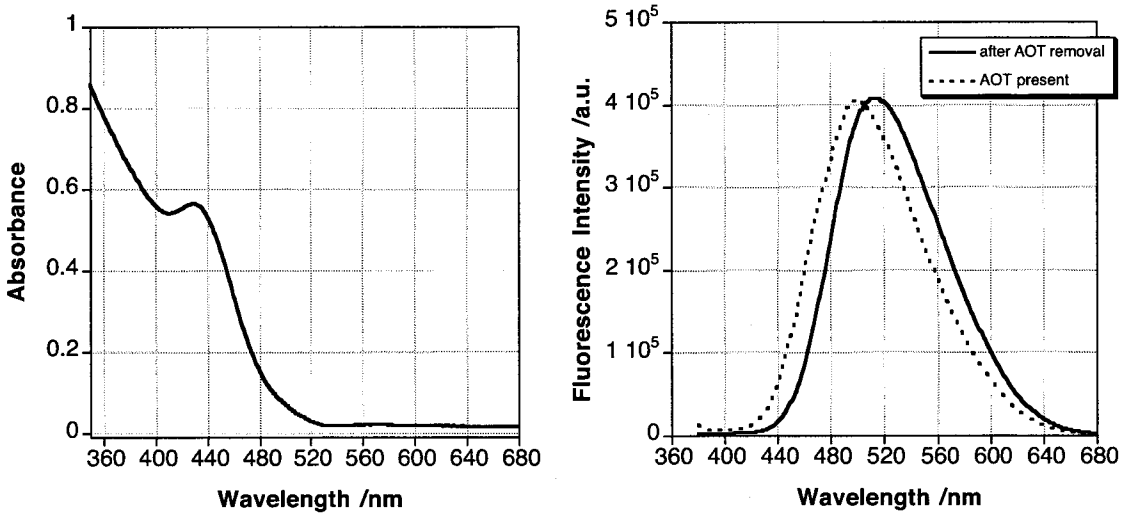

Figure 14. Absorbance [LEFT] and normalized photoluminescence emission [RIGHT] spectra of CdSe QDs synthesized in reverse micelle solution (0.1 M AOT, w = 4.9) and extracted from the surfactant using ethanol precipitation after 7-day aging period.

Ethanol precipitation seems to slightly red-shift the emission and absorbance (not shown) spectra. This can be explained by nanoparticle growth following the removal of the surfactant, which acts as a stabilizer and protecting agent by impeding nanoparticle coalescence.

CONCLUSION

The nanoconstruction of quantum dots is a highly versatile process leading to diverse end-products that have controllable properties depending on size, shape and functionalization, making nanoparticles ideal building blocks for nanotechnology.[45] Indeed, nanoparticles possess an array of unique properties associated with their core materials, including distinct magnetic, photonic and electronic behavior.[45]

For instance, while many organic molecules also fluoresce, quantum dots have special characteristics that make them interesting candidates for a wide range of applications, notably as labels and markers in life sciences.[46] Indeed, the emission color can be readily tailored to the demands of the application simply by changing the nanoparticle size. Furthermore, the emission is narrow which allows the use of several distinguishable labels within a particular sample. In this case, the broad absorbance profile of quantum dots also becomes useful as a single excitation wavelength will effectively cause all markers to emit. It is noteworthy that quantum dots are not as susceptible to photobleaching as organic fluorophores, which means that their emission does not fade after exposure to excitation light.

Thus, a detailed method by which CdSe quantum dots are readily synthesized in water at room temperature using reverse micelles was presented here. This synthetic path made possible the synthesis of highly luminescent yet very small, "blue" quantum dots. The growth of the quantum dots was monitored in real time by tracking their photoluminescence and absorbance. The photoluminescence decay lifetime of the quantum dot solution was also measured. The reaction was successfully stopped by capping with MPSA, which rendered synthesized quantum dots highly luminescent and stable for more than a year. Furthermore, the quantum dots were successfully extracted from the reverse micelle system by ethanol precipitation of the surfactant.

The synthesis of TOPO capped dots, which are formed at very high temperatures, is still the most reliable method to obtain monodisperse nanoparticles. Nevertheless, the method proposed here could be acceptable for some applications that require

room temperature synthesis for instance. Using this method, we have shown size control both with nanoreactor confinement and a capping agent. Furthermore, the lifetime of the quantum dots was measured and studied which led to the observation that the quantum dot luminescence decay was comprised of likely two components, the longer one of which increased as the quantum dots grew larger. This, to our knowledge, has not yet been studied or reported for CdSe quantum dots synthesized at room temperature under air, in an aqueous environment.

It should be highlighted that CdSe nanoparticles having stoichiometric Cd:Se composition were reported to be more stable against oxidation and exhibited less signs of abundant surface defects, while Cd-rich nanoparticles such as the ones synthesized herein showed significant emission broadening and surface trap sites.[47] *Future work might include a decrease of the cadmium precursor concentration to assess the impact on luminescence intensity of the synthesized nanoparticles.*

REFERENCES

1. Rossetti, R.; Nakahara, S.; Brus, L. E., Quantum Size Effects in the Redox Potentials, Resonance Raman Spectra, and Electronic Spectra of of CdS Crystallites in Aqueous Solutions. Journal of Chemical Physics **1983**, 79, 1086 - 1088.

2. Capek, R.; Lambert, K.; Dorfs, D.; Smet, P.; Poelman, D.; Eychmuller, A.; Hens, Z., Synthesis of Extremely Small CdSe and Bright Blue Luminescent CdSe/ZnS Nanoparticles by a Prefocused Hot-Injection Approach. Chemistry of Materials **2009**, 21, (8), 1743-1749.

3. Woll, A. R.; Rugheimer, P.; Lagally, M. G., Self-Organized Quantum Dots. International Journal of High Speed Electronics and Systems **2002**, 12, (1), 45 - 78.

4. Fisher, B. R.; Eisler, H.; Stott, N. E.; Bawendi, M. G., Emission Intensity Dependence and Single-Exponential Behavior In Single Colloidal Quantum Dot Fluorescence Lifetimes. Journal of Physical Chemistry B. **2004**, 108, 143 - 148.

5. Brus, L. E., Electron-electron and Electron-hole Interactions in Small Semiconductor Crystallites: The Size Dependence of the Lowest Excited State. Journal of Chemical Physics **1984**, 80, 4403 - 4409.

6. Alivisatos, A. P., Semiconductor Clusters, Nanocrystals and Quantum Dots. Science **1996**, 271, (5251), 933 - 937.

7. Alivisatos, A. P., Colloidal Quantum Dots. From Scaling Laws to Biological Applications. Pure Applied Chemistry **2000**, 72, 3 - 9.

8. Skaff, H.; Emrick, T., Semiconductor Nanoparticles: Synthesis, Properties, and Integration Into Polymers for the Generation of Novel Composite Materials. In Nanoparticles - Building Blocks for Nanotechnology, Rotello, V., Ed. Kluwer Academic/Plenum Publishers: New York, 2004.

9. El-Sayed, M. A., Small is Different: Shape-, Size-, and Composition-Dependent Properties of Some Colloidal Semiconductor Nanocrystals. Accounts of Chemical Research **2004**, 37, 326 - 333.

10. Zhou, X.; Shao, Z.; Kobayashi, Y.; Wang, X.; Ohuchi, N.; Taketa, M.; Kasuya, A., Photoluminescence of CdSe and CdSe/CdO nH20 Core/Shell Nanoparticles Prepared in Aqueous Solution. Optical Materials **2007**, 29, 1048 - 1054.

11. Murray, C. B.; Norris, D. J.; Bawendi, M. G., Synthesis and Characterization of Nearly Monodisperse CdE (E = S, Se, Te) Semiconductor Nanocrystallites. Journal of the American Chemical Society **1993**, 115, 8706 - 8715.

12. Peng, Z. A.; Peng, X., Formation of High-quality CdTe, CdSe, and CdS Nanocrystals Using CdO as Precursor. Journal of the American Chemical Society **2001**, 123, 183 - 184.

13. Chandrasekharan, N.; Kamat, P. V., Tuning the Properties of CdSe Nanoparticles in Reverse Micelles. Research on Chemical Intermediates **2002**, 28, (7-9), 847 - 856.

14. Steigerwald, M. L.; Alivisatos, A. P.; Gibson, J. M.; Harris, T. D.; Kortan, R.; Muller, A. J.; Thayer, A. M.; Duncan, T. M.; Douglass, D. C.; Brus, L. E., Surface derivatization and isolation of semiconductor cluster molecules. Journal of the American Chemical Society **1988**, 110, 3046 - 3050.

15. Holmberg, K., Surfactant-templated Nanomaterials Synthesis. Journal of Colloid and Interface Science **2004**, 274, 355 - 364.

16. Pileni, M. P.; Zemb, T.; Petit, C., Solubilization by Reverse Micelles: Solute Localization and Structure Perturbation. Chemical Physics Letters **1985**, 118(4), 414-420.

17. Yang, Y.; Xiang, B., Wet Synthesis of Nearly Monodisperse CdSe Nanoparticles at Room Temperature. Journal of Crystal Growth **2005**, 284, (3-4), 453-458.

18. Peng, Z. A.; Peng, X., Nearly Monodisperse and Shape-controlled CdSe Nanocrystals via Alternative Routes. Science **2001**, 124, 3343 – 3353, and Mechanisms of the Shape Evolution of CdSe Nanocrystals. Journal of the American Chemical Society **2001**, 123, 1389 - 1395.

19. Yochelis, S.; Hodes, G., Nanocrystalline CdSe Formation by Direct Reaction between Cd Ions and Selenosulfate Solution. Chemical Materials **2004**, *16,* 2740-2744.

20. Yu, W. W.; Qu, L.; Guo, W.; Peng, X., Experimental Determination of the Extinction Coefficient of CdTe, CdSe, and CdS Nanocrystals. Chemical Materials **2003**, 15, 2854 - 2860.

21. Burda, C.; Chen, X.; Narayanan, R.; El-Sayed, M. A., Chemistry and Properties of Nanocrystals of Different Shapes. Chemical Reviews **2005**, 105, 1025 - 1102.

22. Chen, X.; Hutchison, J. L.; Dobson, P. J.; Wakefield, G., A One-step Aqueous Synthetic Route to Extremely Small CdSe Nanoparticles. Journal of Colloid and Interface Science 2008, 319, 140 - 143.

23. Zhelev, Z.; Jose, R.; Nagase, T.; Ohba, H.; Bakalova, R.; Ishikawa, M.; Baba, Y., Enhancement of the Photoluminescence of CdSe Quantum Dots During Long-term UV-irradiation: Privilege or Fault in Life Science Research? Journal of Photochemistry and Photobiology B. **2004**, 75, (1-2), 99-105.

24. Jin, W.; Costafernandez, J.; Pereiro, R.; Sanzmedel, A., Surface-modified CdSe Quantum Dots as Luminescent Probes for Cyanide Determination. Analytica Chimica Acta **2004**, 522, (1), 1-8.

25. Jones, M.; Nedeljkovic, J.; Ellingson, R. J.; Nozik, A. J.; Rumbles, G., Photoenhancement of Luminescence in Colloidal CdSe Quantum Dot Solutions. Journal of Physical Chemistry B. **2003**, 107, 11346 - 11352.

26. Lisiecki, I., Size control of spherical metallic nanocrystals. Colloids and Surfaces A: Physicochemical and Engineering Aspects **2004**, 250, (1-3), 499-507.

27. Chen, M.; Feng, Y.; Wang, L.; Zhang, L.; Zhang, J.-Y., Study of Palladium Nanoparticles Prepared From Water-in-Oil Microemulsion. Colloids and Surfaces A. **2006**, 281, 119 - 124.

28. Chen, D.-H.; Yeh, J.-J.; Huang, T.-C., Synthesis of Platinum Ultrafine Particles in AOT Reverse Micelles. Journal of Colloid and Interface Science **1999**, 215, 159 - 166.

29. Cao, L.; Huang, S.; Shulin, E., ZnS/CdS/ZnS Quantum Dot Quantum Well Produced in Inverted Micelles. Journal of Colloid and Interface Science **2004**, 273, 478 - 482.

30. Breton, G. W.; Vang, X., Photodimerization of Anthracene: A (4p + 4p) photochemical cycloaddition. Journal of Chemical Education **1998**, 75, (1), 2.

31. Cordero, S. R.; Carson, P. J.; Estabrook, R. A.; Strouse, G. F.; Buratto, S. K., Photo-activated Luminescence of CdSe Quantum Dot Monolayers. Journal of Physical Chemistry B. **2000**, 104, 12137 - 12142.

32. Talapin, D. V.; Rogach, A. L.; Shevchenko, E. V.; Kornowski, A.; Haase, M.; Weller, H., Dynamic Distribution of Growth Rates within the Ensembles of Colloidal II-VI and III-V Semiconductor Nanocrystals as a Factor Governing Their Photoluminescence Efficiency. Journal of the American Chemical Society **2002**, 124, 5782 - 5790.

33. Li, J. H.; Ren, C. L.; Liu, X. Y.; Hu, Z. D.; Xue, D. S., "Green" Synthesis of Starch Capped CdSe Nanoparticles at Room Temperature. Materials Science & Engineering **2007**, 458, 319 - 322.

34. Xu, L.; Chen, K.; El-Khair, H. M.; Li, M.; Huang, X., Enhancement of Band-edge Luminescence and Photo-stability in Colloidal CdSe Quantum Dots by Various Surface Passivation Technologies. Applied Surface Science **2001**, 172, 84 - 88.

35. Harruff, B. A.; Bunker, C. E., Spectral Properties of AOT-protected CdS Nanoparticles: Quantum Yield Enhancement by Photolysis. Langmuir **2003**, 19, 893 - 897.

36. Zhou, X.; Kobayashi, Y.; Ohuchi, N.; Taketa, M.; Kasuya, A., Strong Luminescencing CdSe Nanoparticles by Surface Modification with Cadmium (II) Hydrous Oxide. International Journal of Modern Physics B. **2005**, 19, 2835 - 2840.

37. Wuister, S. F.; De Mello Donega , C.; Meijerink, A., Influence of Thiol Capping on the Exciton Luminescence and Decay Kinetics of CdTe and CdSe Quantum Dots. Journal of Physical Chemistry B. **2004**, 108, 17393 - 17397.

38. Caponetti, E.; Pedone, L.; Martino Chillura, D.; Panto, V.; Turco Liveri, V., Synthesis, Size Control and Passivation of CdS Nanoparticles in Water/AOT/n-heptane Microemulsions. Materials Science & Engineering C. **2003**, 23, 531 - 539.

39. Gaponik, N.; Talapin, D. V.; Rogach, A. L.; Hoppe, K.; Shevchenko, E. V.; Kornowski, A.; Eychmuller, A.; Weller, H., Thiol-Capping of CdTe Nanocrystals: An Alternative to Organometallic Synthetic Routes. Journal of Physical Chemistry B. **2002**, 106, 7177 - 7185.

40. Rogach, A. L.; Kornowski, A.; Gao, M.; Eychmuller, A.; Weller, H., Synthesis and Characterization of a Size Series of Extremely Small Thiol-Stabilized CdSe Nanocrystals. Journal of Physical Chemistry B. **1999**, 103, 3065 - 3069.

41. Ross, S.; Morrison, I. D., Colloidal Systems and Interfaces. John Wiley and Sons: New York, 1988.

42. Weisbecker, C. S.; Merritt, M. V.; Whitesides, G. M., Molecular Self-Assembly of Aliphatic Thiols on Gold Colloids. Langmuir **1996**, 12, 3763 - 3772.

43. Agostiano, A.; Catalano, M.; Curri, M. L.; Della Monica, M.; Manna, L.; Vasanelli, L., Synthesis and Structural Characterisation of CdS Nanoparticles Prepared in a Four-components "Water-in-Oil" Microemulsion. Micron **2000**, 31, 253 - 258.

44. Pileni, M. P., II-VI semiconductors made by soft chemistry: Synthesis and optical properties. Catalysis Today **2000**, 58, 151 - 166.

45. Rotello, V. M., Nanoparticles - Building Blocks of Nanotechnology. Kluwer Academic/Plenum Publishers: New York, 2004.

46. Whitesides, G.; Love, J., The Art of Building Small. Scientific American **2001**, 285, (3), 39 - 47.

47. Sharma, H.; Sharma, S. N.; Singh, G., Effect of Oxidation Induced Surface State Formation on the Properties of Colloidal CdSe .... Journal of Nanoscience and Nanotechnology **2007**, 7, (6), 1953 - 1959.

CHAPTER 3

A PROMISING WINDOW FOR NANOLITHOGRAPHY – PHOTOREVERSIBLE CYCLOADDITION

A PROMISING WINDOW FOR NANOLITHOGRAPHY – PHOTOREVERSIBLE CYCLOADDITION

The needs of the computer industry have generated much interest in a variety of approaches for creating increasingly smaller devices. Integrated circuit manufacturing, currently based on the top-down approach, is experiencing a surge of difficulties as the size of the components establish themselves in the nanometer scale.[1] As the demand for faster and more powerful computer processors increases, new strategies are being developed to improve lithographic resolution. Nanolithography has become a field of ingenious innovations and fast advances in the race brought on by Moore's Law.[2, 3]

The physical limits that govern optical photolithography techniques have rendered the steady reduction in lithographic features a difficult task. To dodge these limitations, the industry has been forced to play complex tricks in order to fabricate lithographic features with sizes that follow Moore's Law. For instance, water immersion lithography has notably offered a larger numerical aperture (maximum achievable NA ~ 1.35) which opened the door to lithography beyond the 45 nm half-pitch node.[4]

Current photolithography techniques could also achieve smaller half pitch critical dimensions by reducing the lithographic wavelength using electron beams or x-rays in nanofabrication. Electron beams however are costly and slow, while X-rays can too easily damage the equipment used in the chip making process.[5, 6] Extreme ultraviolet light (EUV, 13.4 nm) has also been proposed as a lithographic wavelength,[7] but will likely not be viable before 2013.[8]

Thus, using the lithographic wavelengths currently available, masks with increasingly high feature densities are becoming difficult to resolve in imaging processes. Having said that, a single high feature density mask can be divided in two complementary masks, each having a lower feature density, but replicating the original mask when sequentially exposed. Two approaches open way to this double mask method: double-exposure and double-patterning, shown below in Figure 15.

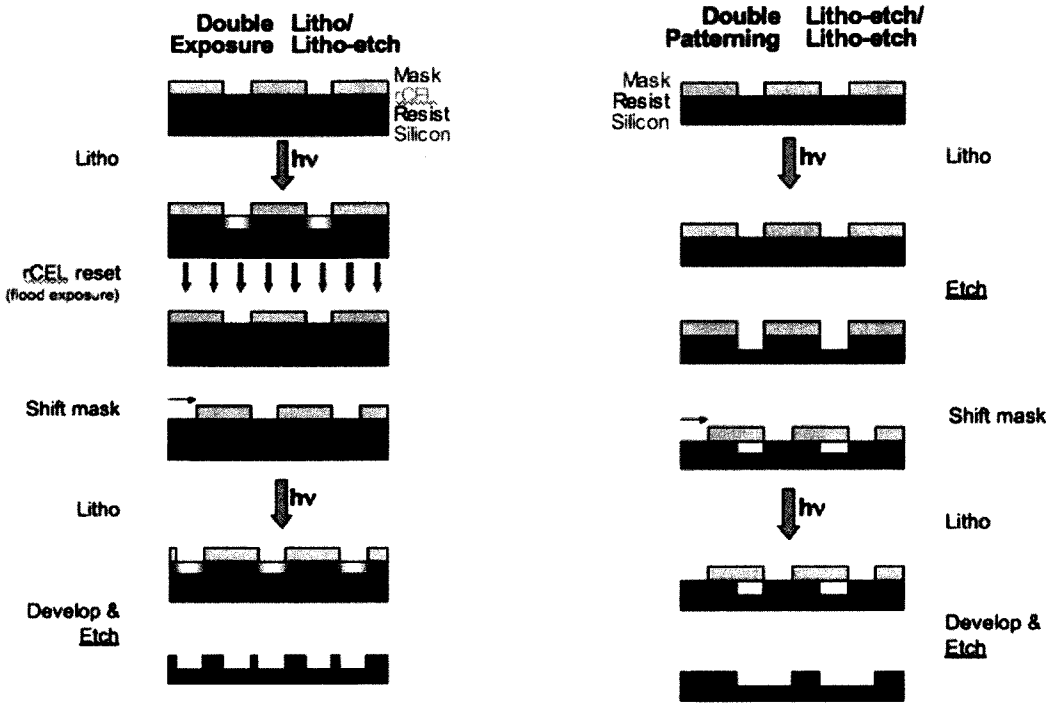

Figure 15. Comparative scheme of double-exposure and double-patterning (with development and etch steps shown).[8] This scheme also shows the utility of a reversible contrast enhancement layer (rCEL), which will be discussed further.

While double-patterning requires the development of the resist between passes and therefore also the removal of the substrate (silicon wafer) from the exposure tool, double-exposure is based on the use of staggered exposures and can be performed sequentially without moving the wafer. Although both methods are viable for implementation in current lithographic facilities, double-exposure offers the advantage of faster throughput by avoiding the intermediate development step.[8] Generally, the overall reduced costs of double-exposure lithography suggests that the industry would preferentially implement it rather than double-patterning.[9]

The double-exposure method could in principle be deployed directly in today's exposure tools and lithographic facilities.[9] However, an implementation roadblock is encountered with current resists which possess a "memory effect".[8] The memory effect is significant for double-exposure methods because it essentially blurs the features that are imaged sequentially. This is due to sub-threshold exposure in the first pass reducing the exposure dose required in the second pass to cause an

unwanted chemical change (usually a solubility switch) in the resist. In other words, an area that is meant to be unexposed (dark) will absorb sufficient irradiation and undergo the solubility switch. Such behavior occurs in linear response resist materials, as the exposure doses are directly additive. This can be derived mathematically, as shown below, using the normalized aerial image intensity (I) defined by Equation 3:

$$I = A\cos^2\left(\frac{\pi x}{pitch}\right) + B$$

Equation 3.

where A is a constant describing the amplitude and B is the minimum.[8] At the pitch limit of the exposure tool, the waves of the sequential exposures are 180° out of phase. If Equation 3 represents the first exposure pass, then the second exposure pass would be described by Equation 4:

$$I = A\sin^2\left(\frac{\pi x}{pitch}\right) + B$$

Equation 4.

The photochemical response of a linear resist results in a summation of the two image intensities and this leads to a total intensity of A + 2B, which is a constant thereby blurring the imaged features. The response to exposures must therefore not be linear, such that that the dose response of the resist must not simply be a function of the sum of the total absorbed dose such that $f(I_1 + I_2) \neq f(I_1) + f(I_2)$.[10]

Provided new resist materials are developed, double-exposure appears to be an apt method for reducing lithographic feature sizes and meeting the needs of the integrated circuit industry.[9, 11] Indeed, it has been shown that resists must show reversibility and nonlinearity in order to overcome dose reciprocity limitations.

Two-photon materials have generated some interest because of their inherent nonlinearity. These materials typically contain a photoacid generator (PAG) that requires simultaneous two-photon absorption to initiate the acid generation, as described by the following equation: PAG + $I(h\nu) + I(h\nu) \rightarrow$ *acid. The probability for*

the conversion is therefore proportional to the intensity squared: $f(I) \alpha I^2$, such that $f(I_1) + f(I_2) = f(I_1^2 + I_2^2) \neq f(I_1 + I_2)$. Unfortunately, simultaneous two-photon absorption materials are inconvenient because of low quantum yield limitations and laser pulse doses of current exposure tools.[9]

Another promising approach offering nonlinear response to exposure dose is the use of contrast enhancement layers, applied on top of existing resists, that act as photochromic windows placed between the exposure tool and the resist. Contrast enhancement layers are composed of strongly absorbing materials that photobleach. The exposure energy is therefore used at first to render the window transparent (photobleaching). As photobleaching occurs, the increasingly transparent layer allows light through to the resist which initiates the solubility switch.[8] *The light will therefore be able to reach the resist only in areas where the exposure intensity is high and cannot cause changes in the dark regions of the resist. Reversible contrast enhancement layers (rCEL) can be returned to their opaque state following, for instance, irradiation at a different wavelength. This is highly advantageous for double exposure applications, where the rCEL can effectively be 'reset' between exposures to ensure better resolution.*

In this collaboration with microprocessor giant Intel Corporation, we have investigated a possible compound for lithographic rCEL applications. Our strategy makes use of the well known photoreversible cycloaddition of anthracenes.[12, 13]

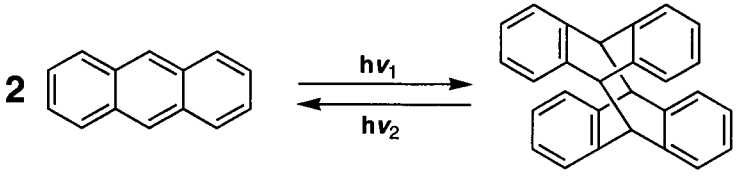

Scheme 2. Reversible anthracene photocycloaddtion.

The use of the dimeric form of anthracenes holds promise as a rCEL material because of the importance of reversibility in these materials. Tethered anthracenes were of particular interest, due to the proximity of anthracene moieties, which allows for more efficient photodimerization. We report here the results obtained concerning the "instantaneous" efficiency of these processes in free and tethered anthracenes in solution and in polymeric materials.

Photoreversible Cycloaddition of Anthracenes

The anthracene dimer can be generated from anthracene with irradiation at wavelengths longer than 230 nm ($h\nu_1$), where anthracene begins to absorb. In fact, although anthracene monomer does not significantly absorb below 230 nm, the absorbance of the dimer is mainly located in this spectral region. Irradiation in this region cleaves the dimer and regenerates anthracene ($h\nu_2$). This provides an interesting transparency photoswitch. For instance, anthracene which is opaque at 250 nm can be transformed with 254 nm irradiation into the anthracene dimer, transparent at 250 nm and highly absorbing at 193 nm. This dimer can then be cleaved using 193 nm irradiation, reverting back to the anthracene monomer compound.

This photoreversible transparency switch can also be exploited for anthracene derivatives that are specifically geared towards nanolithography. Tethered anthracenes, such as DAME, are appealing compounds due to the proximity of anthracene moieties which favors efficient cycloaddition.

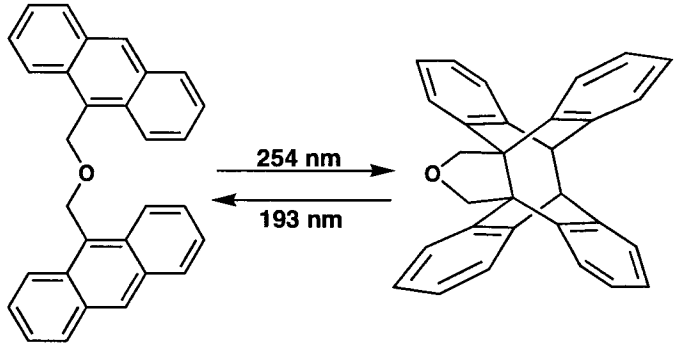

Scheme 3. Photoreversibility of DAME cycloaddition.

We have used spectroscopic techniques to study the reversible DAME system including fluorimetry, UV-Visible absorbance spectroscopy and laser flash photolysis. To investigate further the reactions occurring in this system we also employed nuclear magnetic resonance and mass spectrometry.

METHODS

Irradiation and Spectroscopy

Continuous lamp irradiation was carried out in a Luzchem photoreactor, model LZC-4. Luzchem was also the source of UV bulbs: UVA irradiation centered at 350 nm (3 W/m^2 per bulb) and UVC irradiation centered at 254 nm (12 W/m^2 per bulb). Visible irradiation spanning the whole visible range (400 - 700 nm) was provided by Sylvania® Cool White bulbs (4.8 W/m^2 per bulb). Continuous irradiation was also supplied by a xenon lamp with 320 nm cutoff filter (193 W/m^2) and 280 nm cutoff filter (198 W/m^2), calculated irradiance from 300 to 400 nm.

The energy of continuous lamp irradiation was determined with a Luzchem SPR-01 spectroradiometer, with software version 3.1. The irradiance profiles of each lamp were recorded with this instrument and can be found in Appendix I.

Laser exposure at 193 nm was obtained with the ArF transition of a GSI-Lumonics Pulsemaster model 846 excimer laser (1 Hz pulse frequency unless otherwise noted, ~10 ns pulse duration). Note that all solution experiments with 193 nm irradiation are performed on samples purged with nitrogen, unless otherwise noted. Laser pulses of 266 and 355 nm light were generated by a Continuum Nd-YAG Surelite SLII-10 pulsed laser (1 Hz pulse frequency, 5 ns pulse duration).

The energy of incident laser beams was measured at the sample with a Molectron JD2000 joulemeter radiometer and Thorlabs PM100D Powermeter coupled with a Thorlabs ES245C High Energy Pyroelectric Sensor.

Light energy will be expressed either as (i) irradiance: the irradiation power per area (J/m^{2}s) measured at the sample, (ii) total dose or total energy: light energy delivered to entire sample (J), or (iii) total energy absorbed: light energy delivered to sample, corrected for absorbance of compound at irradiation wavelength. Note that energy is commonly referred to as power in the context of laser exposure, though still a measurement in joules (rather than watts).

Laser flash photolysis (LFP) was performed using a customized version of a Luzchem LFP-111 system, including Hamamatsu photomultiplier detector and Tektronix-3012 digital scope.[14] Excitation flash pulses were provided by previously described laser systems with a Xenon short arc lamp (150 W) as monitoring beam. Samples in a typical experiment were either static (7 x 7 mm^2 quartz cuvette, 3 mL volume) or flowed in an 'L-shaped' quartz flow cell which ensures that a fresh volume of sample is irradiated each laser pulse.

UV-Visible spectra were recorded on Varian Cary-50 and Cary-100 single beam spectrometers with zero/baseline corrections, using air and solvent as the zero and baseline absorbance curves, respectively unless otherwise noted. Film absorbances were recorded on a custom mount, built using a ThorLabs lens tube and aluminum support. Total energy for film samples was adjusted for monitored sample area (area of monitoring beam), which was measured and found to be 6.2 mm^2. Extinction coefficients at specific wavelengths were calculated with a calibration curve, using at least n = 3. A Varian single cell peltier thermostatted cell holder was employed with the Cary-50 for absorbance measurements with controlled temperature.

Steady-state fluorescence spectroscopy was carried out with an instrument from Photon Technology International utilizing a continuous xenon lamp for excitation and Felix32 Analysis software version 1.2. Spectral resolution was set at 2 nm.

Spectrometry

Nuclear magnetic resonance (NMR) spectrometry was conducted using a Bruker Avance 400MHz and analyzed with Bruker Topspin software version 1.3. All spectra were recorded in deuterated chloroform (99.8 atom % D, Aldrich) and calibrated to residual solvent peaks at ^{1}H-NMR δ = 7.26 and ^{13}C-NMR δ = 77.16 ppm.

Mass spectrometry (MS) samples were submitted to the University of Ottawa's Mass Spectrometry Center and carried out on a Kratos Concept II-S spectrometer. Samples were submitted in acetonitrile for electrospray ionization (ESI-MS).

The Wave Experiments

i. Laser-Laser Time Resolved Wave Experiment

Using the LFP system to monitor changes in absorbance, a sample was irradiated with 2 sequential laser pulses (193 nm then 355 or 266 nm), separated by a 100 μs delay. Laser beams were directed perpendicular to the monitoring beam and irradiated the solution sample from either sides [left]. In films, laser beams were directed to irradiate the sample from the back face, in order to reduce incident light reaching the detector [right].

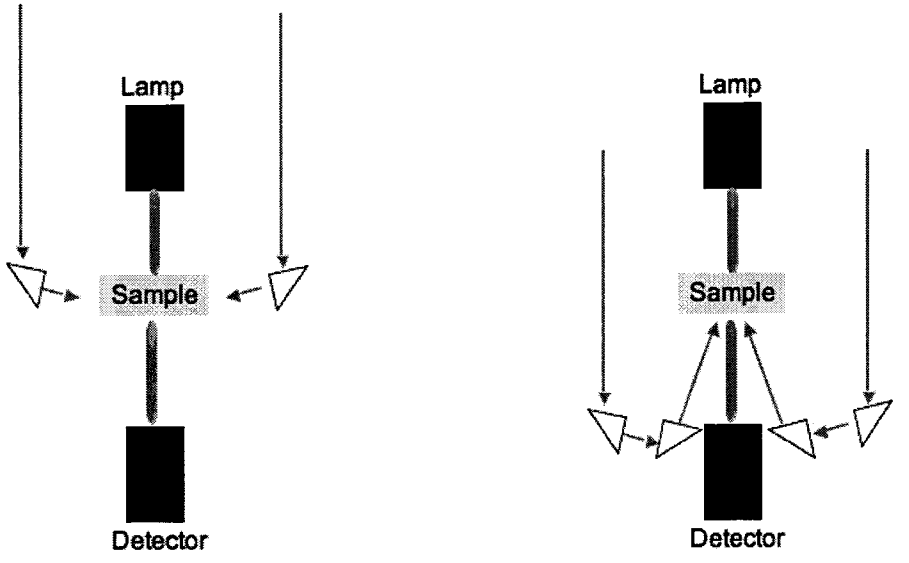

Figure 16. Laser-laser time resolved wave experiment setup.

ii. Laser-Lamp Wave Experiment

This experiment was devised in order to monitor the opening-closing cycle of the cycloadduct by UV-Visible spectroscopy. The sample was directly exposed to 193 nm light pulses until further irradiation led to no increase in the 250 nm band of the absorbance spectrum, attributed to anthracene moieties. Direct irradiation with a continuous UV light source then caused cycloaddition, which was monitored by the decrease in the 250 nm absorbance band.

Film Preparation

Thin films were prepared by spin coating solutions containing 7 % weight polymer dissolved in 2-heptanone or diglyme, on one-inch diameter quartz discs at 2000 rpm for 30 seconds, using a spin coater from Specialty Coatings, Inc. After coating, the films were baked over an aluminum plate in an oven at 95 - 98 °C for 60 seconds, allowing for evaporation of the solvent.

The thickness of polymer films was measured by interferometry with a TFA-11 thin film analyzer from Luzchem Research Inc., and determined to be approximately 500 nm thick using Luzchem TFA software version 2.1.

MATERIALS

Acetonitrile (≥99.9 % Chromasolv® HPLC-grade, Aldrich) was scanned before use with UV-Vis absorption spectra to ensure spectral purity. Disposable glass Pasteur pipettes could not be used with acetonitrile because of an impurity contained in the pipettes with very significant absorbance in the 190 - 220 nm region. Rubber septa were also avoided for spectroscopic measurements, as even extracted septa were found to contaminate our samples.

All other solvents used in synthesis, as well as 2-heptanone and bis(2-methoxyethyl) ether (diglyme), were purchased from Aldrich and used as received.

Diphenylcyclopropenone (DPCP, 98 %, Aldrich), 2-Aminopyridine (98 %, Sigma) anthraquinone (AQ, 97 %) and polymethylmethacrylate (PMMA, ~120 000 m.w., T_g 105 °C,[15] Aldrich) were used as received without any further purification.

A polymer sent to us by Intel Corporation and originating from Dupont, was used as received. The composition of this copolymer was disclosed to be 58 % a-GBLMA and 42 % MAMA:

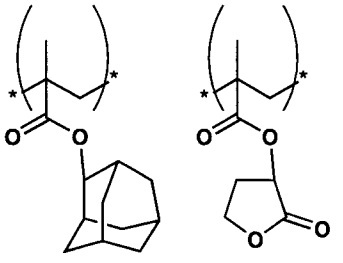

Structure 2. Dupont polymer components.

Anthracene (≥99 %, Aldrich), ^{1}H-NMR (400 MHz, $CDCl_3$) δ = 8.43 (s, 2H), 8.01 (m, 4H) and 7.47 (m, 4H) ppm, ^{13}C-NMR (400 MHz, $CDCl_3$) δ = 131.8, 128.3, 126.4, 125.5

ppm, and rose Bengal B bound to polystyrene (0.3 mmol/g, 200-400 mesh, Aldrich) were used as received.

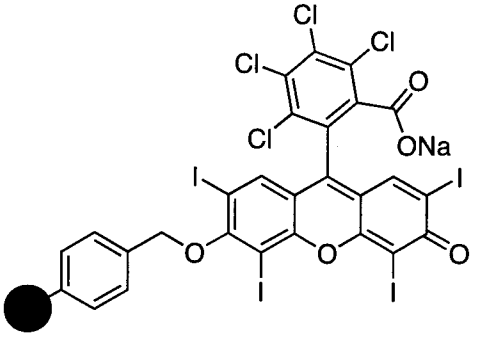

Structure 3. Rose Bengal B bound to polystyrene (represented by a black circle).

Anthracene dimer was synthesized by irradiating a nitrogen purged solution of anthracene in tetrahydrofuran (0.06 M) overnight with UVA light (24 W/m^2).[13]

Anthracene endoperoxide (APO) was first synthesized following the method published by Schmidt et al.[16] *Anthracene (0.1 g) and polystyrene-bound rose Bengal B (0.3 g) were dissolved in carbon disulfide. The solutions were saturated with O_2 and then irradiated with visible light (51 W/m^2), being continuously stirred and periodically monitored by TLC. After irradiation, the crude was purified by column chromatography using hexanes and ethyl acetate (90:10) as eluent. Anthracene, identified by NMR and UV-Vis spectroscopy, was contained in the first fraction. The second fraction was identified as anthracene endoperoxide, pure by NMR. Endoperoxide product yield was 64 % in CS_2 (18 hour irradiation) and 13 % in dichloromethane (3 hour irradiation), as calculated by ^{1}H-NMR.*

APO was verified by electron impact mass spectrometry (EI-MS, m/z = 210.1), UV-Vis absorbance spectroscopy ($\varepsilon_{192\ nm}$ = 33 700 M^{-1}cm^{-1} and $\varepsilon_{214\ nm}$ = 43 000 M^{-1}cm^{-1}), and NMR spectrometry with the following shifts: ^{1}H-NMR (400 MHz, $CDCl_3$) δ = 6.03 (s, 2H), 7.29 (m, 4H) and 7.42 (m, 4H). Note that the ^{13}C-NMR spectrum could not recorded because of thermal decomposition.

Endoperoxide syntheses should be performed in an ice bath to avoid thermal decomposition of the endoperoxide. Rotary evaporation can be used, without heating. If endoperoxide is heated it may decompose to anthraquinone. To confirm the anthraquinone decomposition product, we heated the anthracene endoperoxide and employed UV-Vis spectroscopy ($\varepsilon_{203\ nm}$ = 39 700 $M^{-1}cm^{-1}$, $\varepsilon_{250\ nm}$ = 56 600 $M^{-1}cm^{-1}$, $\varepsilon_{273\ nm}$ = 18 300 $M^{-1}cm^{-1}$, $\varepsilon_{323\ nm}$ = 5 800 $M^{-1}cm^{-1}$) as well as NMR to characterize the product: ^{1}H-NMR (400 MHz, $CDCl_3$) δ = 8.32 (m, 4H) and 7.81 (m, 4H) ppm; ^{13}C-NMR (400 MHz, $CDCl_3$) δ = 134.3 and 127.4 ppm.

DAME and cycloDAME were sent to us by James R. Blackwell and Katherine Esswein from the Intel Corporation in Portland, Oregon. They were both used as received. They were prepared by the following method: in a round bottom flask, 9-anthracenemethanol (0.002 mol) is dissolved in 20 mL of chlorobenzene and allowed to stir under N_2 at 50 °C for 20 minutes. A few milliliters of an aqueous solution of potassium hydroxide (1.2 M) and tetrabutylammonium bromide (0.14 M) are then added to the flask. Following this, 9-chloromethyl anthracene (0.0022 mol) is added to the flask. The temperature is increased to 65 °C and left for 3 to 4 days. After drying under reduced pressure, the residues are treated with 30 to 40 mL of 60 % dichloromethane in water and extracted three times with dichloromethane. The organic phase is collected and dried over $MgSO_4$ and the solvent removed. The crude product is rinsed with ethanol to remove anthracenemethanol and recrystallized in dichloromethane. The reaction yield is typically around 60 %.

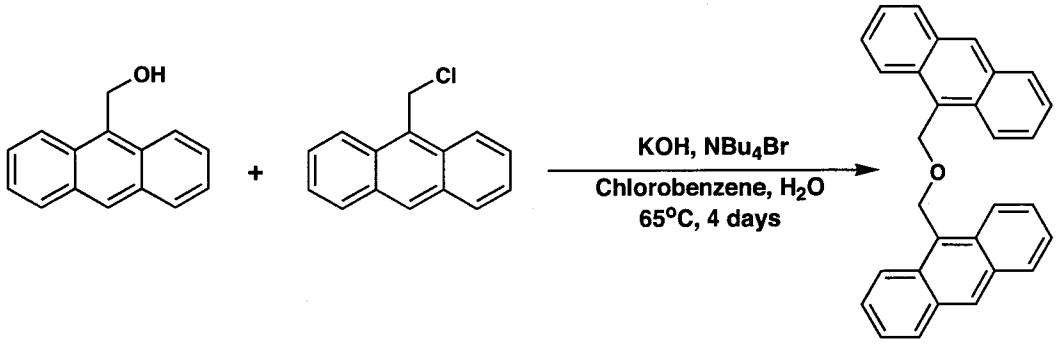

Scheme 4. Dianthracene methyl ether (DAME) synthesis.

Cycloaddition of DAME was performed by UVA irradiation of an argon purged solution of DAME (6.7 mM) in benzene. This synthesis must be carried out under

high dilution to avoid intermolecular addition.[12] The solvent is removed under reduced pressure and the residue rinsed with benzene. The solution is centrifuged and the solvent is removed by decantation.

The products received were characterized by UV-Vis absorbance and NMR:

DAME ($C_{30}H_{22}O$): $\varepsilon_{247\ nm}$ = 133 000 $M^{-1}cm^{-1}$, $\varepsilon_{254\ nm}$ = 131 000 $M^{-1}cm^{-1}$, $\varepsilon_{347\ nm}$ = 7 200 $M^{-1}cm^{-1}$, $\varepsilon_{366\ nm}$ = 11 700 $M^{-1}cm^{-1}$ and $\varepsilon_{386\ nm}$ = 12 200 $M^{-1}cm^{-1}$; ^{1}H-NMR (400 MHz, $CDCl_3$) δ = 8.47 (s, 2H), 8.28 (m, 4H), 8.01 (m, 4H), 7.42 (m, 8H), 5.66 (s, 4H) ppm; ^{13}C-NMR (400 MHz, $CDCl_3$) δ = 138.7, 131.6, 131.3, 129.1, 126.2, 125.1, 124.5 and 64.7 ppm, as shown in Appendix II.

cycloDAME ($C_{30}H_{22}O$): $\varepsilon_{197\ nm}$ = 111 200 $M^{-1}cm^{-1}$; ^{1}H-NMR (400 MHz, $CDCl_3$) δ = 7.16 (m, 4H), 6.94 (m, 4H), 6.86 (m, 8H), 4.85 (s, 4H), 4.54 (s, 2H) ppm; ^{13}C-NMR (400 MHz, $CDCl_3$) δ = 144.0, 143.0, 127.7, 126.1, 125.7, 124.2, 73.2, 63.9 and 54.0 ppm, as shown in Appendix III.

DAME endoperoxide (DAMEPO: $C_{30}H_{22}O_3$) was synthesized as described above for anthracene endoperoxide, in dichloromethane for 3 hours. The product was purified by column chromatography using hexanes and ethyl acetate (95:5) as eluent, to provide better separation. The DAME endoperoxide product was identified by electrospray ionization mass spectrometry in acetonitrile (ESI-MS, m/z = 429.3) and product yield was 40 %, calculated by ^{1}H-NMR. Appendix IV shows the ^{1}H-NMR spectrum of DAME endoperoxide and the chemical shifts of the product were as follows: ^{1}H-NMR (400 MHz, $CDCl_3$) δ = 8.54 (s, 2H), 8.51 (s, 1H), 8.06 (m, 2H), 7.58 (m, 2H), 7.52 (m, 2H), 7.36 (m, 2H), 7.28 (m, 2H), 7.20 (m, 2H), 7.09 (m, 2H), 5.96 (s, 1H), 5.84 (s, 2H), 4.70 (s, 2H) ppm. Note that the ^{13}C-NMR spectrum could not recorded because of thermal decomposition.

RESULTS

Spectroscopic Properties of Studied Compounds

A calibration curve for anthracene was first constructed for future reference in this study and determination of anthracene concentration present in sample after exposure.

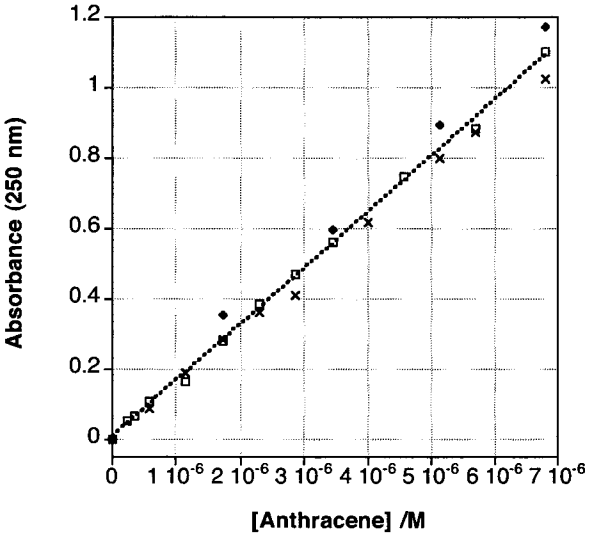

Figure 17. Absorbance calibration curve for anthracene in acetonitrile at room temperature (10 mm path length). Data points for n = 3 shown.

The Beer-Lambert equation described by Equation 5 allows us to use Figure 17 to determine the extinction coefficient (ε) of anthracene, where c is the concentration and l is the path length.

Equation 5. Beer-Lambert Law. $A = \varepsilon cl$

The extinction coefficient of anthracene at 250 nm was calculated to be 160 000 $M^{-1}cm^{-1}$ with less than 5 % error (using standard deviation for n = 3). The same calibration was performed for DAME and cycloDAME compounds and their extinction coefficients can be found in Table 1 below, with no more than 10 % error.

ε (M^{-1} cm^{-1})	DAME	cycloDAME
193 nm	26 000	100 000
250 nm	120 000	3 800
254 nm	131 000	3 400
385 nm	6 000	100

Table 1. Extinction coefficients of DAME and cycloDAME in acetonitrile at room temperature.

Table 1 shows an important feature of this system, which is the transparency switch at 193 and 250 nm explained earlier. This switch is also illustrated in Figure 18 below. Indeed, as DAME is converted to cycloDAME with 254 nm irradiation, the absorbance decreases in the 250 nm region and increases in the 200 nm region. Similarly, absorbance in the 200 nm region decreases when cycloDAME is converted to DAME with 193 nm irradiation, and increases in the 250 nm region.

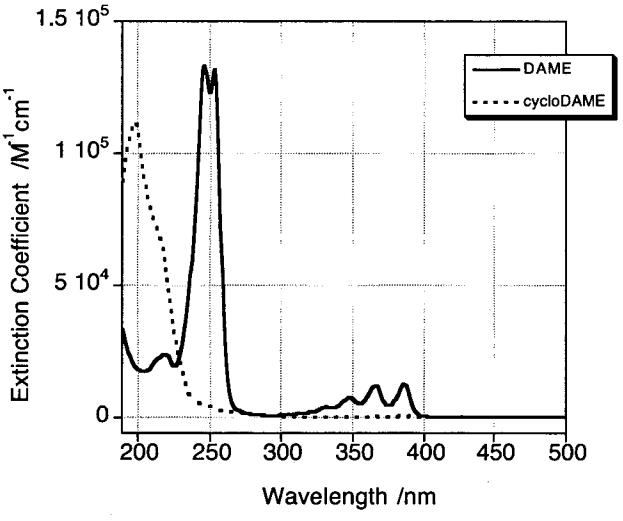

Figure 18. Extinction coefficients of DAME and cycloDAME in acetonitrile, average of three samples is shown.

The absorbance spectrum of DAME shown above closely resembles the absorbance profiles of anthracene and its dimer, that were recorded but are not shown. We can identify the $S_0 \rightarrow S_1$ transition, visible between 350 and 400 nm.[17] We speculate that the double peak observed at 250 nm ($S_0 \rightarrow S_2$) could be caused by DAME conformers present in the system, as previously observed for other tethered anthracenes.[18]

Optimization experiments for cycloaddition of anthracene and DAME were performed with irradiation centered at 254 and 350 nm, as well as with light from a xenon lamp with 280 and 320 nm cutoff filters. Irradiance spectra of sources employed is shown in Appendix I. For equal amounts of energy delivered (irradiance, W/m^2), cycloaddition was quickest with 254 nm irradiation as expected from the absorbance spectra of both anthracene and DAME, which have large extinction coefficients at that wavelength. Cycloaddition was carried out using 254 nm for all subsequent manipulations, unless otherwise noted.

We note here that anthracene cycloaddition occurs via the singlet manifold.[12] In fact, a singlet excited anthracene forms an excimer with the unexcited anthracene, and this short-lived species undergoes bond formation resulting in the formation of the dimer. [19, 20] We speculate that DAME photophysics also operate within the singlet manifold and explore this further in the following section.

Photophysical Pathways

It is important to understand the possible photophysical pathways of cycloDAME, which are shown in Scheme 5. The high quantum yield of cleaving combined with the very low fluorescence quantum yield suggests that DAME cleaving occurs diabatically, as explained below.

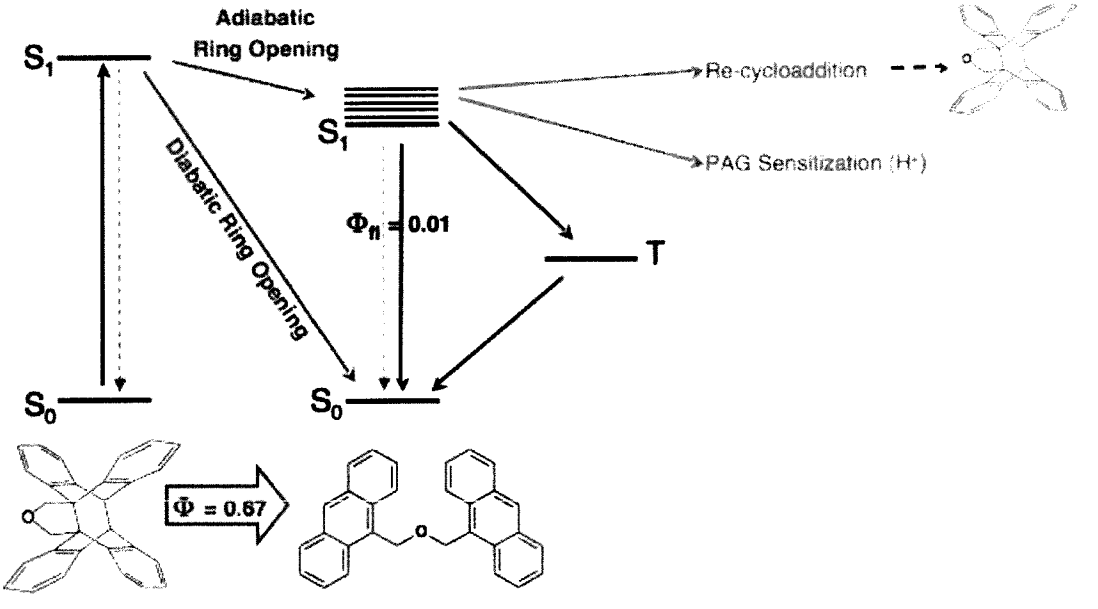

Scheme 5. Possible photophysical pathways of cycloDAME.

i. Cleaving quantum yield

Cleaving of cycloDAME was performed with 193 nm irradiation. The quantum yield (Φ) of cycloDAME cleaving was determined to be 0.67 ± 0.04 by comparison to the decomposition yield of diphenylcyclopropenone (Φ = 1.00 ± 0.03).[21] The quantum yield of disappearance of diphenylcyclopropenone was first determined by Fessenden and coworkers, by comparison to the yield of production of acetophenone from valerophenone in benzene solution (Φ = 0.30).[22]

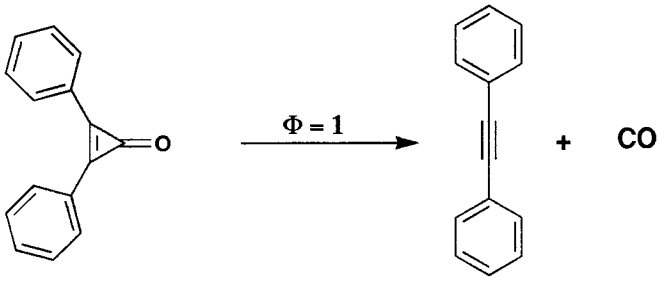

Scheme 6. Diphenylcyclopropenone (DPCP) decomposition as reference for quantum yield measurement.

This measurement was performed for irradiation at 337 nm, by nitrogen laser pulses. We assume that the quantum yield is unchanged with 193 nm irradiation for our purposes. We rationalize this because no new products were formed and a higher energy is employed in this case. Samples of both DPCP and cycloDAME were exposed to a known number of pulses from the ArF laser. The decomposition of diphenylcyclopropenone was determined by the decrease in absorbance of the solution at 310 nm (quantum yield calculation shown in Appendix V). Note that the product, diphenylacetylene, does not absorb appreciably at this wavelength. Given the excellent quantum yield, cycloDAME can be used as a new reference for cleaving yield at 193 nm, for compounds investigated in future studies.

ii. Fluorescence quantum yield

The high cleaving quantum yield led us to expect that DAME fluorescence was not a major photophysical pathway. This was confirmed by the fluorescence quantum yield of DAME, which was determined to be very low (Φ_{fl} = 0.01, with less than 3 % error). This further supports our claim that diabatic cleaving is most favored. Indeed, the adiabatic population of the excited singlet state of DAME might lead to both re-cycloaddition (giving a lower ring opening quantum yield) as well as more significant fluorescence which is not observed.

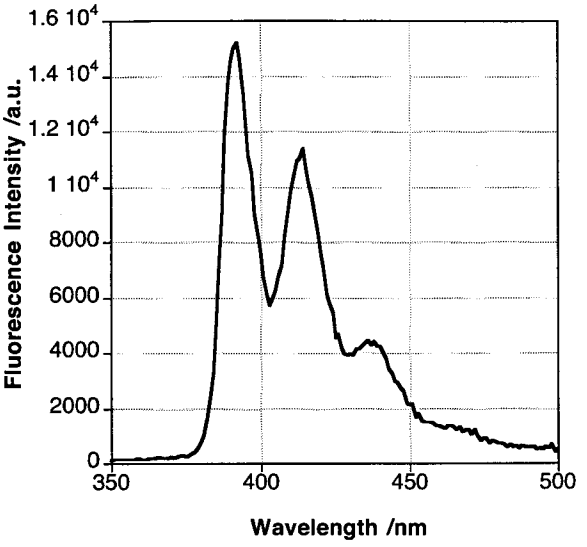

Figure 19. Fluorescence spectrum of DAME in acetonitrile (22 μM), under air (λ_{exc} = 254 nm).

The fluorescence quantum yield was determined using 254 nm light excitation to reflect DAME cycloaddition experiments, though fluorescence quantum yield is theoretically wavelength independent as long as no chemistry occurs from upper excited states. The quantum yield was determined using 2-aminopyridine in 1 N H_2SO_4 (Φ_{fl} = 0.60, λ_{em} = 360 nm) as a reference,[23] which provided excellent spectral overlap with the fluorescence of DAME. The reference compound and DAME were absorbance matched at the excitation wavelength ($A_{254\ nm}$ = 0.1). The quantum yield was corrected for the different refractive indices of acetonitrile (η = 1.344) and sulfuric acid (η = 1.33) as shown by Equation 6, where Φ is the quantum yield, I is the intensity of the fluorescence signal, OD is the absorbance at the excitation wavelength, η is the refractive index and subscript R denotes the reference compound.[23]

Equation 6. $$\Phi_{fl} = \Phi_R \cdot \frac{I}{I_R} \frac{OD_R}{OD} \cdot \frac{\eta^2}{\eta_R^2}$$

As previously mentioned, the low fluorescence quantum yield combined with the high ring opening quantum yield suggest that cycloDAME cleaving occurs diabatically from the singlet excited state, similarly to anthracene dimer cleaving.[12] Although excited state cycloDAME could also revert back to the

cycloDAME ground state rather than to DAME, we can conclude that this is a disfavored relaxation pathway given the high quantum yield of DAME ring opening.

It is interesting to note that this was not the case in other experiments carried out on a compound synthesized in our group, which we named the "methoxyanthracene tether" shown below.

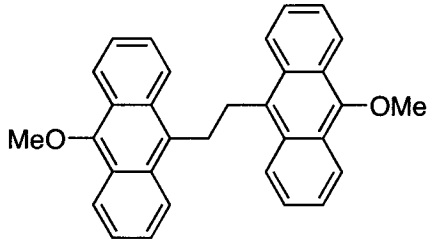

Structure 4. 9-Methoxyanthracene tethered dimer.

Indeed, the quantum yield of cleaving for this compound was very low. We propose that this is due to a favored adiabatic pathway followed by immediate ring closing, through relaxation directly back to the closed-form ground state, in cyclic photochemistry reminiscent of a "clapping"-like motion.

iii. Transients

Laser flash photolysis studies were carried out on both DAME and cycloDAME and the results are presented herein. Firstly, anthracene dimer was studied as a reference. The transient spectra as well as ground state growth and triplet decay were recorded.

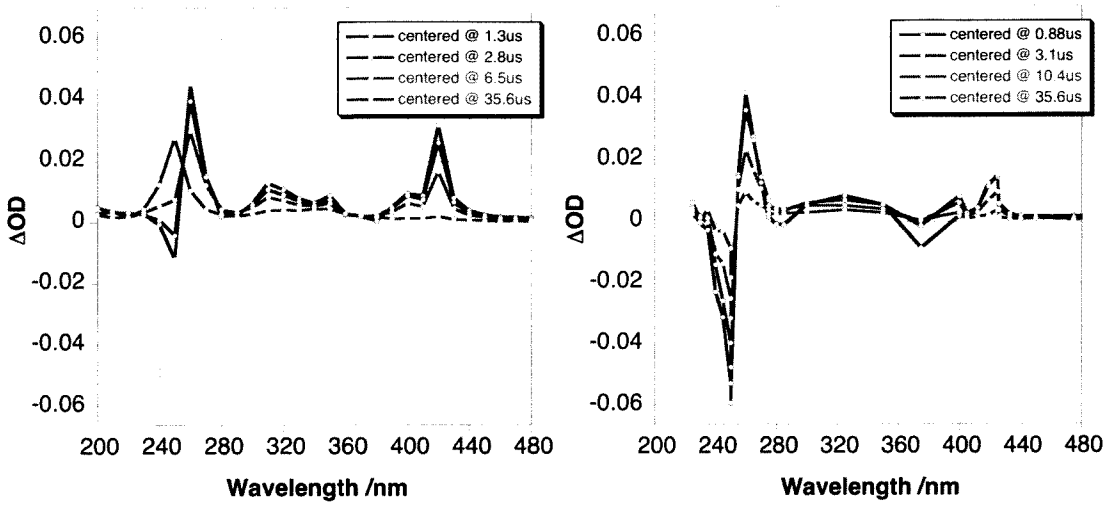

Figure 20. Full transient spectra of anthracene dimer (10 μM) in nitrogen purged acetonitrile solution, using 193 nm laser pulse as excitation source (30 mJ total energy), under flow [LEFT] and static conditions [RIGHT].

Figure 20 [LEFT] shows the anthracene ground state band around 250 nm as well as triplet signals. Though some ground state is observed after 35.6 μs, this spectrum was recorded under flow conditions where anthracene dimer was readily replenished. Bleaching of the anthracene ground state signal occurred when the flow was stopped [RIGHT] and anthracene accumulated in the monitored sample. In this spectrum, ground state bleaching is apparent at 250 and 380 nm, both anthracene ground state absorbance bands.

Ground state anthracene was monitored at 250, while we monitored the anthracene triplet state by detection of the triplet-triplet absorption at 420 nm.[19, 24]

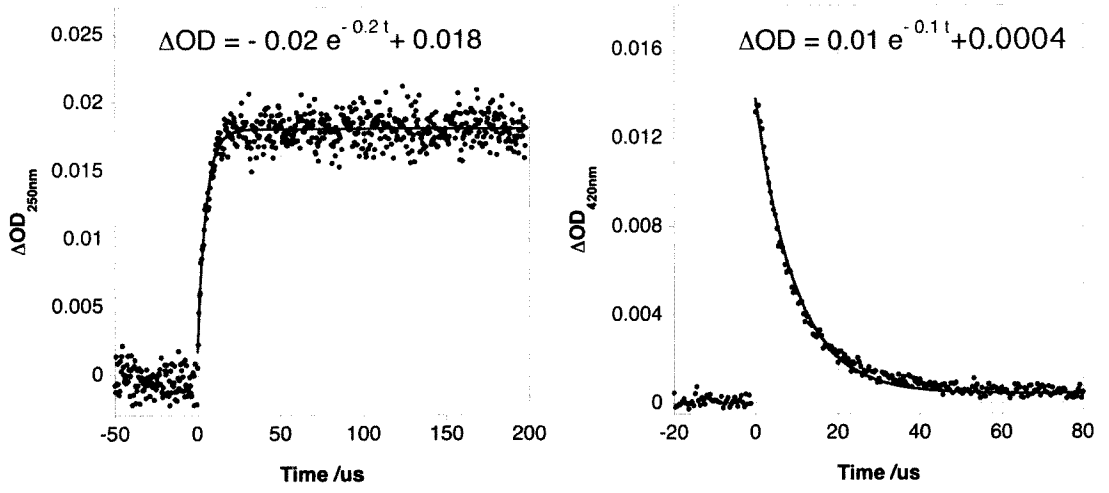

Figure 21. Anthracene dimer (5 μM) in nitrogen purged acetonitrile solution, under flow conditions. Ground state monitored at 250 nm [LEFT] and triplet monitored at 420 nm [RIGHT], following 193 nm laser pulse (5 mJ total energy).

The traces were fit to first order kinetics, as described by Equation 7, where ΔOD is the change in absorbance after time t, k is the rate constant and A is the pre-exponential factor corresponding to the absorbance at time zero for this simple monoexponential decay.

Equation 7. $$\Delta OD = Ae^{-kt}$$

The lifetime can be calculated from the rate constant, according to the relationship shown in Equation 8 where k is the rate constant and τ is the lifetime (in seconds).

Equation 8. $$\tau = 1/k$$

From the slope of the decay, the triplet lifetime of anthracene (λ_{abs} = 420 nm) was thus found to be 10 μs, giving a decay rate constant of 1.0 x 10^5 s^{-1}. Anthracene triplet decay lifetimes can be found in the literature for solvents other than acetonitrile.[25-27] These do not correspond to the lifetimes we consistently observed in acetonitrile, though Nielsen and coworkers did observe a triplet decay of 1.31 x 10^5 s^{-1} at 428 nm in toluene,[28] which compares well with our value.

Similar kinetic analysis led to a growth lifetime of 5 μs for anthracene ground state (λ_{abs} = 250 nm) and a cleaving rate constant of 2.0 x 10^5 s^{-1}. This relatively long lifetime likely reflects a triplet-mediated process, as processes occurring within the singlet manifold are much faster. Thus, we believe that the observed decay is consistent with a triplet formed following re-excitation from the ground state. As this experiment was conducted under flow conditions, no anthracene ground state is expected to be present in solution after dimer excitation and cleavage. However, the observed signal is very low considering the large extinction coefficient of triplet anthracene. It follows that the observed triplet signal can be attributed to excitation of ground state anthracene traces left behind despite flow conditions.

The same study was conducted for cycloDAME:

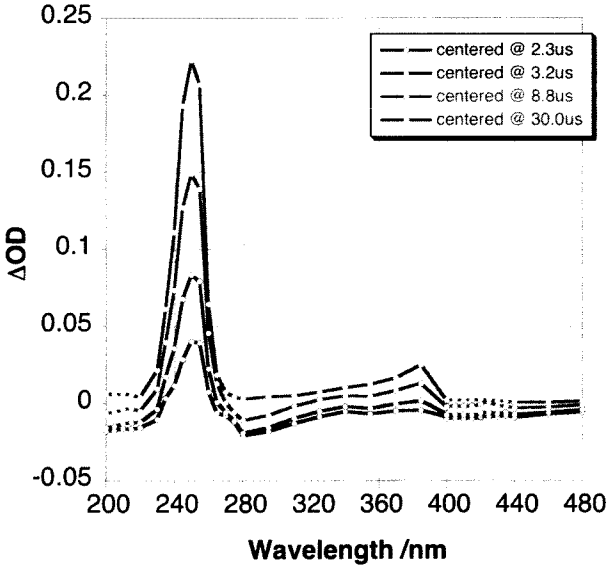

Figure 22. Transient spectra of cycloDAME (12 μM) in nitrogen purged acetonitrile solution, using a 193 nm laser pulse as excitation source (10 mJ total energy).

The increasing absorbance seen in the transient spectra above indicate the formation of products. Indeed, ground state DAME absorbance bands centered at 250 and 380 nm are increasing as DAME is formed following exposure to 193 nm pulses.

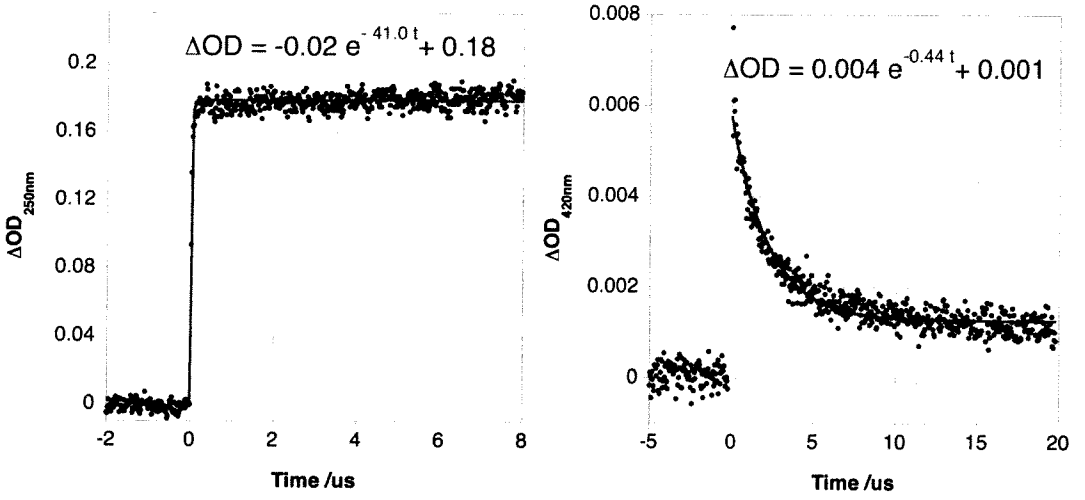

Figure 23. cycloDAME (12 μM) in nitrogen purged acetonitrile solution, under flow conditions. Ground state monitored at 250 nm [LEFT] and triplet monitored at 420 nm [RIGHT], following 193 nm laser pulse (5 mJ total on sample).

The growth of ground state DAME (open-form product) was recorded having a lifetime of 25 ns along with a rate constant of 4.1 x 10^7 s^{-1}. This value is very low and we observed significant variation between experiments for the growth lifetime of ground state DAME, though all on the order of tens of nanoseconds. This appears to be at the detection limit of the LFP system used and we cannot ascertain this lifetime value. Indeed, the time resolution for the system was set a 20 MHz (50 ns), which prevents rise time measurement below about 20 ns.

Nevertheless we can assume that the DAME growth lifetime is shorter than for anthracene. This might be explained by the readiness of DAME to cleave due to the added strain of the tetrahydrofuran-like bridge linking the two anthracene moieties.

The triplet-triplet absorption band monitored at 420 nm showed a decay lifetime of 2.3 μs, from which a rate constant of 4.4 x 10^5 s^{-1} was calculated. This lifetime was found to be consistently shorter than that of triplet anthracene, which could be explained by more abundant deactivation pathways in the case of the tethered anthracene compound. It can be presumed that π-π interactions that can cause self-quenching and reduce the triplet lifetime will be more significant when the aromatic rings are tethered to each other.[29] Furthermore, the amount of anthracene moieties present in the cycloDAME sample is approximately five times

higher (12 μM cycloDAME = 24 μM anthracene moieties) than the anthracene sample used in previous experiments (5 μM), which could contribute to even more π-π interactions. This short lifetime explains why the triplet was not observed in the transient spectra time windows of Figure 22. It should be noted that the observed triplet signal is very weak, indicating that this is minor pathway, consistent with re-excitation of traces of open-form DAME as previously seen for anthracene.

Irradiation dose response of cycloDAME to 193 nm laser excitation

Optical threshold materials may also hold a key to smaller lithographic features.[8] *In order to fulfill their purpose adequately, these materials must have a non linear response to dose, which is why a power dependence study of cycloDAME cleavage was performed.*

In these experiments, cycloDAME was irradiated with 193 nm laser pulses of varying power. Figure 24 illustrates one of these experiments.

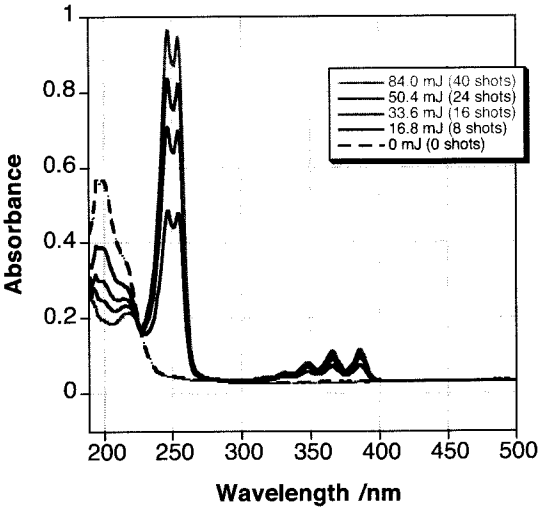

Figure 24. Cleaving cycloDAME (5 μM) in nitrogen purged acetonitrile solution, using 193 nm laser pulses (2.1 mJ total per pulse: 0.7 mJ/cm^2 irradiance, 3 cm^2 sample irradiation area).

To maintain a constant total irradiation dose, the number of shots delivered was increased as the laser power was decreased. The total irradiation dose was matched and equal to approximately 84 mJ. Cleavage was monitored using the absorbance value at 250 nm, as shown in Figure 25 below. This absorbance band is a suitable probe for DAME formation, due to the important extinction coefficient switch at that wavelength (see Table 1). The dose is shown as the total dose on sample (for instance, 28 mJ/cm^2 with 3 cm^2 sample irradiation area is a total dose of 84 mJ).

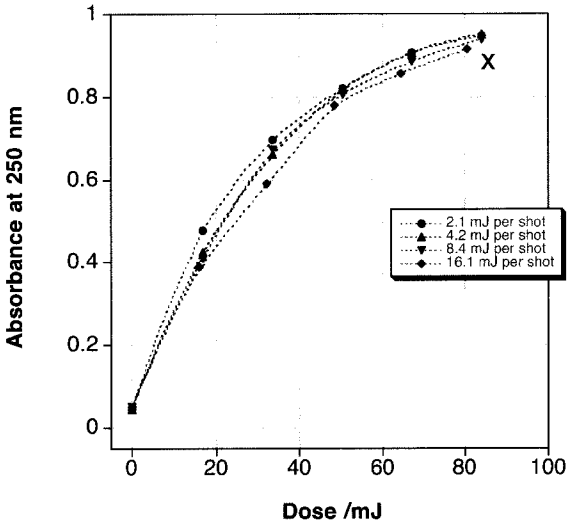

Figure 25. Monitoring cycloDAME cleaving (5 μM) in nitrogen purged acetonitrile solution, using 193 nm laser pulses at multiple powers. Matched total dose for all samples (approximately 84 mJ) after five exposures, marked by an "x".

As expected, cycloDAME readily cleaved under 193 nm irradiation to produce open form DAME. It is evident from this experiment that cycloDAME responds linearly to irradiation dose. Indeed, the final concentration of DAME formed (monitored using the absorbance value at 250 nm) is dependent on the total amount of light energy delivered, whether it be with numerous low power pulses or only a few high power ones.

Though DAME has a linear response to dose, the compound can still be useful as a contrast enhancement layer (CEL). However, much of the advantages in using CELs is lost if the system is not reversible, which is why we designed the "Wave Experiments" to study the reversibility of DAME photoinduced cleavage.

DAME Cycloaddition and Cleavage (The Wave)

The wave experiments are investigations of the photoreversibility between DAME (open form) and cycloDAME (closed form).

The process was first studied at short timescales, using laser flash photolysis with a double laser irradiation source. We then studied the reversibility over several cycloadd-cleave cycles, using pulsed 193 nm irradiation and continuous UVC irradiation.

i. Laser-Laser Time Resolved Wave Experiments

As described in the Methods section of this chapter (see Figure 16), this study makes use of a two-color, two-laser experimental setup where the two pulses are separated in time by an adjustable microsecond time delay. The light pulses are aligned to irradiate an overlapping region of the sample, where a third light beam provides for monitoring absorbance changes within the sample.

It is important to mention that although DAME cycloaddition is the most efficient with 254 nm irradiation, due to the high extinction coefficient of DAME at that particular wavelength as shown earlier (see Table 1 and Figure 18), irradiation at wavelengths absorbed by DAME (such as 355 nm) will also lead to cycloaddition, albeit less efficiently. Although our Nd-YAG laser also operates at 266 nm, it is ineffective for cycloaddition because of the sharp drop in extinction coefficient at this wavelength (see Figure 18).

The power of the 355 nm laser pulses were firstly varied to observe the effect on cycloaddition. To probe the system we chose to monitor DAME absorbance at 385 nm, as is shown in Figure 26, although monitoring can be carried out at any wavelength corresponding to absorbance bands of either DAME or cycloDAME. The experiments here were carried out under static as well as slow and fast flow conditions, with no difference in the recorded change in absorbance (Δ OD), reflecting the low single shot conversion.

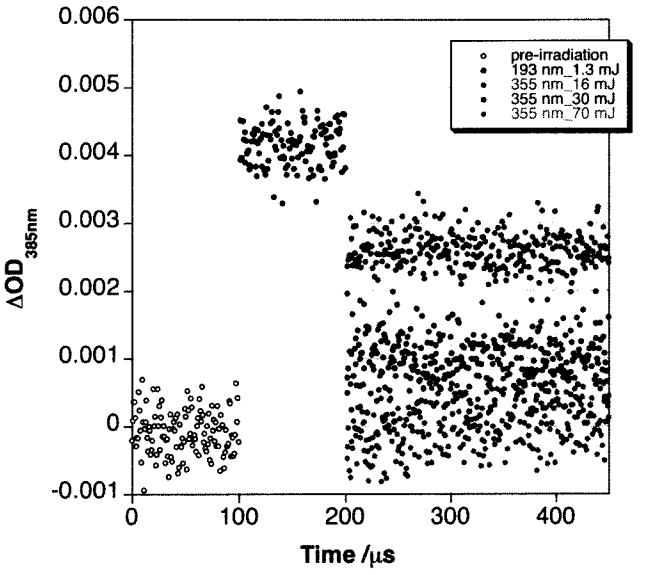

Figure 26. Cleaving cycloDAME (10 μM) in nitrogen purged acetonitrile solution (3 cm^2 sample irradiation area), with one pulse of 193 nm light (1.3 mJ total on sample). Cycloaddition performed in situ after 100 μs delay, by one pulse of 355 nm light at varying irradiance powers (16, 30 and 70 mJ total on sample). Open-form DAME is monitored at 385 nm.*

As expected, a significant difference can be seen between the varying powers of 355 nm irradiation. Taking into account the extinction coefficients of the irradiated compounds, the light energy absorbed by cycloDAME is equivalent to 6 x 10^{-17} einsteins per 193 nm pulse at 1.3 mJ power, whereas energy absorbed by DAME at 355 nm is 1.7, 3.2 and 7.5 x 10^{-16} einsteins for 16, 30 and 70 mJ output powers, respectively. These powers were converted to energy absorbed by the irradiated compound using calculations described on page 69 in the Laser-Lamp Wave Experiments section. The results of this calculation are shown in Table 2 below.

* Note that powermeter readings for this experiment are known to be inaccurate, instrument was displaying approximately twice the real power. Relative values are reliable and can be compared, but not absolute power values. For consistency, the original power measurements are used, actual values are about one half of those in Table 2.

	Energy of pulse		% Abs *	Energy absorbed	
	(10^{-3} J)	(10^{-8} einsteins)		(10^{-3} J)	(10^{-8} einsteins)
193 nm	1.3	210	94	1.2	198
355 nm	16	4.8	12	1.9	0.6
355 nm	30	8.9	12	3.6	1.1
355 nm	70	20.8	12	8.4	2.5

* at wavelength of irradiation for 10μM cycloDAME (193 nm) and DAME (355 nm)

Table 2. Energy of laser pulse absorbed by irradiated compound in laser-laser experiment.

The results first illustrate the energetic difference between 355 nm photons and 193 nm photons, which have higher energy per einstein. We then can observe that, although comparable amounts of joules are required for cleaving and cycloaddition, a lower energy in einsteins is needed to cleave cycloDAME than to cycloadd DAME.

It should be highlighted that the 193 nm dose reaching the far side of the sample cuvette is considerably less than that of the near side, due to the strong absorbance of cycloDAME at this wavelength. It follows that a relatively high dose of light is required to reach the far side. Nevertheless, such optical path issues are of little concern in commercial lithographic applications due to the thickness of the films used, which are very thin and consequently have short optical paths.

The clean steps in the graph indicate that DAME generation and cycloaddition is a fast process, even on the microsecond timescale. Indeed, very little growth is observed for either process and only plateaus are seen.

The most convenient way of improving the signal would be to increase the concentration of DAME generated. Unfortunately, due to power limitations of the 355 nm irradiation source, it was not possible to increase the power of 193 nm

irradiation. Thus we opted for a different irradiation wavelength for cleaving (266 nm), which we projected would be better absorbed by DAME because of its higher extinction coefficient in that region. Note that what appears as better signal-to-noise in Figure 27 is only a reflection of higher extinction coefficients at the monitored wavelength (250 nm).

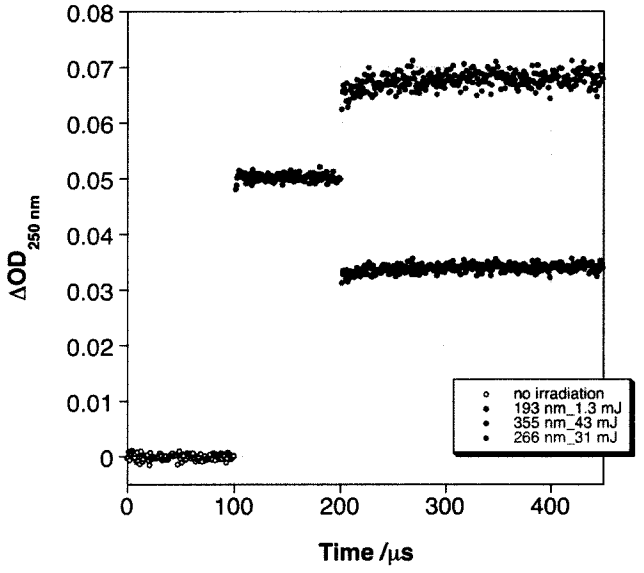

Figure 27. Cleaving cycloDAME (5 μM) in nitrogen purged acetonitrile solution (3 cm^2 sample irradiation area), with 193 nm light (1.3 mJ/cm^2 irradiance). After 100 μs delay, sample underwent second irradiation with 355 nm light pulses (43 mJ/cm^2, blue points) or 266 nm (31 mJ/cm^2, green points). Open-form DAME is monitored at 250 nm.*

Though it was originally our thought that 266 nm light could cause cycloaddition, careful inspection of the absorbance profile of DAME shows a sharp drop off at approximately 260 nm (see Figure 27 above). Therefore, although highly efficient cycloaddition would likely occur with 248 nm laser pulses,+ which is readily absorbed by our compound (as described in Table 1), irradiation using 266 nm light does not cause DAME cycloaddition which would have shown absorbance decreasing at the monitored wavelength (250 nm). To the contrary, the absorbance in Figure

* Note that powermeter readings for this experiment are known to be inaccurate, instrument was displaying approximately twice the real power. Relative values are reliable and can be compared, but not absolute power values.

+ This could not be verified experimentally in the two-laser setup for practical reasons: 193 nm and 248 nm irradiation are generated by the same laser source using different gas fills. Furthermore it should be noted that monitoring at 250 nm is difficult when using a 248 nm laser source and special precautions must be taken to avoid high power laser light to reach the photomultiplier.

27 shows a general increase after 266 nm irradiation as well as a slight growth immediately following the laser pulse.

This is a surprising observation because the extinction coefficient of DAME at 266 nm is very low ($\varepsilon_{266\ nm}$ = 5 500 $M^{-1}cm^{-1}$) and the extinction coefficient of cycloDAME at this wavelength is almost zero. This led us to carry out 266 nm irradiation experiments (8mJ total on sample) on open-form DAME.

Although this series of experiments was inconclusive, we observed the clear growth of a product absorbing at 250 nm. The growth lifetime was fit to a first order exponential and determined to have a 15 μs lifetime. This growth lifetime corresponds to the decay lifetime of a transient found absorbing between 400 and 440 nm which was previously attributed to the triplet.

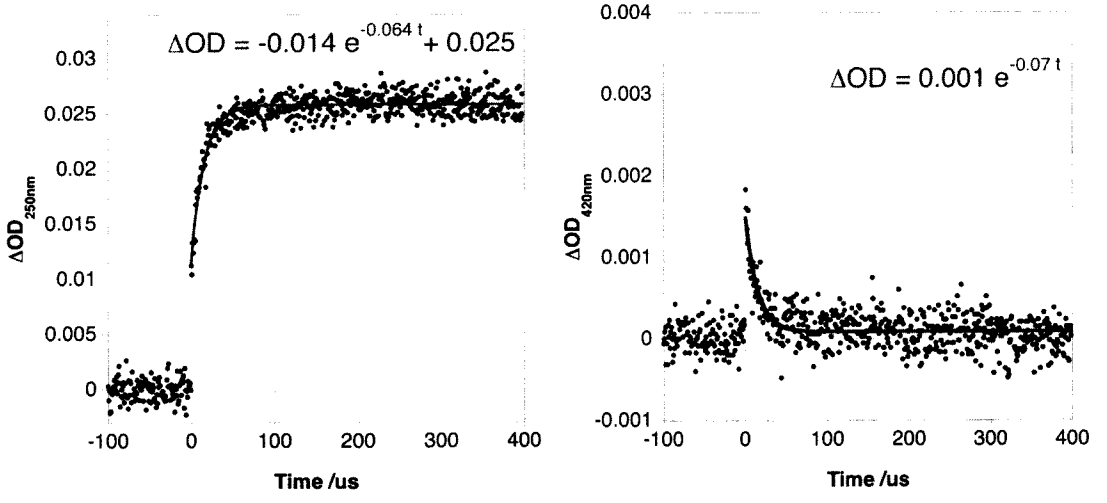

Figure 28. DAME (10 μM) in nitrogen purged acetonitrile solution, under flow conditions. Ground state monitored at 250 nm [LEFT] and transient monitored at 420 nm [RIGHT], following 266 nm laser pulse (8 mJ total on sample).

The lifetime recorded for the transient at 420 nm in previous cycloDAME experiments was 2.3 μs. Interestingly, shorter time scale monitoring in this experiment uncovered another decay at 420 nm with a lifetime comparable to the triplet found in experiments carried out on cycloDAME with 193 nm excitation (~ 2 μs, see Figure 28). This signal is shown below, though the signal-to-noise ratio was poor and it is difficult to ascertain the validity of this trace.

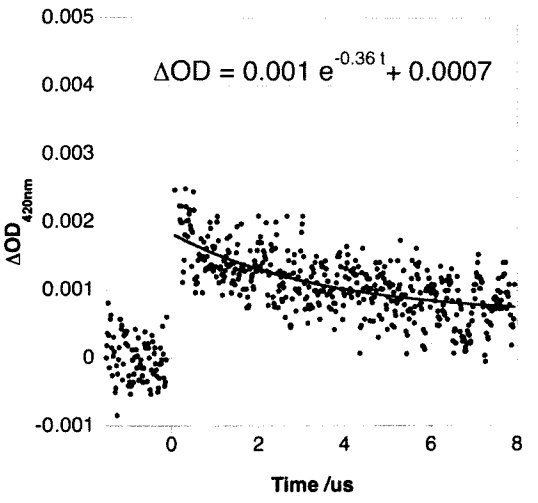

Figure 29. DAME (10 μM) in nitrogen purged acetonitrile solution, under flow conditions. Transient monitored at 420 nm with 1μs per division time resolution, following 266 nm laser excitation (8 mJ total on sample).

The transient spectrum was recorded at time windows based on the growth of the product absorbing at 250 nm. It is important to realize that DAME fluorescence emissions can interfere with measurements where DAME fluoresces (375 to ~ 500 nm), due to possible DAME excitation by the monitoring beam. We disregard these concerns because the absorbance increase observed in the transient spectra is present at wavelengths not only higher than 375 nm, but also in the 320 and 375 nm spectral range where there is no DAME fluorescence.

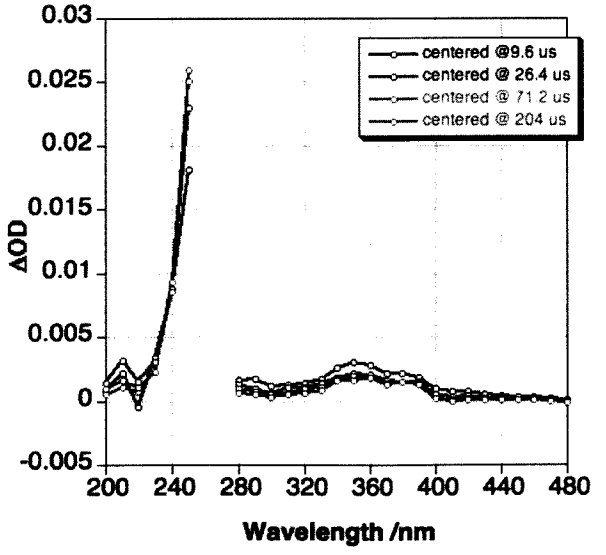

Figure 30. Transient spectra of DAME in nitrogen purged acetonitrile solution (10 μM), excitation with 266 nm laser (8 mJ). Monitoring suspended between 250 and 280 nm to avoid detector saturation by excitation light pulses.

Although some uncertainty persists concerning these transients, it is clear that a long lived species is formed, absorbing not only at 250 nm, but also in the 320 to 400 nm range. Kinetic traces taken in the 320 to 400 nm range show a transient decaying to a value above zero, usually indicative of a product. This decay explains the ΔOD decrease in the transient spectrum of Figure 30 and some are shown below.

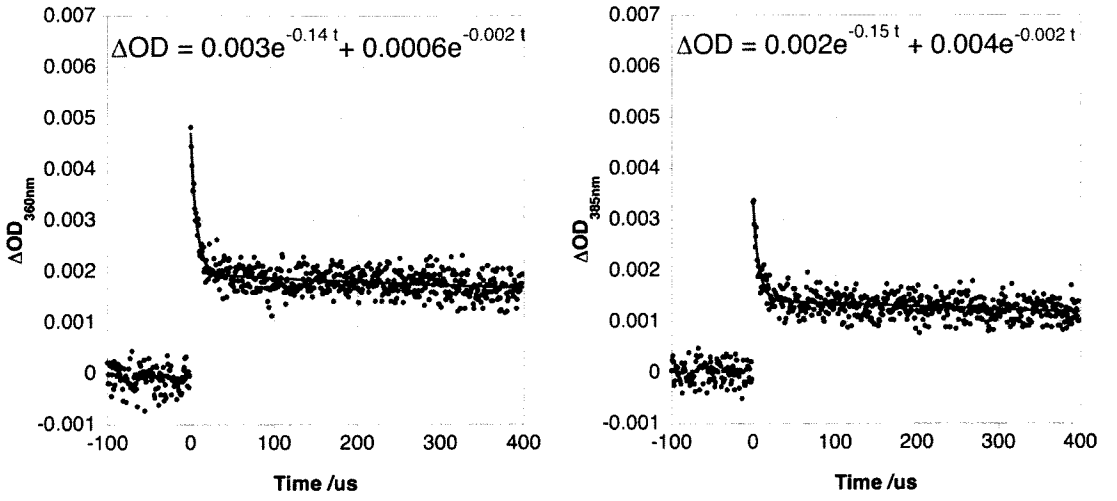

Figure 31. DAME (10 μM) in nitrogen purged acetonitrile, under flow conditions. Transient monitored at 360 and 385 nm following 266 nm laser excitation (8 mJ total on sample).

Kinetic analysis of the decay traces and fitting to 2-exponential decays of the form shown in Equation 9, suggest that the longer lived species is in fact an intermediate, itself decaying to a more stable product with a rate constant of 2 x 10^3 s^{-1} (500 μs). The fast component of these decays have a lifetime of approximately 7 μs, suggesting a triplet pathway since this decay is typically too slow for singlet processes.

Equation 9. Two-exponential decay. $\Delta OD = A_1 e^{-k_1 t} + A_2 e^{-k_2 t}$

It is worthwhile to mention here the well-known decomposition pathway of anthracene to anthraquinone via an endoperoxide. This pathway corresponds nicely to the kinetics observed and will be discussed further in this chapter.

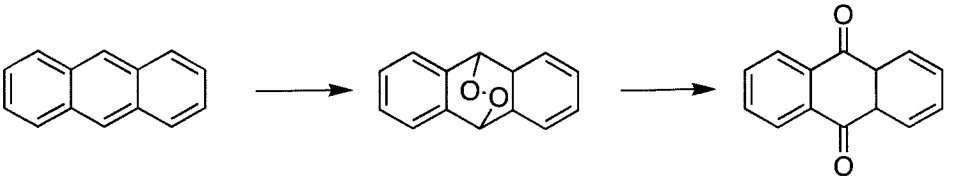

Scheme 7. Decomposition of anthracene to anthraquinone.

ii. Laser-Lamp Wave Experiments

In the second wave study, a solution of the open form (DAME) is first irradiated with UVC light to form the cycloadduct (cycloDAME), which is then cleaved using 193 nm irradiation.

Photocycloaddition was achieved with continuous UVC irradiation (254 nm, 9 x 10^{-9} einsteins, 1500 mJ/cm^2 per second, calculated from 235 to 300 nm), while pulsed laser irradiation at 193 nm (4 x 10^{-9} einsteins, 8 mJ/cm^2 per pulse) caused photocleavage. Absorbance values at irradiation wavelengths were kept low to avoid inner filter effects, though these effects would decrease as the conversion increases at higher irradiation doses.

Formation of cycloDAME and subsequent cleaving of the compound formed were monitored with the absorbance of the solution at 250 nm, which indicates presence of open form DAME. The sample was irradiated until no absorbance change was observed with a dose that was double the previous irradiation. These limit doses were determined with another solution, to avoid photoproduct formation due to over-exposure. The results were compiled for a new solution and are shown in Figure 32 for five cycloadd-cleave cycles.

It is important to note that A_0 is the initial absorbance of the solution, before any type of irradiation. This value was carried through for all cycles (A_0 = 0.13). Furthermore, the energy absorbed shown in the graph is displayed as a total cumulative value in both einsteins and joules.

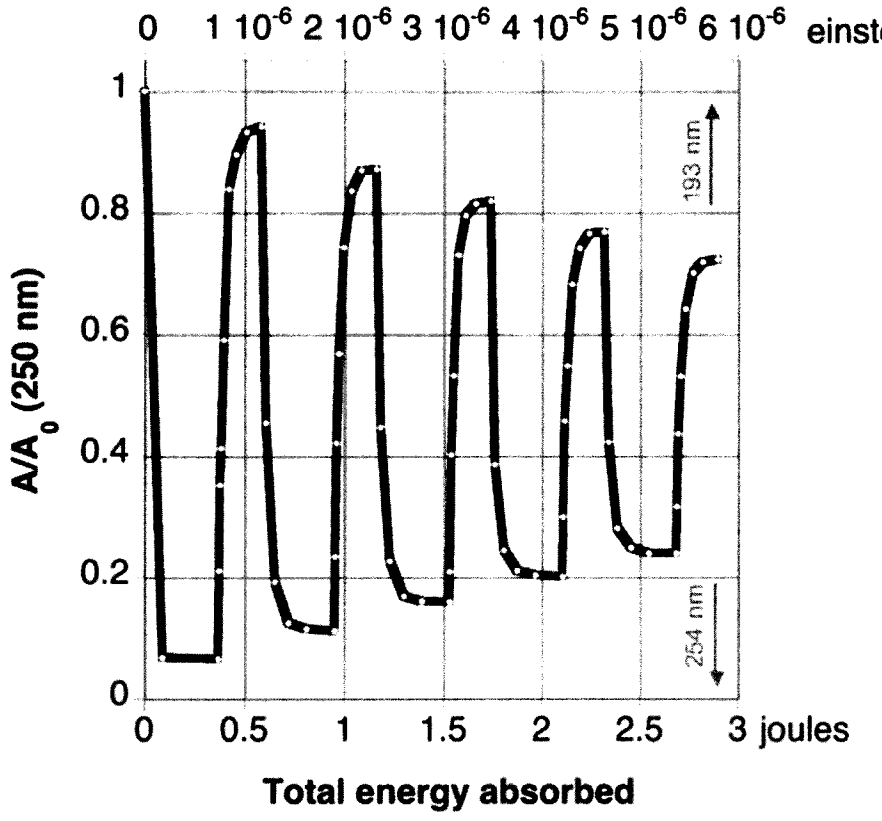

Figure 32. Wave experiment for DAME (10 μM) in nitrogen purged acetonitrile solution (3.5 mL). Total amount of light energy absorbed by the sample is shown in both einsteins and joules.

The data analysis for this experiment is not trivial and is worthy of note, especially for the calculated energy absorbed. This variable is considered as the spectral overlap integral between the output of the light source and the absorbance of the sample. The irradiance of the lamp used (I, J/m²s) is first measured and recorded in joules per area, in order to calculate the total energy delivered to the sample (E_λ in joules) according to Equation 10 where a is the area and t is the time:

Equation 10. $$E_\lambda(J) = I_\lambda \cdot a \cdot t$$

This energy can also be expressed in the unit of einsteins. To do so we calculate the energy in joules of one mole of photons at each irradiation wavelength ($\xi_\lambda = N_A hc/\lambda$) and convert the lamp energy in joules to einsteins by using Equation 11:

Equation 11. $$E_\lambda(eins) = \frac{E_\lambda(J)}{\xi_\lambda}$$

The energy that is delivered to the sample is not necessarily absorbed, and we therefore correct the total energy delivered (E_λ) with the percent absorbance of the compound at each irradiation wavelength ($1-\%T_\lambda$), over the spectral range of irradiation using Equation 12 to finally obtain to total absorbed energy, E_{abs} :

$$E_{abs} = \int E_\lambda (1 - \%T_\lambda) d\lambda$$

Equation 12. Spectral overlap integral.

We integrated over the 235 - 400 nm spectral range for continuous lamp irradiation. A similar analysis was carried out for laser irradiation, though it was for a single irradiation wavelength (193 nm) which rendered the integration unnecessary.

The wave experiment shows clear fatigue, even after the first cycle where the absorbance at 250 nm is not completely regenerated (see Figure 32 at total energy of 5×10^{-6} einsteins).

To ensure that this was not an impurity problem, we tested a highly pure sample of cycloDAME as determined by NMR and UV-Vis spectroscopy, with no absorbance band indicating presence of DAME (250 nm). This sample underwent the irradiation cycle described above, starting with 193 nm light to form DAME. The cycloDAME absorbance band around 200 nm seemed to disappear completely with 193 nm irradiation, although the sample did still absorb in that region due to DAME. The cycloaddition step, on the other hand, did not go to completion. A residual absorbance band centered at 250 nm remained, regardless of UVC irradiation time. It is therefore concluded that the cycloaddition step is limiting even with the tetrahydrofuran-like tether and leads to inefficiencies in the system. Sources of other inefficiencies will be discussed further and are speculated to be due to side-reactions of the anthracene moiety.

Though a wave experiment in film was also performed, the fatigue of the system combined with the extremely thin film made it impossible to measure reliable absorbance spectra after more than one cycle as can be seen in Figure 33, where only 30 % of the signal can be recovered after the second cleaving step. Note that because this experiment began with the cycloadduct, the graph shows the

absorbance ratio (A/A_0) at 250 nm where A_0 is the maximum absorbance at 250 nm obtained after the first cleaving step, in order to compare with the wave in solution.

Nevertheless, it was quite evident that both cleavage and cycloaddition in films are less efficient than in solution. An expansion of the wave in films is also presented to compare with the wave experiment in solution. It shows that cleaving in films is slightly more difficult than in solution while cycloaddition is vastly more difficult.

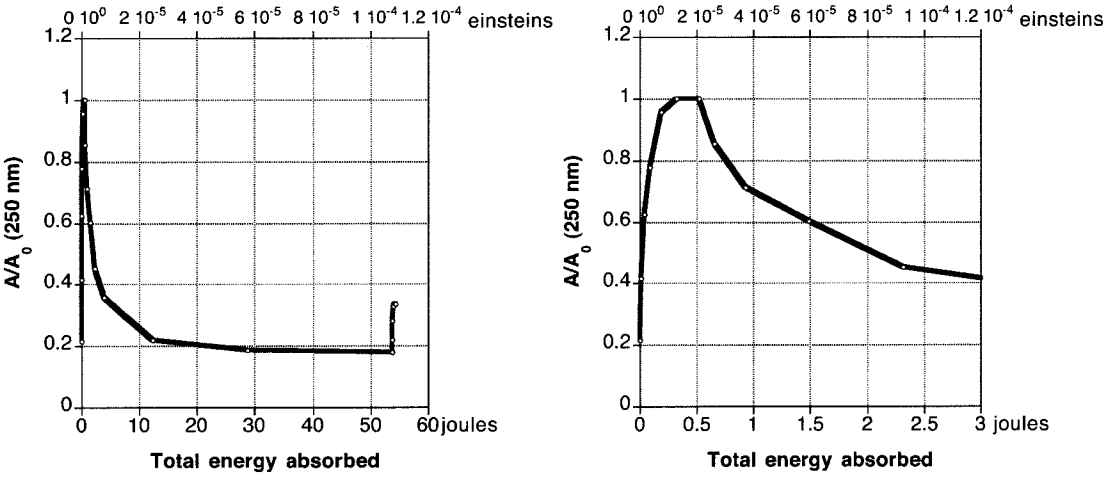

Figure 33. Attempted wave experiment for cycloDAME in Dupont polymer (5 % w/v in diglyme, 1 mM cycloDAME) film, under air. Total amount of light energy absorbed by the sample over monitoring area (6.2 mm^2) is shown in both einsteins and joules. Graph on right shown with expanded energy axis.

The wave experiment in film was conducted with both DAME and cycloDAME as starting material, to investigate the possible rearrangement of molecules in a rigid matrix after opening of the cycloadduct. No detectable difference was recorded between these films. Furthermore, post-193 nm exposure bake (100 °C) did not render subsequent cycloaddition more difficult. It can be postulated that local heating, caused by 193 nm laser pulses used to cleave the cycloadduct, is sufficient to allow opened DAME to rearrange into a more relaxed conformation immediately after ring opening.[30] One could argue that this, probably stretched, conformation is unfavorable for cycloaddition.

The wave experiment in films was carried out in both Dupont polymer (Figure 33) and PMMA (not shown) films. When control films composed of only polymer were

irradiated with large amounts of 193 nm light, important absorbance changes were observed in the 200 nm region of the spectrum. This was a photoreaction of concern for our wavelength region of interest and we investigated this further by exposing films to laser pulses and monitoring the absorbance changes in the 190 - 300 nm spectral region.

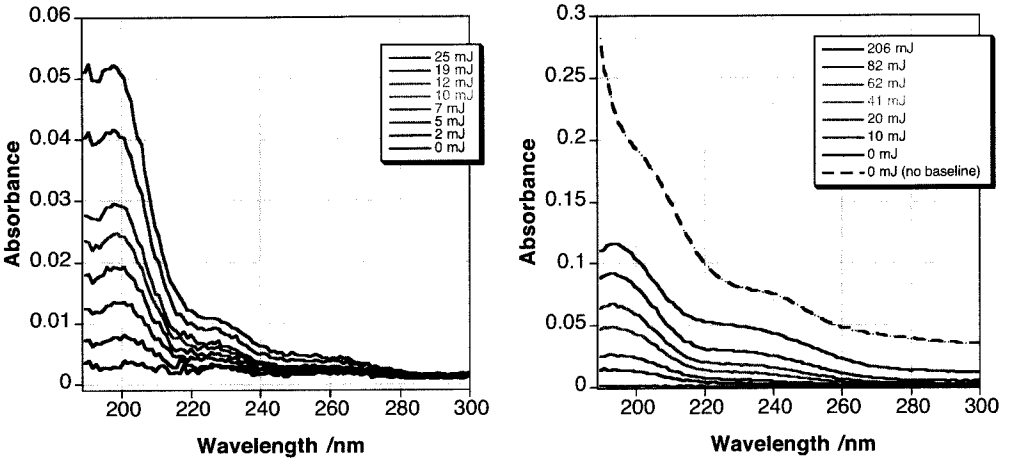

***Figure 34.** [LEFT] Degradation of PMMA film (7 % w/v in 2-heptanone) and [RIGHT] Dupont polymer film (10 % w/v in diglyme), spin-coated with 60 s PAB at 98 °C. Degradation caused by 193 nm light pulses (~ 4 mJ/cm² irradiance per pulse, 6.5 cm² irradiation area). Spectra baselined with non-irradiated polymer film. Power shown is total energy delivered on area monitored (6.2 mm²) by UV-Vis absorbance.*

It is clear from Figure 34 that 193 nm irradiation causes significant absorbance changes. For both experiments, absorbance seemed to be constantly increasing as the irradiation dose was increased. In the right graph, it is interesting to note that the absorbance of the irradiated film tends towards the absorbance profile of non-irradiated polymer with only a quartz disk baseline (black dashed trace). We also note that after 25 mJ of energy delivered to the film, the absorbance at 200 nm increased by approximately 0.05 for PMMA while it was necessary to expose the Dupont polymer film with twice that energy to observe the same absorbance change.

To verify that photoproducts were not being generated by remaining solvent in the film, PMMA (7 % w/v) were cast from 2-heptanone and spun onto quartz disks as described in our methods, but post-application bake (98 °C) times were varied (30, 60, 180 and 300 s). These disks were then irradiated with 193 nm light pulses (2

mJ/cm^2 per pulse, 6.5 cm^2 sample irradiation area). The absorbance change between 190 nm and 500 nm was monitored for irradiation doses up to 2 J (1000 pulses). No detectable difference was observed between disks, though significant increases in absorbance were present in the 200 nm region, as previously seen. It was therefore concluded that heptanone does not play a role in this absorbance increase and that photodegradation must be of the polymer itself. This photodegradation can be dismissed for our experiments because of the low total energy delivered to the film at energies relevant to lithography.

The fatigue of this system is important and it is vital to understand its source. As mentioned earlier, it was speculated that anthracene side-reactions were an important source of our system's inefficiency.

Investigation of possible side-reactions leading to fatigue

Endoperoxides of anthracene and other aromatic compounds have long been of great interest and are studied to this day, notably in the context of photodynamic therapy and the photoreversible release of singlet oxygen.[31-33] Anthracene endoperoxide is a well known product of anthracene when in presence of singlet oxygen.

Disputes persist however concerning the photophysical pathways of aromatic endoperoxides in general and anthracene endoperoxide in particular. Literature generally agrees however that adiabatic cycloreversion occurs from upper excited $\pi\pi^*$ singlet states and forms $^1O_2$ (excitation at 435 nm or shorter). Schmidt has reported that the quantum yield of cycloreversion is dramatically increased (1.5 to 22 %) when excitation is changed from 313 nm to 270 nm.[16] Fidder also demonstrated that cycloreversion occurs with excitation ranging from 260 - 280 nm (Φ_{rev} ~ 30%),[32] which corresponds well with the upper singlet excited states established by Corral (S_4 at 37 000 cm^{-1}, 270 nm; S_2 at 35 900 cm^{-1}, 279 nm),[32] from which cycloreversion is thought to occur. These assignments of upper singlet excited state energies agree with Schmidt's findings. Klein and coworkers dispute these claims however and affirm that cycloreversion occurs from the first singlet

excited state S_1 (36 300 cm^{-1}) when excited at 275 nm.[34] Interestingly, Klein's results remain consistent with other findings if the S_1 assignment is disregarded.

The transition of interest for our research, the one which generates product through homolytic O-O cleavage, has been disputed. Though it is generally accepted that cleavage originates from S_1 ($\pi_{OO}^* \rightarrow \sigma_{OO}^*$).[35] Rigaudy et al. observed that irradiation at wavelengths longer than 435 nm lead to cleavage and rearrangement products.[36, 37] Homolytic O-O cleavage was determined to occur from S_1 at ≤ 23 000 cm^{-1} (435 nm), because irradiation below this wavelength mostly led to anthraquinone and derivatives,[16] though it was recently noted that no experimental evidence had yet to be brought forward to support the existence of the $\pi_{OO}^* \rightarrow \sigma_{OO}^*$ transition.[38] Thus, the $S_0 \rightarrow S_1$ was recently observed for the first time at 291 nm by Corral and coworkers.[38] Their calculations have confirmed this band to be the $\pi_{OO}^* \rightarrow \sigma_{OO}^*$ transition and they have established that S_1 is a diradical, responsible for cleavage and rearrangement products.

In line with Corral's findings, Fidder et al. have also detected the 291 nm band. Fidder has also shown that photogeneration of rearrangement products is not limited to excitation at wavelengths that are above 435 nm, which no longer provides support for the claim that the $S_0 \rightarrow S_1$ transition lies at ≤ 23 000 cm^{-1}. Indeed, Fidder has notably generated anthraquinone with 289 nm excitation of APO (Φ_{AQ} ~ 11 %), bicyclic acetal with 300 nm excitation ($\Phi_{c\text{-}Ac}$ ~ 50 %) as well as diepoxide with 330 nm (Φ_{DE} ~ 75 %).[32]

Semi-empirical calculations performed by Klein have proposed that homolytic cleavage occurs from the triplet manifold. This claim is supported by previous literature, that describes interesting similarities between the triplet and singlet manifold processes.[39] In fact, it was demonstrated that sensitization of APO T_n ($\pi\pi^*$) induces cycloreversion[40] while sensitization of APO T_1 ($\pi^*\sigma^*$) leads to the formation of rearranged products.[37]

We can conclude from the literature that although some confusion remains concerning the exact pathway, photodecomposition of endoperoxides does in fact occur, leading to varied oxidation products of anthracene. Needless to say, this is a

suitable explanation for the fatigue observed in the photocycloreversion. Hence, we performed a series of experiments to synthesize and characterize anthracene as well as DAME endoperoxides.

i. Endoperoxide synthesis (by pulsed Far-UV irradiation)

To emulate the conditions of previous laser irradiation experiments, while keeping a simple product analysis, anthracene was used as a model to generate endoperoxide in solution with laser irradiation at 193 nm.

A solution of anthracene in acetonitrile was irradiated under air with pulses of 193 nm light. The sample was monitored by UV-Vis spectrometry until a significant absorbance was measured at around 270 nm. ^{1}H-NMR analysis of the irradiated sample confirmed the presence of anthraquinone multiplets (δ = 8.33 and 7.81 ppm).

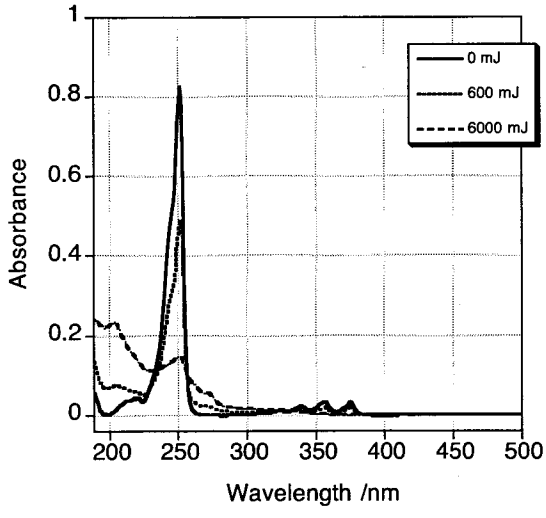

Figure 35. Absorbance profiles of anthracene solution (5 μM, in acetonitrile) irradiated under air by 193 nm laser pulses (1 mJ/cm^2 per pulse, 3 cm^2 sample irradiation area). Total energy on sample shown.

It is apparent from this experiment that high doses of 193 nm light will generate the anthraquinone, likely via the endoperoxide. Indeed, our results indicate that the endoperoxide has a strong absorbance around 193 nm. Absorption of 193 nm photons by the endoperoxide could cleave the endoperoxide bond and yield

anthraquinone. It was discussed by Rigaudy et al. that irradiation of anthracene endoperoxide with wavelengths shorter than 435 nm yields mainly anthraquinone.[37]

To confirm that this applies to the system under investigation, a large volume of DAME solution in acetonitrile (50 mL) underwent 193 nm irradiation in order to produce enough anthraquinone for NMR analysis. The sample was divided in five aliquots to reduce the path length of irradiation. The constantly stirred samples were irradiated under air with high doses of 193 nm light (0.8 mJ/cm^2 per pulse, 9 cm^2 sample irradiation area). The progress of the photoreaction was monitored by UV-Vis spectroscopy. When the absorbance spectrum showed a significant band around 270 nm (after 6 000 mJ delivered), irradiation was terminated and the solvent was removed under high vacuum, thus avoiding heating the endoperoxide and artificially generating anthraquinone.

The irradiated DAME sample, as well as a DAME sample dissolved in acetonitrile and subsequently dried in vacuo, were submitted for NMR analysis. The NMR spectrum of the reference DAME sample was identical to previous spectra of DAME that had not been dissolved in acetonitrile. We conclude that acetonitrile does not affect DAME on the time scale of this experiment. Not surprisingly, the ^{1}H-NMR spectrum of the irradiated sample contained small DAME peaks as well as anthraquinone multiplets at δ = 8.33 and 7.81 ppm. This experiment is therefore further evidence that DAME can photodecompose, likely via the endoperoxide, when irradiated with high doses of 193 nm light.

ii. Endoperoxide synthesis (by continuous visible irradiation)

Anthracene endoperoxide can be chemically generated directly from anthracene and singlet oxygen[41-43] *as shown in Scheme 8.*

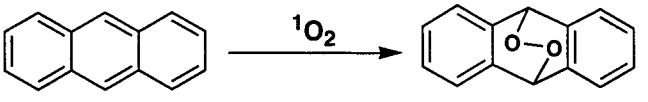

Scheme 8. Anthracene endoperoxide synthesis.

Rose Bengal can be used as a photosensitizer, producing singlet oxygen with visible light excitation and thus avoiding anthracene photodimerization which occurs with irradiation below 385 nm.

Anthracene endoperoxide was first synthesized following the method published by Schmidt et al. in carbon disulfide,[16] irradiated overnight. This crude product mixture displayed incomplete hydrocarbon conversion as well as side products in the NMR spectra (full table of NMR shifts on pages 81 and 83). The crude product mixture was nevertheless purified by column chromatography. After purification, ^{1}H-NMR revealed that the characteristic vicinal proton signal of the endoperoxide (δ = 6.03 ppm) had almost completely disappeared and anthraquinone multiplets appeared in the aromatic region. As it is well known that anthracene endoperoxide thermally decomposes to anthraquinone,[32, 36, 37] we conclude that the synthesized endoperoxide was converted to anthraquinone in the purification process due to heating. Stability of the endoperoxide on silica was later confirmed using two-dimensional thin layer chromatography.

Anthracene endoperoxide was therefore synthesized for a second time, this time in dichloromethane. Irradiation time was reduced to 3 hours, to limit secondary product formation as well as the amount of rose Bengal leaching into solution.

^{1}H-NMR analysis of the crude product mixture showed a strong singlet at δ = 6.03 ppm, attributed to the endoperoxide vicinal proton. The NMR spectrum displayed a clean aromatic region, showing only anthracene starting material and two multiplets attributed to anthracene endoperoxide aromatic protons (δ = 7.29 and 7.42 ppm), shifted slightly up-field with respect to anthracene.

Products were also characterized by UV-Vis spectroscopy:

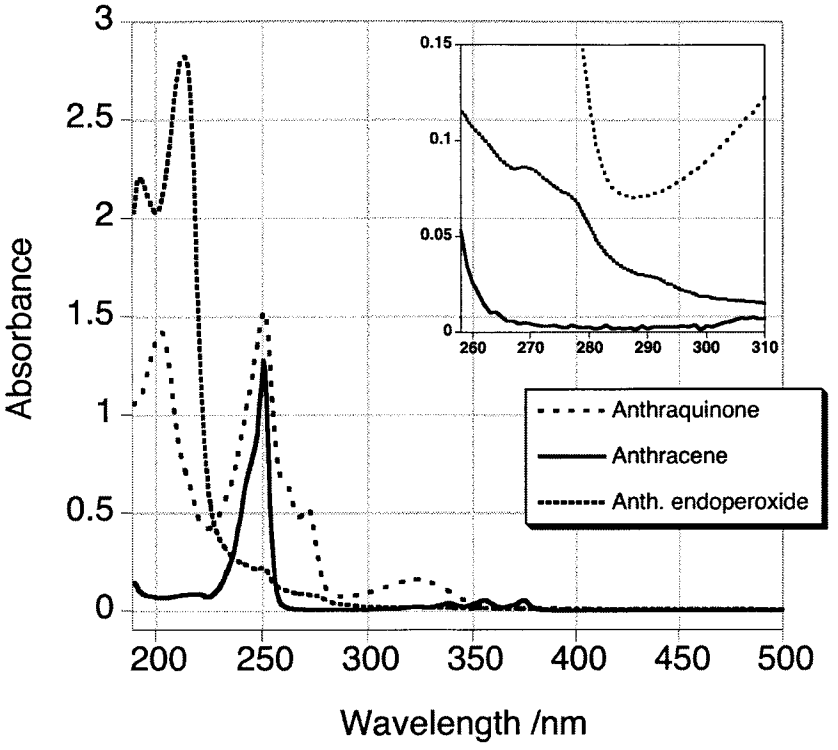

Figure 36. Anthracene starting material (5 μM), endoperoxide oxidation product (60 μM) and its thermal decomposition product anthraquinone (30 μM) in acetonitrile, measured in a 10 mm path length cuvette. Inset showing anthracene endoperoxide absorbance bands in 260 to 310 nm region.

Interestingly, the endoperoxide displays a peak around 192 nm. This would make it highly susceptible to excitation at 193 nm during laser cleaving experiments. The extinction coefficient of anthracene endoperoxide can be obtained from our results and we calculated that in acetonitrile, APO $\varepsilon_{193\ nm}$ *= 33 200* $M^{-1}\ cm^{-1}$*. Note that the absorbance of anthracene endoperoxide at 250 nm indicates a minor anthracene starting material impurity.*

Anthraquinone on the other hand, retains the characteristic anthracene band at 250 nm but also displays a strong absorbance at 200 nm, slightly to the red of the endoperoxide. A significant shoulder to the red of the anthracene band is also present at approximately 270 nm. Finally, a characteristically broad peak centered at 323 nm can be observed, which is likely the ketone-like $n\pi^*$ *transition.*

DAME endoperoxide (DAMEPO) was synthesized with the same method used for anthracene endoperoxide.

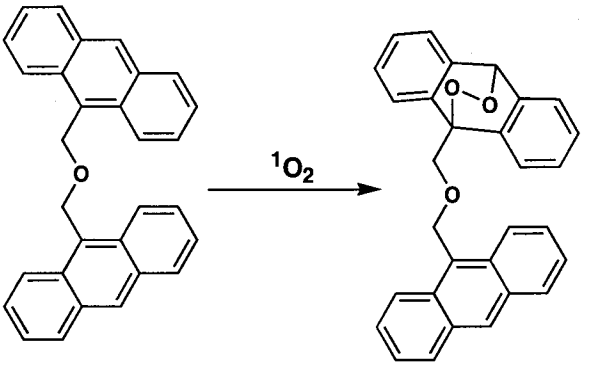

Scheme 9. DAME endoperoxide synthesis.

^{1}H-NMR was used to characterize the products obtained from this synthesis and NMR spectra of commercial anthracene and anthraquinone were obtained as references for NMR studies.

^{1}H-NMR shifts, in $CDCl_3$	9, 10 - positions	1, 4, 5, 8 - positions	2, 3, 6, 7 - positions	Tether (if applicable)
Anthracene	8.43 (2H, s)	8.01 (4H, m)	7.47 (4H, m)	-
Anthraquinone	-	8.32 (4H, m)	7.81 (4H, m)	-
Anthracene endoperoxide (APO)	6.03 (2H, s)	7.42 (4H, m)	7.29 (4H, m)	-
DAME	8.47 (2H, s)	8.28 (4H, dd) 8.01 (4H, dd)	7.42 (8H, m)	5.66 (4H, s)
cDAME	4.54 (2H, s)	7.16 (4H, m)	6.94 (4H, m) 6.86 (8H, m)	4.85 (4H, s)
DAMEPO endoperoxide ring	5.96 (1H, s)	7.36 (2H, dd) 7.28 (2H, dd)	7.20 (2H, td) 7.09 (2H, td)	4.70 (2H, s)
anthracene ring	8.51 (1H, s)	8.54 (2H, m) 8.06 (2H, dd)	7.58 (2H, m) 7.52 (2H, m)	5.84 (2H, s)

Table 3. ^{1}H-NMR shifts of anthracene and derivatives, in deuterated chloroform and calibrated to residual solvent peak at δ = 7.26 ppm

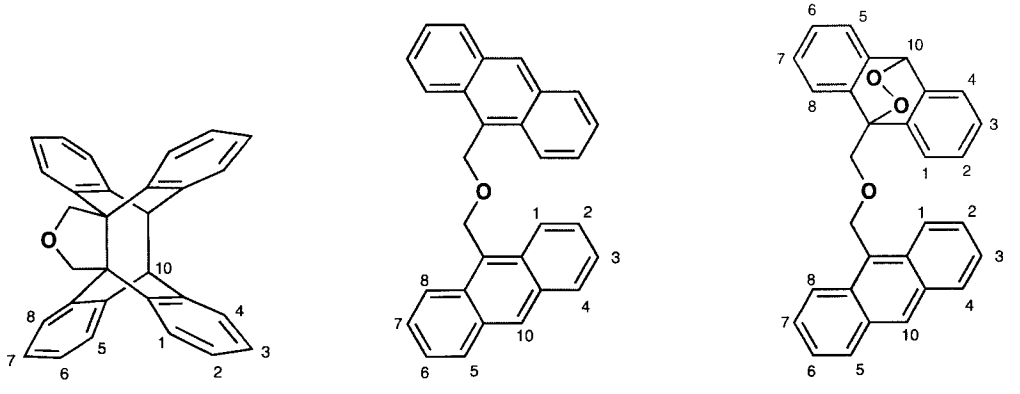

Structure 5. cycloDAME, DAME and DAMEPO proton labeling.

Aside from DAME starting material, the crude product mixture ^{1}H-NMR spectrum displayed a strong singlet at δ = 5.96 ppm, which we attributed to the proton vicinal to the endoperoxide bridge (H_{10}) though showing up at slightly higher field than the anthracene endoperoxide (δ = 6.03 ppm).

Low intensity anthraquinone-like multiplets were also observed (δ = 8.32 and 7.81 ppm) in the aromatic region, which integrate equally with respect to themselves. This compound eluted in fractions preceding the endoperoxide-containing fraction, probably anthraquinone. The absorbance of this fraction suggests the presence of an anthraquinone, though the fraction was not pure enough for conclusive characterization.

The proton splitting pattern of DAME is interesting and in itself worthy of note. First of all, protons in the 10-position (abbreviated H_{10}) appear as a singlet at δ = 8.47 ppm. Protons H_1 (δ = 8.28 ppm) are split by adjacent H_2 into a doublet (J = 8.8 Hz) and these peaks are broadened by long-range coupling with meta-H_3 (J < 1 Hz), which brings this signal close to a doublet of doublets.‡ In fact, several other examples of long-range coupling can be observed. Indeed, the H_4 signal (δ = 8.01 ppm) is split first into a doublet (J = 8.6 Hz) by adjacent H_3 and then again by meta-H_2 (J = 1.1 Hz), which leads to a doublet of doublets. However, H_3 couples to adjacent H_4 (J = 8.6 Hz) and H_3 with a very similar J-value, which leads to a triplet rather than a doublet of doublets. H_3 is also coupled to meta-H_1 (J < 1 Hz), which splits the triplet into a triplet of doublets. Although H_2 and H_3 are very similar, they are not perfectly symmetric because of the tether. Thus, H_2 is coupled similarly with H_1, H_3 and H_4 to generate a second triplet of doublets. The combined signals of H_2 and H_3 gives the multiplet at δ = 7.42 ppm.

The splitting of DAME endoperoxide (DAMEPO) protons is similar to that of DAME. One notable difference is the separation of the signal assigned to H_2 and H_3. Indeed, the multiplet that is observed at δ = 7.42 ppm for DAME is much more clearly resolved for DAMEPO and seen as two true triplets of doublets at δ = 7.09 and 7.20 ppm, with J = 1.1 and 7.5 Hz.

---

‡ For the remainder of this description we will refer to protons 1 through 4 only and these will be meant to represent protons 1 to 8 ($H_1 = H_8$, $H_2 = H_7$, $H_3 = H_6$ and $H_4 = H_5$).

^{13}C-NMR, in $CDCl_3$	Chemical shift, δ (ppm)
Anthracene 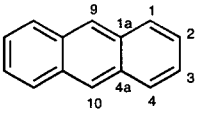	131.8 (C_{1a}, C_{4a}) 128.3 (C_1, C_4) 126.4 (C_9, C_{10}) 125.5 (C_2, C_3)
Anthraquinone 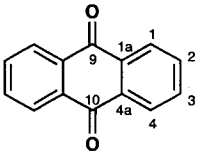	183.3 (C_9, C_{10}) 134.3 (C_2, C_3) 133.7 (C_{1a}, C_{4a}) 127.4 (C_1, C_4)
DAME 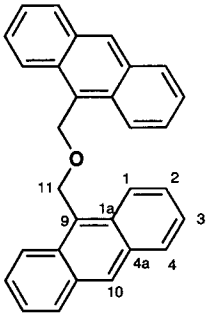	138.7 (C_9) 131.6 (C_{4a}) 131.3 (C_{1a}) 129.1 (C_4) 126.2 (C_{10}) 125.1 (C_1) 124.5 (C_2, C_3) 64.5 (C_{11})
cycloDAME 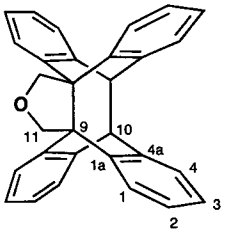	144.0 (C_{1a}) 143.0 (C_{4a}) 127.7, 126.1, 125.7, 124.2 (C_1, C_2, C_3, C_4) 73.2 (C_{11}) 63.9 (C_9) 54.0 (C_{10})

Table 4. ^{13}C-NMR shifts of anthracene and derivatives, in deuterated chloroform and calibrated to residual solvent peak at δ = 77.16 ppm.

Although the DAME spectrum was contaminated with a small amount of cycloDAME, we were able to identify peaks by comparing to the cleaner cycloDAME spectrum. As expected, aromatic quaternary carbons were of low intensity and at shifts close to δ = 140 ppm (DAME C_9; cycloDAME C_{1a} and C_{4a}). Aliphatic quaternary C_9 and tertiary C_{10} present only in cycloDAME had easily identifiable high field shifts (δ = 63.9 and 54.0 ppm) as well as a characteristic low intensity. Interestingly, DAME-C_{10} (δ = 126.2 ppm) was essentially not shifted from anthracene (δ = 126.1 ppm), though necessarily at much lower field than cycloDAME-C_{10}. Also note the shift of C_{11}, at a lower field than expected for a -CH_2- group because of the adjacent electron density withdrawing oxygen atom.

After characterization of the DAME endoperoxide by NMR and MS, we obtained the absorbance profile of our product:

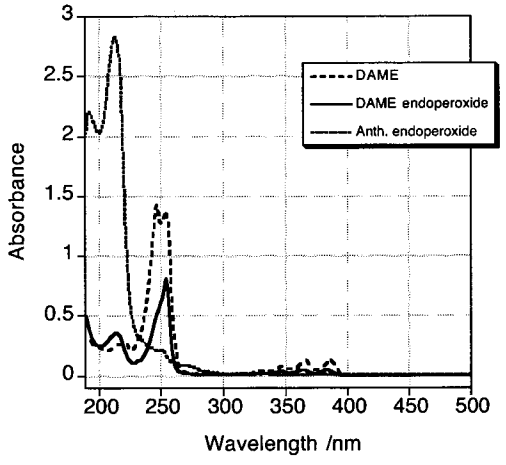

Figure 37. DAME starting material (10 μM), DAME endoperoxide (~5 μM)* as well as anthracene endoperoxide for comparison (60 μM), all in acetonitrile (10 mm path length).

NMR and MS results indicate that only one anthracene moiety is bridged by an endoperoxide, thus the characteristic bands at 250 nm and 320 - 400 nm of the unmodified anthracene moiety are visible in the absorbance profile.

Note that the ^{13}C-NMR of DAMEPO could not be recorded due to decomposition of the compound over the time that was attempted to record the spectrum. Thermal

* Because of limited DAME endoperoxide product obtained from synthesis, it was impossible to accurately weigh exact DAMEPO mass used in this solution.

decomposition of DAMEPO at room temperature in deuterated chloroform was indeed observed over a period of a few weeks and monitored by ^{1}H-NMR. Initially, the spectrum of DAME endoperoxide was clean in the aromatic region, with no peaks showing to indicate presence of a quinone-like compound. Several days later, multiplets centered at δ = 8.3 and 7.8 ppm, characteristic of anthraquinone shifts, appeared. We calculated DAMEPO decomposition to be 30 % after 5 days and 95 % after 15 days at room temperature. Indeed, thermolysis of anthracene endoperoxide (APO) performed by Corral et al. indicated the likely existence of the diradical intermediate reachable by thermal activation from the APO ground state.[38]

iii. Heating the endoperoxide: rate constant of O-O thermal cleavage

To investigate the endoperoxide thermal decomposition, solutions of anthracene and DAME endoperoxides were heated in solution and monitored by UV-Vis spectrometry and ^{1}H-NMR. We show the results obtained by heating of anthracene endoperoxide in Figure 38.

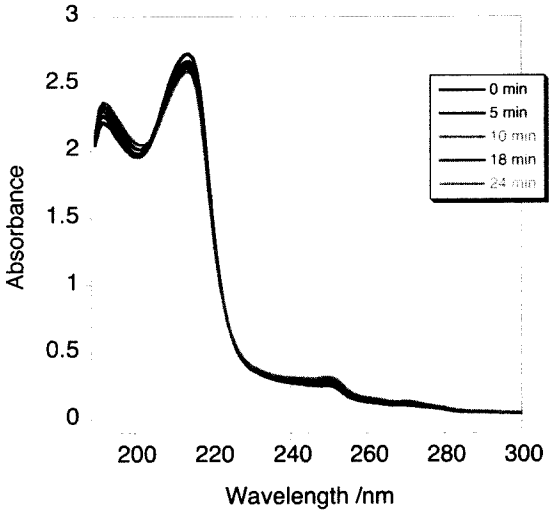

Figure 38. Absorbance profiles of anthracene endoperoxide in acetonitrile (65 μM, 3 mL) heated and continuously stirred at 74 °C for increasing amounts of time, showing the onset of its decomposition.

The absorbance profiles showed at least two clean isosbestic points, located around 205 and 225 nm. These indicate that the endoperoxide (λ_{abs} = 192 and 214 nm) is cleaving to generate anthraquinone (λ_{abs} = 203, 250, 273 nm). The absorbance

decrease at 214 nm shows the endoperoxide concentration decreasing, while the absorbance increase in the 200 nm range, as well as 240 to 280 nm range, shows the anthraquinone concentration increasing. We speculate that the decrease of the endoperoxide absorbance band at 192 nm is not visible because it is masked by the anthraquinone band growing in around 200 nm. A graph was therefore constructed to observe these changes more accurately, by monitoring the relevant wavelengths as shown in Figure 39.

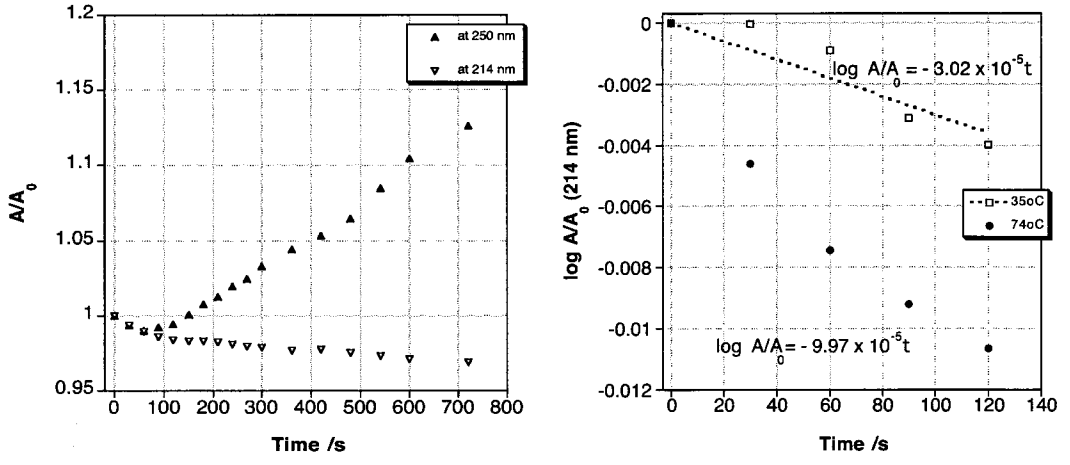

Figure 39. Anthracene endoperoxide (65 μM) in a constantly stirred acetonitrile solution. [LEFT] Absorbance peak monitoring of endoperoxide (214 nm) and anthraquinone (250 nm) with increasing heating time at 74 °C and [RIGHT] thermal decomposition of anthracene endoperoxide monitored by absorbance change at 214 nm at 35 and 74 °C.

This analysis makes the absorbance changes quite clear, showing definite loss of endoperoxide and significant subsequent generation of anthraquinone. The data treatment, using the initial absorbance (A_0), allows us to properly compare these changes and also safely disregard the initial endoperoxide absorbance at 250 nm due to impurities.

The kinetics of endoperoxide thermal decomposition were also studied at temperatures ranging from 35 to 78 °C, in order to stay below the boiling point of the solvent (b.p. acetonitrile = 82 °C). The absorbance change (A/A_0) at 214 nm was used as a probe and not surprisingly showed a faster rate of change at higher temperatures, shown in Figure 39. This data can be used to extract the rate constant using the a simple exponential decay function as shown in Equation 13

below, where A_0 is the initial absorbance before heating, k is the rate constant and A is the absorbance after heating time t.

Equation 13. $$A = A_0 e^{-kt}$$

From the results obtained in the thermal decomposition study, we calculate the rate constants, k = 3.0 x 10^{-5} and 10.0 x 10^{-5} s^{-1}, for 35 and 74 °C respectively. The latter is only an approximation given the deviations from linearity present in Figure 39.

The Arrhenius Equation relates the temperature to the observed rate constant (k), where B is the pre-exponential factor, E_A is the activation energy, R is the gas constant (8.314 J $K^{-1}mol^{-1}$, 1.985 cal $K^{-1}mol^{-1}$) and T is the temperature (in Kelvin).

Equation 14. Arrhenius Equation.[44] $$k = Be^{-E_A/RT}$$

Manipulations to the Arrhenius Equation allow us to determine the activation energy, using rate constants measured at different temperatures, as shown in Equation 15.

Equation 15. $$\ln\frac{k_1}{k_2} = -\frac{E_A}{R}\left(\frac{1}{T_2} - \frac{1}{T_1}\right)$$

On the basis of the limited data available, we therefore estimate the thermal decomposition activation energy of anthracene endoperoxide to be 6.5 kilocalories, or 27.2 kilojoules. It is important to note that this value is not precise, as we are dealing with only two rate constants from which to calculate E_A, one of which is only an approximation.

Thermal decomposition studies were also carried out for DAME endoperoxide at varying temperatures. Endoperoxide decomposition was monitored at 214 nm as in the previous experiments with APO. Because the decomposition was significantly slower for DAMEPO, we obtained a curve fitting well to an exponential decay of the form shown in Equation 13, with the addition of a pre-exponential factor and a shift

to account for the decay not returning to zero. We fit the exponential decay directly to the curve in Figure 40 below.

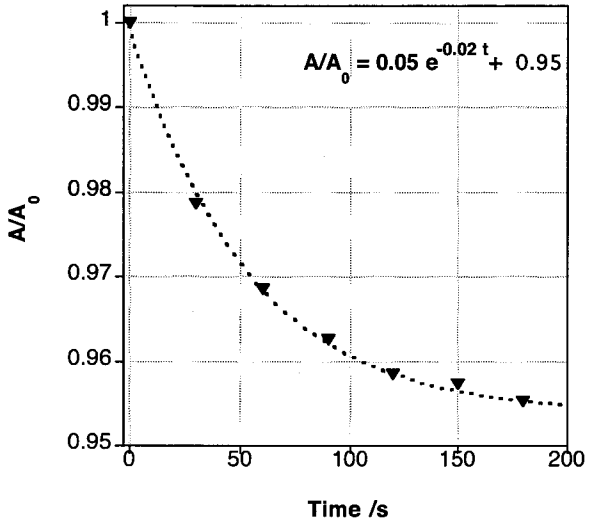

Figure 40. Thermal decomposition of DAMEPO (~5 μM)* at 74 °C in a constantly stirred acetonitrile solution monitored by absorbance change at 214 nm with increasing heating time.

Using this data, the thermal decomposition rate constant of DAME endoperoxide was determined to be approximately 2.0 x 10^{-3} s^{-1} at 74 °C, which gives a lifetime of 50 s. This measurement was repeated for three DAMEPO samples and the error was found to be less than 5 %.

It is important to point out that the rate constants of DAME and anthracene endoperoxides differ by more than one order of magnitude. DAMEPO is therefore much less stable than APO which has a lifetime of almost 30 hours at 74 °C.

* Because of limited DAME endoperoxide product obtained from synthesis, it was impossible to accurately weigh exact DAMEPO mass used in this solution.

CONCLUSION

The tethered anthracene derivative DAME was studied as a candidate for photochromic layers in lithographic applications. Although an ideal compound would show no fatigue and perfect reversibility; high cleaving quantum yields and efficient cycloaddition make DAME a continuing molecule of interest.

Obvious problems with anthracene derivatives are highly common endoperoxide formation and subsequent decomposition products. These reactions effectively remove photoactive material from the photochromic layer and contribute to permanent darkening of that layer.

Reversion of endoperoxide formation has been studied and found to occur both via thermolysis and photolysis.[45-47] *To reduce the fatigue of the DAME system, these processes could be used in conjunction with specifically functionalized systems to regenerate active material. It should be noted that DAME endoperoxide was found to be less thermally stable than anthracene endoperoxide - a possible advantage for reversion.*

Processes occurring with 266 nm excitation of DAME and cycloDAME are of interest and should be investigated further. Notably, the possibility of radical reactions could be confirmed. The intermediate as well as product occurring after excitation should be identified.

The DAME system could likely be tuned and optimized in order to take advantage of the photochromic switch it provides in lithographic applications and in particular, as a component of reversible contrast enhancement layers.

REFERENCES

1. Yu, B.; Meyyappan, M., Nanotechnology: Role in Emerging Nanoelectronics. *Solid State Electronics* **2006**, 50, 536 - 544.

2. Moore, G. E., Cramming More Components Onto Integrated Circuits. *Electronics* **1965**, 38, (8), 114 - 117.

3. Thompson, S. E.; Parthasarathy, S., Moore's Law: The Future of Si Microelectronics. *Materials Today* **2008**, 9, (6), 20 - 25.

4. Zimmerman, P.; Byers, J.; Rice, B.; Ober, C.; Giannelis, E.; Rodriguez, R.; Wang, D.; O' connor, N.; Lei, X.; Turro, N.; Liberman, V.; Palmacci, S.; Rothschild, M.; Lafferty, N.; Smith, B., Development and Evaluation of 193 nm Immersion Generation-three Fluid Candidates. *Proc. of SPIE* **2008**, 6923, 69230/A1-10.

5. Whitesides, G.; Love, J., The Art of Building Small. *Scientific American* **2001**, 285, (3), 39 - 47.

6. Vieu, C.; Carcenac, F.; Pepin, A.; Chen, Y.; Mejias, M.; Lebib, L.; Manin Ferlazzo, L.; Couraud, L.; Launois, H., Electron Beam Lithography: Resolution Limits and Applications. *Applied Surface Science* **2000**, 164, (1-4), 111 - 117.

7. Moon, S.; Kim, J., Chemistry of Photolithographic Imaging Materials Based on the Chemical Amplification Concept. *Journal of Photochemistry and Photobiology C: Photochemistry Reviews* **2007**, 8, 157 - 173.

8. Lee, S.; Jen, K.; Willson, C.; Byers, J.; Zimmerman, P.; Turro, N., Materials modeling and development for use in double-exposure lithography applications. *Journal of Micro/Nanolithography* **2009**, 8, (1), 011011/1-11.

9. O'Connor, N. A.; Berro, A.; Lancaster, J. R.; Gu, X.; Jockusch, S.; Tomoki, N.; Ogata, T.; Lee, S.; Zimmerman, P. A.; Wilson, G. C.; Turro, N. J., Toward the Design of a Sequential Two Photon Photoacid Generator for Double Exposure Photolithography. *Chemistry of Materials* **2008**, 20, (24), 7374 - 7376.

10. Bristol, R.; Shykind, D.; Kim, S.; Borodovsky, Y.; Schwartz, E.; Turner, C.; Masson, G.; Min, K.; Esswein, K.; Blackwell, J. M.; Suetin, N., Double-Exposure Materials for Pitch Division with 193nm Lithography: Requirements, Results. *Proc. of SPIE* **2009**, 7273, 727307/1-12.

11. Byers, J.; Lee, S.; Jen, K.; Zimmerman, P.; Turro, N. J.; Wilson, G. C., Double Exposure Materials: Simulation Study of Feasibility. *Journal of Photopolymer Science and Technology* **2007**, 20, 707 - 717.

12. Bouas-Laurent, H.; Desvergne, J.; Castellan, A.; Lapouyade, R., Photodimerization of Anthracenes in Fluid Solutions: (Part 2) Mechanistic Aspects of the Photocycloaddition and of the Photochemical and Thermal Cleavage. *Chemical Society Reviews* **2001**, 30, (4), 248 - 263.

13. Bouas-Laurent, H.; Desvergne, J.; Castellan, A.; Lapouyade, R., Photodimerization of Anthracenes in Fluid Solution: Structural Aspects. *Chemical Society Reviews* **2000**, 29, 43 - 55.

14. Scaiano, J. C., Nanosecond Laser Flash Photolysis: A Tool for Physical Prganic Chemistry. In *Reactive Intermediate Chemistry*, Moss, R. A.; Platz, M. S.; Jones, M., Eds. John Wiley & Sons, Inc.: 2004.

15. Hong, M.; Jen, A. K.-Y., Polymer-Based Optical Waveguide Materials, Processing, and Devices. *Advanced Materials* **2002**, 14, (19), 1339 - 1365.

16. Schmidt, R.; Schaffner, K.; Trost, W.; Brauer, H. D., Wavelength-dependent and Dual Photochemistry of the Endoperoxides of Anthracene and 9,10-Dimethylanthracene. *Journal of Physical Chemistry* **1984**, 88, (5), 956 - 958.

17. Turro, N. J.; Ramamurthy, V.; Scaiano, J. C., *Principles of Molecular Photochemistry*. University Science Books: Sausalito, California, 2009.

18. Becker, H.; Elebring, T.; Sandros, K., Photochemical Intramolecular 4 pi + 4 pi Cycloaddition of 1, 2-Di (9-anthryl) ethanes. *Journal of Organic Chemistry* **1982**, 47, (6), 1064 - 1068.

19. Wang, Z.; Weininger, S.; McGimpsey, G. W., Photochemistry of the Triplet T2 State of Anthracene. *Journal of Physical Chemistry* **1993**, 97, (2), 374 - 378.

20. Tomlinson, W. J.; Chandross, E. A.; Fork, R. L.; Pryde, C. A.; Lamola, A. A., Reversible Photodimerization: A New Type of Photochromism. *Applied Optics* **1972**, 11, (3), 533 - 548.

21. Fessenden, R. W.; Carton, P. M.; Shimamori, H.; Scaiano, J. C., Measurement of the Dipole Moments of Excited States and Photochemical Transients by Microwave Dielectric Absorption. *Journal of Physical Chemistry* **1982**, 86, 3803 - 3811.

22. Wagner, P. J.; Keslo, P. A.; Kemppainen, A. E.; McGrath, J. M.; Scott, H. N.; Zepp, R. G., Type II Photoprocesses of Phenyl Ketones. Glimpse at the Behavior of 1,4 Biradicals. *Journal of the American Chemical Society* **1972**, 94, 7506 - 7512.

23. Lakowicz, J. R., *Principles of Fluorescence Spectroscopy*. Second Edition ed.; Kluwer Academic: New York, 1999.

24. Carmichael, I.; Helman, W. P.; Hug, C. L., Extinction Coefficients of Triplet-Triplet Absorption Spectra of Organic Molecules in Condensed Phases. *Journal of Chemical Reference Data* **1987**, 16, (2), 239 - 260.

25. Jackson, G.; Livingston, R., Unimolecular Decay of the Triplet State of Anthracene in Fluid and Viscous Media. *Journal of Chemical Physics* **1961**, 35, (6), 2182 - 2186.

26. Jackson, G.; Livingston, R.; Pugh, A., Experimental Study of the Triplet State of Anthracene in Fluid Solutions. *Transactions of the Faraday Society* **1960**, 56, 1635 - 1639.

27. Livingston, R.; Tanner, D., The Triplet State of Anthracene in Liquid Solutions. *Transactions of the Faraday Society* **1958**, 54, 765 - 771.

28. Nielsen, B.; Jorgensen, K.; Skibsted, L., Triplet—triplet Extinction Coefficients, Rate Constants of Triplet Decay and Rate Constant of Anthracene Triplet Sensitization by Laser Flash Photolysis. *Journal of Photochemistry and Photobiology A.* **1998,** 112, (2-3), 127 - 133.

29. Hashimoto, S.; Miyashita, T.; Hagiri, M., Hypermobility of Aromatic Guest Species in Zeolite as Observed from Anthracene Triplet Self-Quenching within NaY in the Presence of Critical Amounts of Coadsorbed Solvents. *Journal of Physical Chemistry B* **1999,** 103, 9149 – 9155.

30. Ivan, M. G. Photochemistry Applied in Optical Lithography (Ph.D. Thesis). University of Ottawa, Ottawa, 2007.

31. Bonnett, R., Photosensitizers of the Porphyrin and Phthalocyanine Series for Photodynamic Therapy. *Chemical Society Reviews* **1995,** 24, 19 - 33.

32. Fidder, H.; Lauer, A.; Freyer, W.; Koeppe, B.; Heyne, K., Photochemistry of Anthracene-9,10-endoperoxide. *The Journal of Physical Chemistry A* **2009,** 113, (22), 6289 - 6296.

33. Nagaoka, Y.; Otsu, K.; Okada, F.; Sato, K.; Ohba, H.; Kotani, N.; Fujii, J., Specific Inactivation of Cysteine Protease-type Cathepsin by Singlet Oxygen Generated from Naphthalene Endoperoxides. *Biochemical and Biophysical Research Communications* **2005,** 331, 215 - 223.

34. Klein, A.; Kalb, M.; Gudipati, M., New Assignment of the Electronically Excited States of Anthracene-9,10-endoperoxide and Its Derivatives: A Critical Experimental and Theoretical Study. *The Journal of Physical Chemistry A* **1999,** 103, (20), 3843 - 3853.

35. Brauer, H. D.; Schmidt, R., Comment on "New Assignment of the Electronically Excited States of Anthracene-9, 10-endoperoxide". *Journal of Physical Chemistry A* **2000,** 104, 164 - 165.

36. Rigaudy, J.; Baranne-Lafont, J.; Defoin, A.; Cuong, N. K., Transformations Thermiques des Photooxydes Meso des Acenes—II Cas du Photooxyde d'Anthracene. *Tetrahedron* **1978,** 34, 73 - 82.

37. Rigaudy, J.; Defoin, A.; Baranne-Lafont, J., syn-Anthracene 4a, 10: 9, 9a-Dioxide Dedicated to Professor Egbert Havinga on the occasion of his 70th birthday. *Angewandte Chemie International Edition in English* **1979,** 18, (5), 413 - 415.

38. Corral, I.; Gonz á lez, L.; Lauer, A.; Freyer, W.; Fidder, H., Identifying the Low-lying Electronic States of Anthracene-9,10-endoperoxide. *Chemical Physics Letters* **2008,** 452, 67 - 71.

39. Katscher, U.; Schmidt, R.; Brauer, H. D., Triplet-sensitized Cycloreversion of Endoperoxides of Aromatic Compounds - An Adiabatic Reaction Route. *Chemical Physics Letters* **1993,** 205, (1), 75 - 79.

40. Stevens, B.; Glauser, W. A., The Benzene-sensitized Cycloreversion of 9,10-Peroxy,9,10-dimethylanthracene in Solution. *Chemical Physics Letters* **1986,** 129, 120 - 124.

41. Foote, C. S.; Wexler, S., Singlet Oxygen. A Probable Intermediate in Photosensitized Autoxidations. *Journal of the American Chemical Society* **1964**, 86, 3880 - 3881.

42. Foote, C. S., Photosensitized Oxygenations and the Role of Singlet Oxygen. *Accounts of Chemical Research* **1968**, 1, 104 - 110.

43. Sugiyama, N.; Iwata, M.; Yoshioka, M.; Yamada, K.; Aoyama, H., Photooxidation of Anthracene. *Bulletin of the Chemical Society of Japan* **1969**, 42, 1377 - 1379.

44. Silbey, R. J.; Alberty, R. A.; Bawendi, M. G., *Physical Chemistry.* Fourth Edition ed.; John Wiley & Sons, Inc.: 2005.

45. Aubry, J.; Pierlot, C.; Jean Rigaudy, a.; Schmidts, R., Reversible Binding of Oxygen to Aromatic Compounds. *Accounts of Chemical Research* **2003**, 36, 668 - 675.

46. Turro, N.; Chow, M., Mechanism of Thermolysis of Endoperoxides of Aromatic Compounds - Activation Parameters, Magnetic Field, and Magnetic Isotope Effects. *Journal of the American Chemical Society* **1981**, 103, (24), 7218 - 7224.

47. Turro, N.; Chow, M.; Rigaudy, J., Thermolysis of Anthracene Endoperoxides - Concerted vs. Diradical Mechanisms. *Journal of the American Chemical Society* **1979**, 101, (5), 1300 - 1302.

CHAPTER 4

ASSEMBLER REVERIES –

THE FUTURE OF NANOFABRICATION

FINAL COMMENTS

> *The principles of physics, as far as I can see, do not speak against the possibility of moving things atom by atom. It is not an attempt to violate any laws; it is something, in principle, that can be done; but in practice, it hasn't been done because we are too big.*
>
> - Richard P. Feynman, 1960.[1]

In the 1980's, Eric Drexler's quixotic interpretation of Feynman's vision led him to believe that it would eventually be possible to build a universal nanorobot capable of building almost anything atom-by-atom, which he nicknamed "The Assembler".[2] The Assembler has generally been received with a great deal of well-deserved skepticism and this approach has yet to persuade chemists, who are well aware of the high reactivity of most atomic species, the nature of chemical bonding and of molecular properties which would make atom-by-atom manipulation extremely difficult, if not impossible.[3]

If this particular bottom-up approach has failed to emerge as a nanofabrication process, chemists have answered Feynman's invitation to work from the bottom-up in a multitude of ways including chemical synthesis, as described in Chapter 2. Moreover, many top-down approaches have been developed and successfully implemented in the industry, with optical lithography leading the way as the foremost industrial fabrication method of devices with fine detail on the nanoscale.

However, as it was illustrated in the first chapter, the lithographic fabrication of features that are smaller than the lithographic wavelength poses an immense challenge. This problem was first encountered in the mid-1990's, at which time several tricks such as immersion lithography had to be used to follow Moore's Law and achieve the required feature sizes now significantly smaller than the lithographic wavelength. Nevertheless, as the demands of the integrated circuit industry continued to follow Moore's Law and decreasing sizes of lithographic components, science is struggling to keep pace using more or less conventional lithography and the lithographic wavelengths currently available.

Industrial top-down techniques have been extensively developed and the enhancement of these methods with high numerical aperture, double exposure and other resolution enhancement techniques (RET) similar to those explored in the third chapter, can produce well-defined structures on scales previously thought unreachable.[4, 5] *Indeed, strategies like reversible contrast enhancement layers permit the extension of the current optical lithography lifespan. But while the industry's capabilities improve with each technology generation, the difficulties increase dramatically as the feature size continues to decrease.*[6] *Even with the successful implementation of chemical tricks such as those investigated in Chapter 3 for the next few generations of technology, it is difficult to argue that the industry is reaching the limits of optical lithography at 193 nm.*[7]

While the use of shorter lithographic wavelengths such as extreme-UV (13.4 nm)[7] *is still possible, the photons given by such technology will be rather expensive ones and will be hardly useful in mass production of common inexpensive electronics destined to commercial availability to the public. Beyond lithographic wavelength limitations, there also are diffusion and physical barriers which constitute important difficulties in the lithographic processes used for the fabrication of nanodevices.*[8]

New technologies based on non-traditional routes are needed to continue making progress, particularly in the integrated circuit field.[6] *On this note, it should be highlighted that currently employed top-down techniques have an inherent size limit that is larger that that of bottom-up techniques.*[4] *Thus, although it is still too early to consider radical changes of the technology used in industry, this is the ideal time to investigate the possibilities that lie in bottom-up methods for practical and wide-spread commercial applications.*

In fact, the bottom-up approach may prove be a look into the future, as lithography becomes unable to surpass the challenges brought on by nanoscaled components. Thus confirmed is the incredible foresight of Feynman when he observed that "it is a staggeringly small world that is below".[1] *Indeed, the bottom-up methods may solve the technological challenges faced by the integrated circuit industry and could lead to novel strategies for increasing device density.*[9] *It is new and ingenious strategies such as these that may open the way to the miniaturized devices of tomorrow.*

However if bottom-up methods are to play a role in the industry of the future, it will be necessary to establish methods for reproducible synthesis of nanostructures in conditions that are industry-friendly. In particular, lithography is not foreseen at very high temperatures and thus an approach at room temperature would be vastly encouraged. Furthermore, current syntheses employ harsh and toxic materials which are not appropriate for commercial fabrication and large scale manufacturing.

Milder conditions, such as those detailed in Chapter 2 for the synthesis of nanoparticles, may render similar bottom-up methods attractive to industrial applications. While the method described led to the successful synthesis of highly luminescent nanoparticles, suggesting relatively defect-free surfaces, the reverse micelle system did not appear to strongly restrict nanoparticle growth which leads to issues of undesired polydispersity. It is true that structures are never truly identical, unless they are single atoms or molecules, and that even current industrially fabricated nanostructures must exhibit a certain degree of polydispersity in size and shape.[10] Polydispersity can nevertheless be restricted with the use of self-assembly processes which tend towards the system's thermodynamic minimum, resulting in reproducible, stable and relatively defect-free structures because defects are energetically rejected.[11-13]

Moreover, self-assembly methods are cost-effective and versatile.[12] These properties will likely render them attractive candidates as fabrication tools in materials production, especially in nanomaterials, in the coming years.[14]

More particularly, it is foreseeable that the coalition of bottom-up and top-down methods will unlock the door to future technologies and development of effective nanoscaled devices.[15] Recently, in an extraordinary "tour de force" combining both bottom-up and top-down techniques, a sensor has been constructed by Murray and coworkers using a macroscopic substrate as a template on which nanoparticles assemble.[16, 17] It is expected that such integrated processes, using chemically synthesized nanoparticles that are manipulated by polymeric materials or self-assembly, will open the door to useful nanofabrication applications.[4] In such cases,

the macroscopic material plays the role of a template; a kind of skeleton that organizes the different components and functions of the device under construction.

Furthermore, template-mediated self-assembly can resolve the inherent difficulty associated with bottom-up methods: the missing link to the macroworld. Indeed, while bottom-up methods provide interesting and advantageous alternatives to nanomaterial construction, the materials so constructed are disconnected from the macroworld to which they must attach themselves in order to be of use. As with Murray's sensor, such assembly methods can deliver an interface between the nanoscopic and macroscopic worlds and supply the needed "contacts".[18] *The use of processes based on self-assembly in the integrated circuit industry has the potential of greatly enhancing feature density and delivering rich on-chip functionality.*[6]

In addition, it should be highlighted that although physicists and chemists are currently at the forefront of nanofabrication efforts, biologists are likely to make important contributions. Indeed, ideas are now coming from all directions in a "wonderful free-for-all discovery".[19] *In this era of great intellectual wealth, with overwhelming amounts of research being conducted, it becomes easy to dismiss purely investigational results with the pretext that they are not directed towards concrete applications. George Porter, pioneer in ultrafast chemistry, Nobel laureate and advocate for pure research, fervently opposed this inclination. He noted on this matter that there are two kinds of research: applied research and 'not yet applied research'.*[20, 21] *It remains our task to determine how to use the knowledge gained from all research, more specifically nanoresearch, whether it be pure or applied.*

Massive innovations in the nano realm are leading to extraordinary expectations for the future. Although there is no telling how nanotechnology will enable society to remedy global issues and concerns, there is no shortage of those that dare to imagine. Nobel laureate and professor Richard E. Smalley for instance, was a strong advocate for energy development through nanotechnology.[22] *Beyond energy, nanotechnology is likely to open a multitude of paths to follow in the area of information technology and computing. Some envision the development of the ultimate small storage particle, which would consist of the smallest possible*

particle on which data can be stored. Others dream of making the ultimate small motor or flying machine, which could be used as invisible spy crafts in international surveillance missions.[22] *Those with medical inclinations yearn for robotic submarines designed to repair internal damage and remove chemical toxins in the human body, or nanobiosensors that detect the onset of disease and release drugs that target the diseased cells on site.*[8]

It is true that these futuristic ideas appear to be pure science fiction today, but it is quite obvious that such an observation should not become a barrier for science to explore them. As Einstein astutely noted, imagination is more important than knowledge because knowledge is limited to what is known and understood, while imagination embraces the entire world, including what has yet to be discovered.[23] *It must therefore be that the driving force of innovative science is the creative minds of those who refuse to be bound by our current knowledge. Without imagination, how could a fully functional nanoradio which tunes in a broadcast signal, amplifies it and converts it to an audio signal have been fabricated from a single carbon nanotube?*[24] *Indeed, Moore's Law looked impracticable when considering basic principles of physics, but the misunderstanding of those that didn't grasp these principles has nonetheless pushed those that do to find ways around them.*

Science cannot abandon ideas solely because they are regarded as fantasy today. If that were the case, innovation would be sure to dwindle and fade away, depriving future generations from valuable scientific advances and technologies. It is vital to remind ourselves that, science can not only be the answer to the questions "why?" and "how?" but also to the question "what if?"...[25]

FUTURE DIRECTIONS

1. *Variability in terms of size and luminescence was observed in nanoparticles synthesized. This should be investigated further and reduced as much as possible by determining the variables that impact the final nanoparticle product outside of direct reactants.*
2. *Doping of the nanoparticles with lanthanides during synthesis.*
3. *The removal of surfactant after surface capping of the nanoparticle, which is a vital step on the road of making the synthesized nanoparticles useful for practical applications and flexibility in research.*
4. *Quenching of semiconductor nanoparticle luminescence using various binding and non-binding quenchers on nanoparticles that are either unprotected or protected, which could shed light on the protection offered by the surfactant and the capping agent.*
5. *Decrease of the cadmium precursor concentration used in synthesis with respect to selenium, in order to assess the impact on the synthesized nanoparticle luminescence intensity and the possible reduction of surface trap sites.*
6. *Better elucidation of photophysical pathways of cycloDAME and DAME, possibly using faster laser flash photolysis to observe transients and rapid growth times of products, as well as further 266 nm irradiation LFP studies for identification of transients and products generated.*
7. *Laser-laser wave experiment using 193 nm and 248 nm irradiation wavelengths for cleaving and cycloadding steps.*
8. *Full characterization of DAMEPO (extinction coefficient, product yield, ^{13}C-NMR), as there was too little product synthesized to accurately weigh and perform these experiments.*

CLAIMS TO ORIGINAL RESEARCH

1. *Room temperature reverse micelle synthesis of highly luminescent, and very small core blue quantum dots.*
2. *Surface derivatization of synthesized nanoparticles using reverse-micelles as vehicles to deliver MPSA capping agent.*
3. *AOT surfactant removal from reverse micelle system using ethanol precipitation.*
4. *Nanoparticle growth studies using time-resolved luminescence profile observations as well as nanosecond time-resolved photoluminescence lifetime measurements of nanoparticles growing in reverse micelles.*
5. *Effects of the water-to-surfactant ratio and the surfactant concentration on the formation of nanoparticles within the reverse micelle water pool in terms of nanoparticle size and luminescence.*
6. *^{1}H and ^{13}C-NMR characterization of DAME, cycloDAME and DAME endoperoxide (DAMEPO).*
7. *Determination of extinction coefficients for DAME, cycloDAME and anthracene endoperoxide at irradiation relevant wavelengths and maximum absorbance peak wavelengths.*
8. *Photophysical pathway investigation of DAME cycloaddition and reversion, including quantum yield of cycloDAME ring opening and fluorescence quantum yield of DAME.*
9. *Transient studies of anthracene dimer and cycloDAME by laser flash photolysis following 193 nm excitation.*
10. *In situ monitoring of cycloDAME photochemical reversibility (open to closed form) by laser-laser time-resolved wave experiment studies, and laser-lamp wave studies of DAME reversibility and resiliency over several open-close cycles.*
11. *Dose response evaluation of cycloDAME to cleaving irradiation.*
12. *Direct anthracene endoperoxide synthesis by pulsed far-UV irradiation in acetonitrile solution.*

13. *Rose Bengal sensitized DAMEPO synthesis using continuous visible irradiation.*
14. *Spectroscopic determination of the rate of thermal cleavage for anthracene endoperoxide and DAMEPO peroxide bonds.*
15. *Invention of a new actinometer, using cycloDAME as a reference to measure efficiencies of future candidate compounds.*

REFERENCES

1. Feynman, R. P., There's Plenty of Room at the Bottom. *Engineering and Science* **1960**, 23, 22 - 36.

2. Balzani, V., Nanoscience and Nanotechnology: A Personal View of a Chemist. *Small* **2005**, 1, 278 - 283.

3. Balzani, V.; Credi, A.; Venturi, M., Molecular Devices and Machines. *Nano Today* **2007**, 2, (2), 18 - 25.

4. Skaff, H.; Emrick, T., Semiconductor Nanoparticles: Synthesis, Properties, and Integration Into Polymers for the Generation of Novel Composite Materials. In *Nanoparticles - Building Blocks for Nanotechnology*, Rotello, V., Ed. Kluwer Academic/Plenum Publishers: New York, 2004.

5. Thompson, S. E.; Parthasarathy, S., Moore's Law: The Future of Si Microelectronics. *Materials Today* **2008**, 9, (6), 20 - 25.

6. Yu, B.; Meyyappan, M., Nanotechnology: Role in Emerging Nanoelectronics. *Solid State Electronics* **2006**, 50, 536 - 544.

7. O'Connor, N. A.; Berro, A.; Lancaster, J. R.; Gu, X.; Jockusch, S.; Tomoki, N.; Ogata, T.; Lee, S.; Zimmerman, P. A.; Wilson, G. C.; Turro, N. J., Toward the Design of a Sequential Two Photon Photoacid Generator for Double Exposure Photolithography. *Chemistry of Materials* **2008**, 20, (24), 7374 - 7376.

8. Cao, G., *Nanostructures & Nanomaterials: Synthesis, Properties and Applications*. Imperial College Press: London, UK, 2004.

9. Lu, W.; Lieber, C. M., Nanoelectronics From The Bottom Up. *Nature Materials* **2007**, 6, 841 - 850.

10. Ozin, G. A.; Arsenault, A.; Cademartiri, L., *Nanochemistry - A Chemical Approach to Nanomaterials*. 2nd ed.; The Royal Society of Chemistry Publishing: Cambridge, 2009.

11. Whitesides, G.; Mathias, J. P.; Seto, C. T., Molecular Self-Assembly and Nanochemistry: A Chemical Strategy for the Synthesis of Nanostructures. *Science* **1991**, 254, (5036), 1312 - 1319.

12. Huie, J. C., Guided Molecular Self-assembly: A Review of Recent Efforts. *Smart Materials and Structures* **2003**, 12, 264 - 271.

13. Whitesides, G.; Grzybowski, B., Self-Assembly at All Scales. *Science* **2002**, 295, (5564), 2418 - 2421.

14. Zhang, S., Building From the Bottom Up. *Materials Today* **2003**, 6, (5), 20 - 27.

15. Rotello, V. M., *Nanoparticles - Building Blocks of Nanotechnology*. Kluwer Academic/Plenum Publishers: New York, 2004.

16. Zamborini, F. P.; Leopold, M. C.; Hicks, J. F.; Kulesza, P. J.; Malik, M. A.; Murray, R. W., Electron Hopping Conductivity and Vapor Sensing Properties of Flexible Network Polymer Films of Metal Nanoparticles. *Journal of the American Chemical Society* **2002**, 124, (30), 8958 - 8964.

17. Walt, D. R., Nanomaterials: Top-to-bottom Functional Design. *Nature Materials* **2002**, 1, 17 - 18.

18. Wade, T. L.; Wegrowe, J.-E., Template Synthesis of Nanomaterials. *The European Physical Journal - Applied Physics* **2005**, 29, 3 - 22.

19. Whitesides, G.; Love, J., The Art of Building Small. *Scientific American* **2001**, 285, (3), 39 - 47.

20. Archer, M., George Porter: A Peer Among Scientists. *Comptes Rendus. Chimie.* **2006**, 9, 180 - 187.

21. Phillips, D., Obituary - George Porter. *Nature* **2002**, 419, 578.

22. Hornyak, G. L.; Dutta, J.; Tibbals, H. F.; Rao, A. K., *Introduction to Nanoscience*. CRC Press - Taylor & Francis Group: Boca Raton, 2008.

23. Isaacson, W., *Einstein - His Life and Universe*. Simon & Schuster: New York, 2007, page 7.

24. Jensen, K.; Weldon, J.; Garcia, H.; Zettl, A., Nanotube Radio. *Nano Letters* **2007**, 7, (11), 3508 - 3511.

25. Ozin, G. A.; Arsenault, A.; Cademartiri, L., Foreword by Ludovico Cademartiri. In *Nanochemistry - A Chemical Approach to Nanomaterials*, 2nd ed.; The Royal Society of Chemistry Publishing: Cambridge, 2009.

APPENDIX I – CONTINUOUS IRRADIATION SOURCES

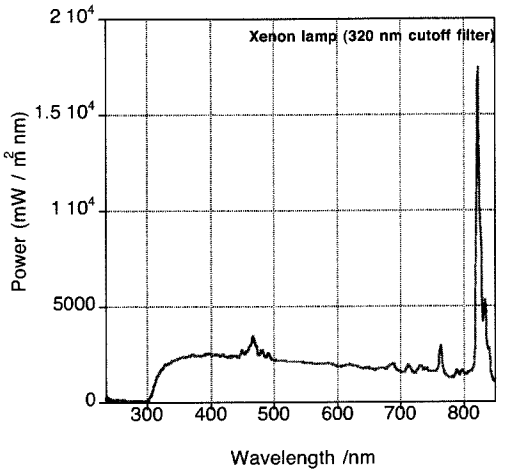

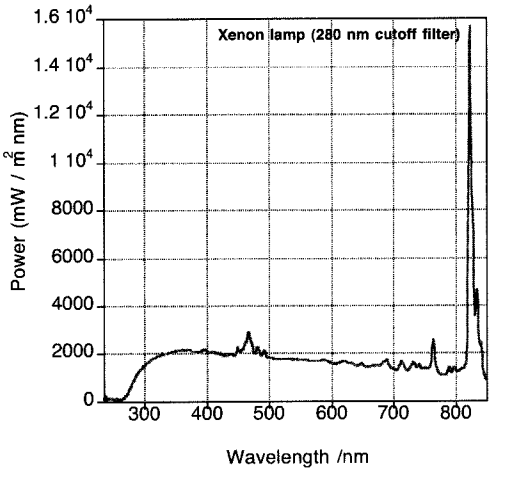

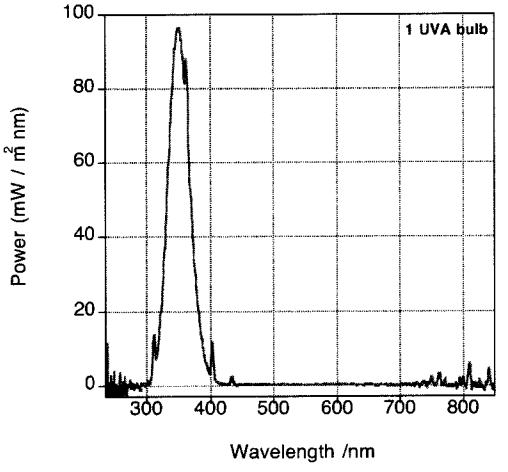

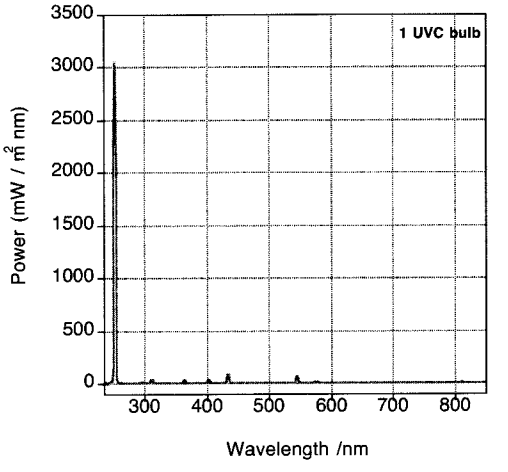

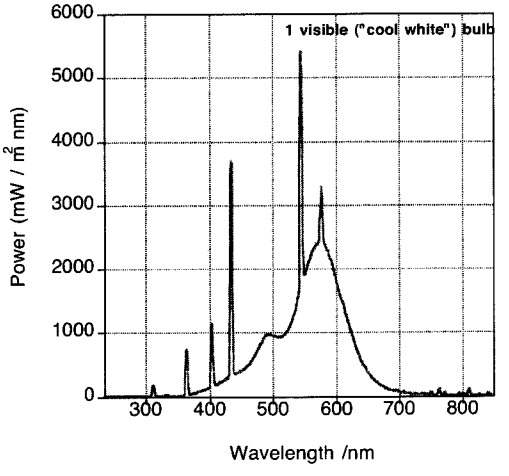

APPENDIX II.1 – ^{1}H NMR (400 MHz, $CDCl_3$) DAME

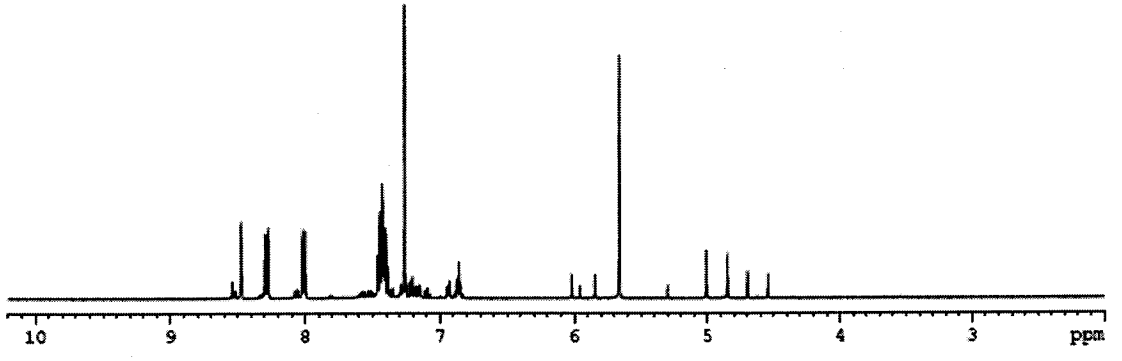

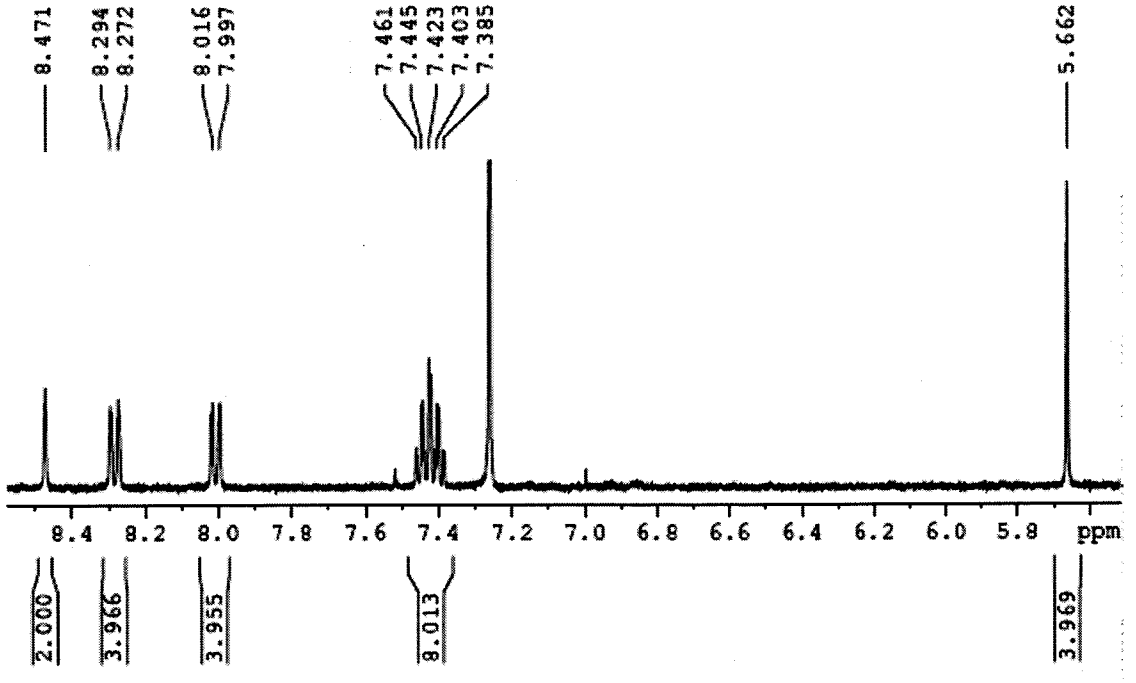

APPENDIX II.2 – ^{13}C NMR (400 MHz, $CDCl_3$) DAME

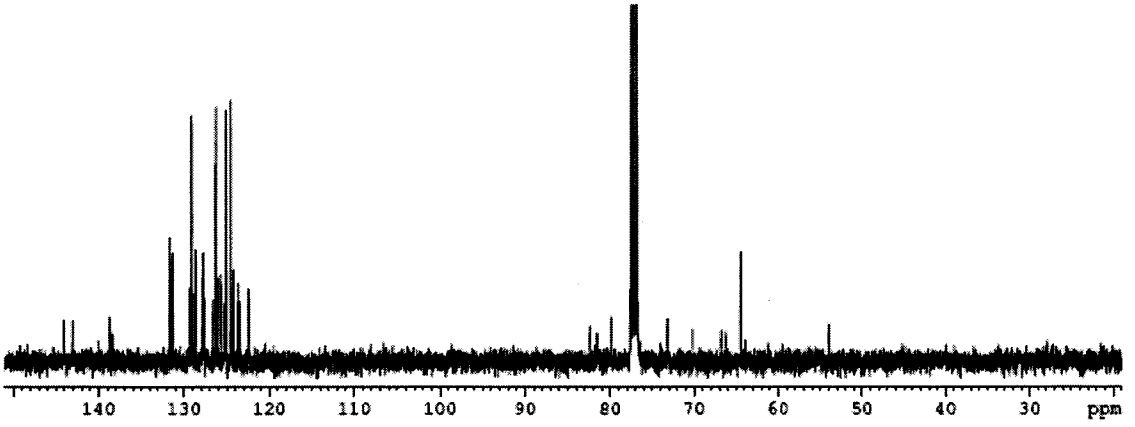

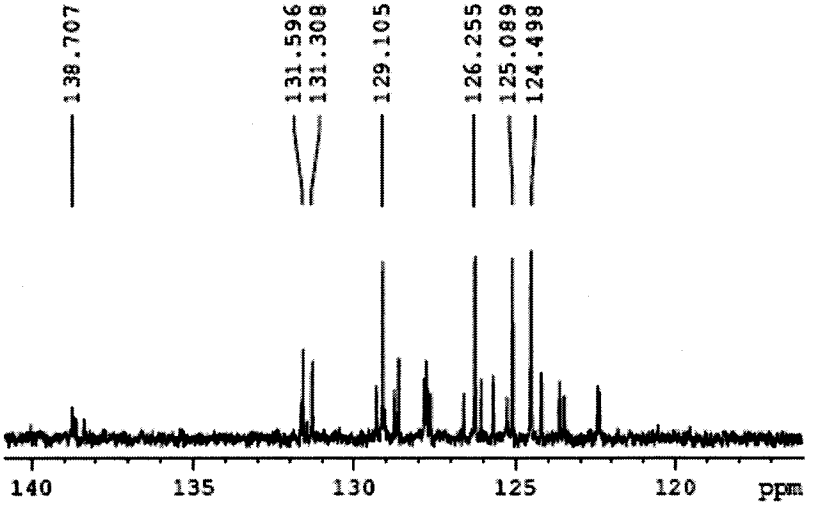

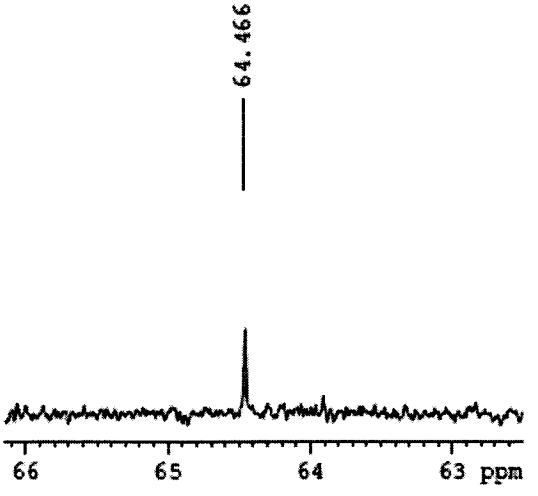

APPENDIX III.1 – ^{1}H NMR (400 MHz, $CDCl_3$)

CYCLODAME

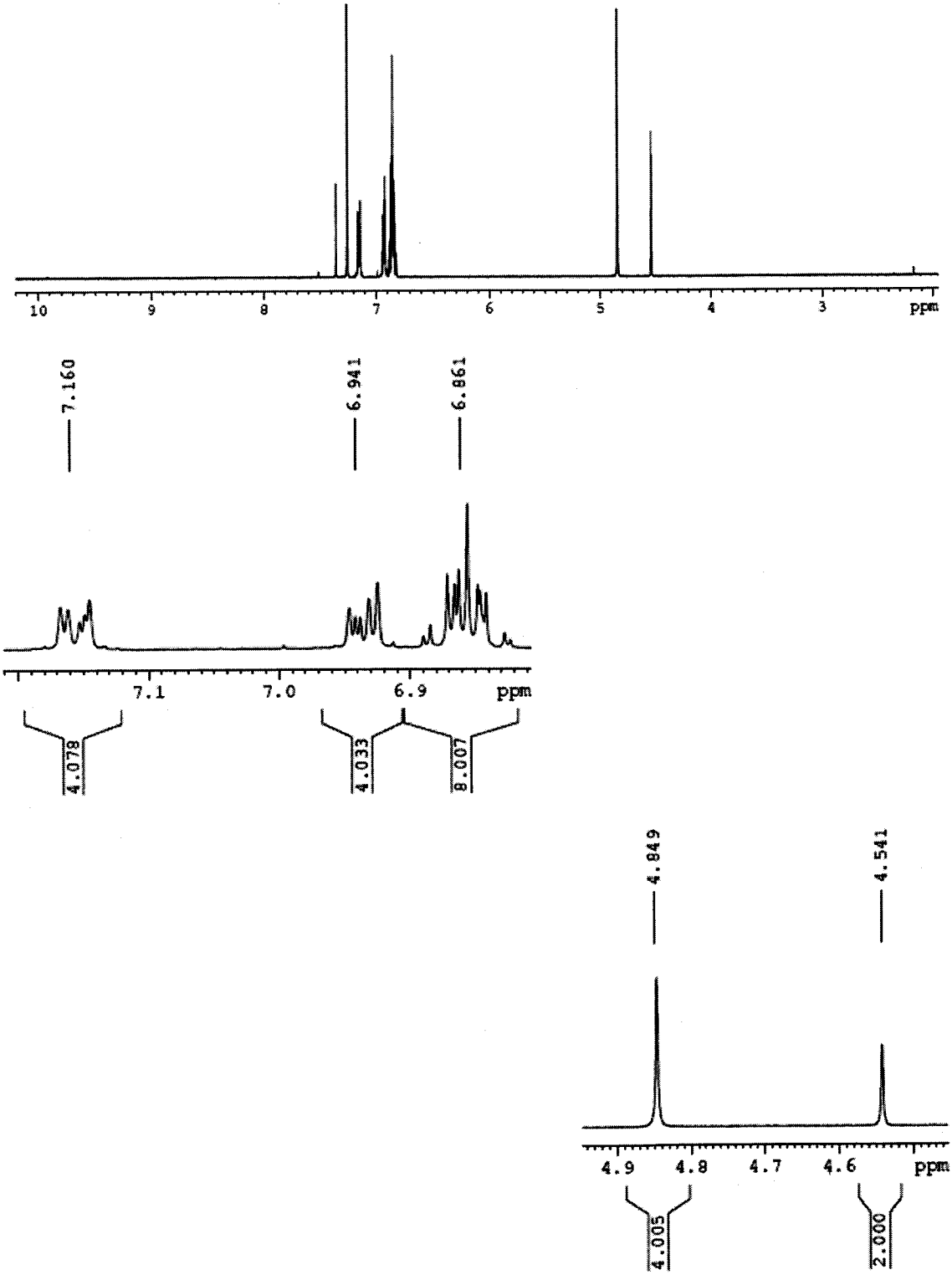

APPENDIX III.2 – ^{13}C NMR (400 MHz, $CDCl_3$)

CYCLODAME

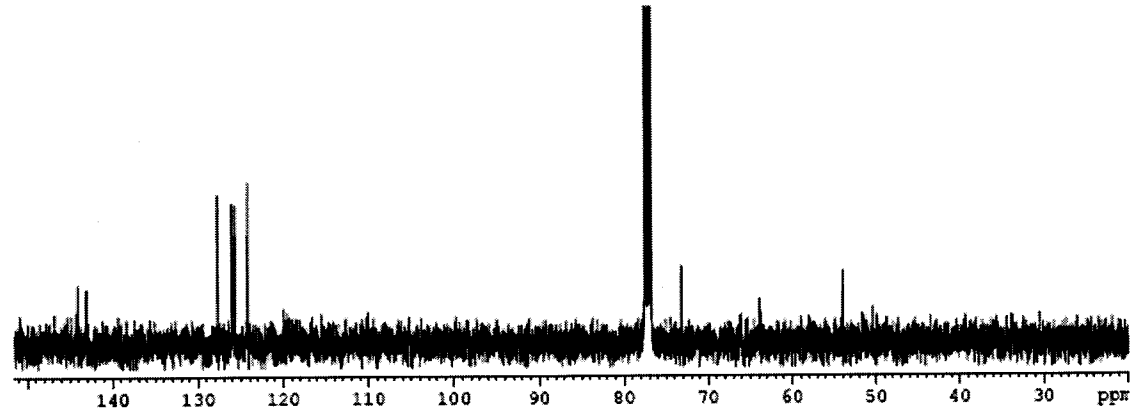

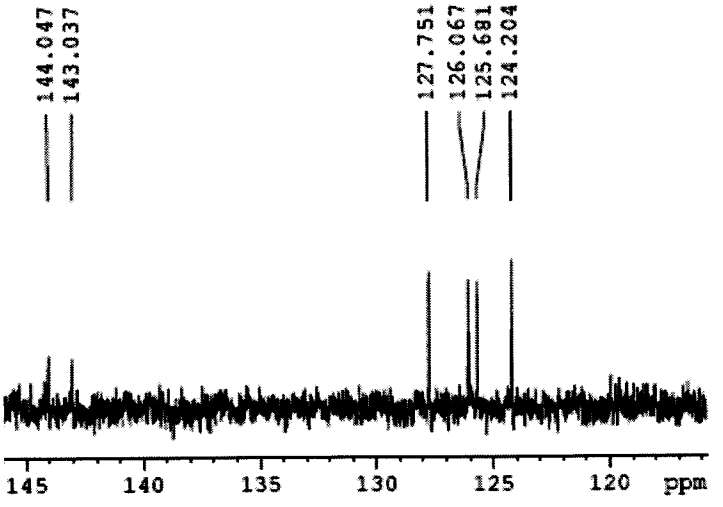

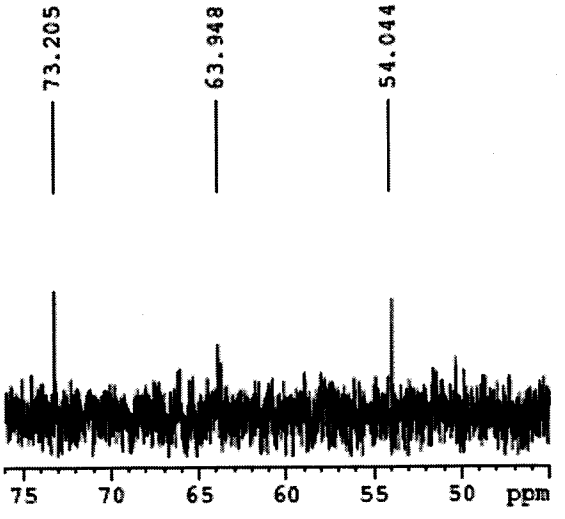

APPENDIX IV – ^{1}H NMR (400 MHz, $CDCl_3$)

DAMEPO

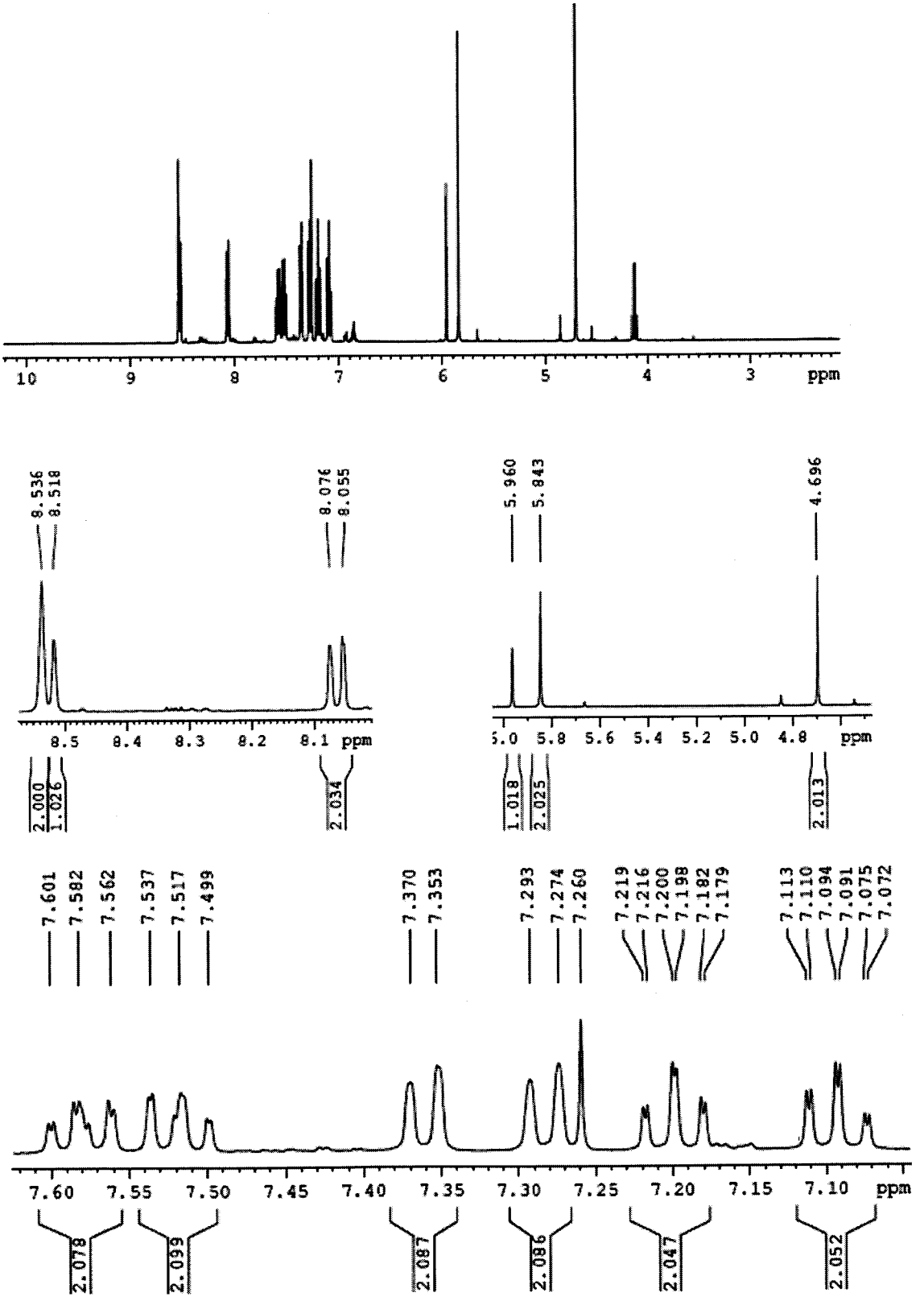

APPENDIX V – CLEAVING QUANTUM YIELD OF CYCLODAME

The quantum of yield of cycloDAME cleaving with 193 nm light was determined against the diphenylcyclopropenone (DPCP) actinometer (Φ = 1). Both samples were contemporaneously irradiated with equal doses of 193 nm light and their absorbance profiles were recorded in function of irradiation dose. The absorbance was converted to concentration using previously determined extinction coefficients:

$\varepsilon_{365\ nm}$ *(DAME) = 14 000* $M^{-1}\ cm^{-1}$ *and* $\varepsilon_{310\ nm}$ *(DPCP) = 19 000* $M^{-1}\ cm^{-1}$.

cycloDAME in acetonitrile (A_{193nm}= 0.54) was cleaved to form DAME (λ_{abs}= 365 nm) and monitored using the absorbance increase at 365 nm:

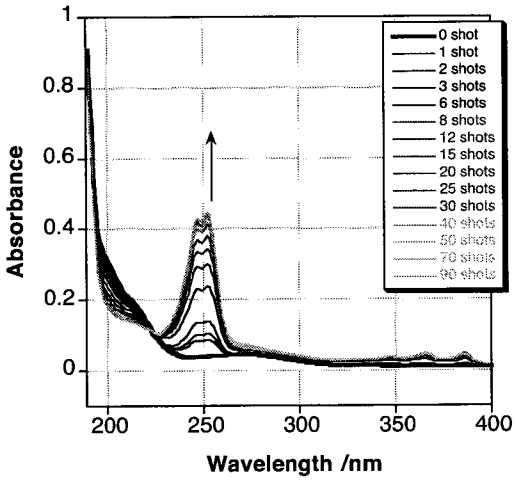

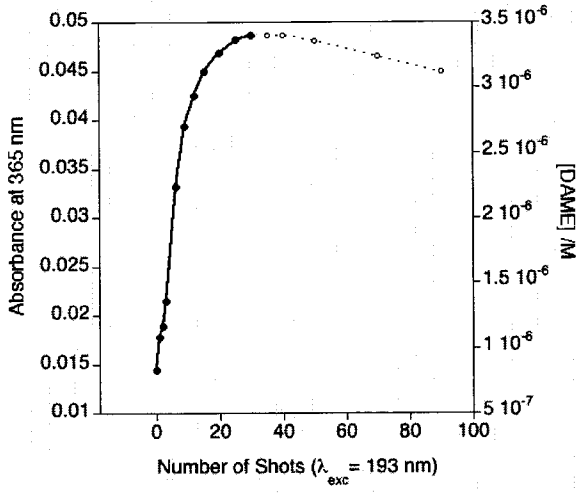

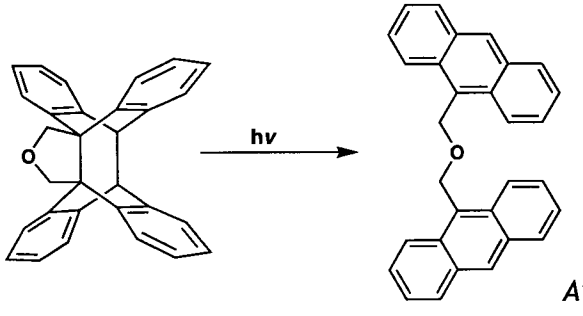

Average initial rate: 1.87 x 10^{-7}*M/shot*

DPCP (λ_{abs}= 310nm) in acetonitrile (A_{193nm}= 0.41), underwent photodecomposition and was monitored using the absorbance decrease at 310 nm:

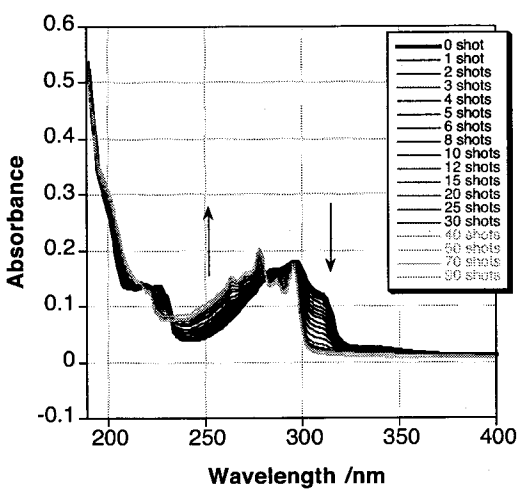

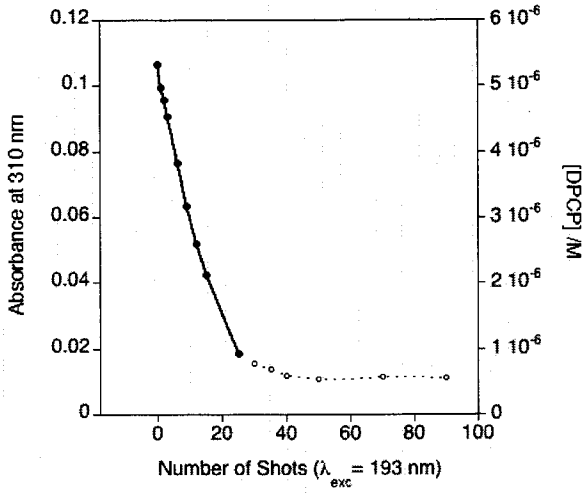

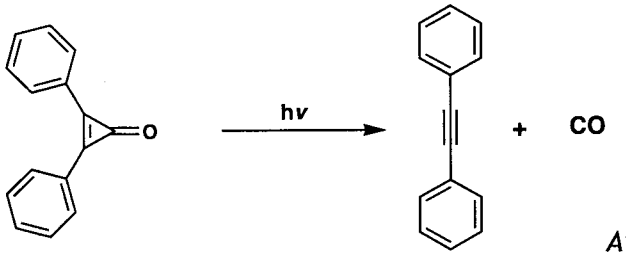

Average initial rate: -2.26 x 10^{-7}M/shot

The average initial rates of DPCP decomposition and cycloDAME cleavage were determined directly from the concentration changes. To correct for the absorbance difference at the excitation wavelength, the following relationship was applied:

$$\frac{\Phi_1}{\Phi_2} = \frac{\dfrac{\text{(number of events for 1)}}{\text{(number of photons absorbed for 1)}}}{\dfrac{\text{(number of events for 2)}}{\text{(number of photons absorbed for 2)}}} = \frac{\dfrac{\text{(initial rate for 1)}}{(1-T_1)}}{\dfrac{\text{(initial rate for 2)}}{(1-T_2)}}$$

where the transmittance (T) can be calculated from the measured absorbance at the excitation wavelength, according to the equation: $T = 10^{-A}$.

The initial rate was then used to calculate the quantum yield of cycloDAME against the actinometer quantum yield (Φ_{DPCP} = 1).

$$\frac{\Phi_{cDAME}}{\Phi_{DPCP}} = \frac{(1.87 \cdot 10^{-7})/(1-0.724)}{(2.26 \cdot 10^{-7})/(1-0.776)} = 0.67$$

This experiment was repeated three times and the error was calculated from the standard deviation obtained. Our final calculated value for the cleaving quantum yield is 0.67 ± 0.04.